UNITED NATIONS UNIVERSITY

UNU-GTP

ORKUSTOFNUN

Silica rich waters in Köldulaugagil, Hengill area, SW-Iceland

Samuel Kinyua Munyiri

STRUCTURAL MAPPING OF OLKARIA DOMES GEOTHERMAL FIELD USING GEOCHEMICAL SOIL GAS SURVEYS, REMOTE SENSING AND GIS

Report 5
December 2016

UNITED NATIONS UNIVERSITY
UNU-GTP
Geothermal Training Programme

Orkustofnun, Grensasvegur 9,
IS-108 Reykjavik, Iceland

Reports 2016
Number 5

STRUCTURAL MAPPING OF OLKARIA DOMES GEOTHERMAL FIELD USING GEOCHEMICAL SOIL GAS SURVEYS, REMOTE SENSING AND GIS

MSc thesis
School of Engineering and Natural Sciences
Faculty of Earth Sciences
University of Iceland

by

Samuel Kinyua Munyiri
Kenya Electricity Generating Company, Ltd. - KenGen
P.O Box 785-20117, Naivasha
KENYA
smunyiri@kengen.co.ke

United Nations University
Geothermal Training Programme
Reykjavík, Iceland
Published in December 2016

ISBN 978-9979-68-409-1
ISSN 1670-7427

This MSc thesis has also been published in June 2016 by the
School of Engineering and Natural Sciences, Faculty of Earth Sciences
University of Iceland

INTRODUCTION

The Geothermal Training Programme of the United Nations University (UNU) has operated in Iceland since 1979 with six month annual courses for professionals from developing countries. The aim is to assist developing countries with significant geothermal potential to build up groups of specialists that cover most aspects of geothermal exploration and development. During 1979-2016, 647 scientists and engineers from 60 developing countries have completed the six month courses, or similar. They have come from Africa (38%), Asia (36%), Latin America (14%), Europe (12%), and Oceania (1%). There is a steady flow of requests from all over the world for the six-month training and we can only meet a portion of the requests. Most of the trainees are awarded UNU Fellowships financed by the Government of Iceland.

Candidates for the six-month specialized training must have at least a BSc degree and a minimum of one-year practical experience in geothermal work in their home countries prior to the training. Many of our trainees have already completed their MSc or PhD degrees when they come to Iceland, but many excellent students with only BSc degrees have made requests to come again to Iceland for a higher academic degree. From 1999 UNU Fellows have also been given the chance to continue their studies and study for MSc degrees in geothermal science or engineering in co-operation with the University of Iceland. An agreement to this effect was signed with the University of Iceland. A similar agreement was also signed with Reykjavik University in 2013. The six-month studies at the UNU Geothermal Training Programme form a part of the graduate programme.

It is a pleasure to introduce the 50th UNU Fellow to complete the MSc studies under a UNU-GTP Fellowship. Samuel Kinyua Munyiri, BSc in Geology, from Kenya Electricity Generating Company, Ltd. – KenGen, completed the six-month specialized training in Borehole Geology through a special advanced 6-month training session given by UNU Geothermal Training Programme in Kenya, from July 2012 – February 2013. His research report, co-authored by Mr. Michael Mwania and Emily Okech, was entitled: *Borehole geology and hydrothermal mineralisation of well OW-35, Olkaria East geothermal field, Central Kenya rift valley.* After one and half year of geothermal work in Kenya, he came to Iceland for MSc studies at the University of Iceland, School of Engineering and Natural Sciences, starting in August 2014. In May 2016, he defended his MSc thesis presented here, entitled: *Structural mapping of Olkaria Domes geothermal field using geochemical soil gas surveys, remote sensing and GIS.* His studies in Iceland were financed by the Government of Iceland and KenGen through a UNU-GTP Fellowship from the UNU Geothermal Training Programme. We congratulate him on his achievements and wish him all the best for the future. We thank the School of Engineering and Natural Sciences, Faculty of Earth Sciences at University of Iceland for the co-operation, and his supervisors for the dedication.

Finally, I would like to mention that Samuel's MSc thesis with the figures in colour is available for downloading on our website *www.unugtp.is*, under publications.

With warmest greetings from Iceland,

Lúdvík S. Georgsson, Director
United Nations University
Geothermal Training Programme

ACKNOWLEDGEMENTS

I wish to sincerely thank the Icelandic Government, United Nations University Geothermal Training Programme (UNU-GTP) and the Kenya Electricity Generating Company, Ltd. (KenGen) for awarding the scholarship for this study. I am greatly indebted to the University of Iceland, Iceland GeoSurvey (ÍSOR) and any other institution that ensured success in my M.Sc. studies.

My appreciation goes to the KenGen management, Olkaria Geothermal Project, for facilitating the study program and providing the sabbatical leave. The role played by Geology, Geophysics and Geochemistry sections in data acquisition and processing is much valued.

Gratitude goes to my advisors Prof. Thorvaldur Thórdarson, Dr. Björn S. Hardarson and Gunnlaugur M. Einarsson for their role in enlightening, valuable discussions and impacted knowledge in structural geology and GIS. It is through them that some of the fundamental problems relating to the project were satisfactorily answered and I particularly cherish their support and advice. Special thanks go to Dr. Björn S. Hardarson who supervised the field work and greatly assisted in collecting data; I am indebted to Gunnlaugur M. Einarsson for his tireless work, great skills and guidance in producing the structural geology map of the study area. Sigurður Kristinsson was also instrumental in reviewing my work. Thank you all.

To my colleagues, friends and the other UNU-GTP fellows who encouraged and facilitated the success of this work in any way, I wish to thank you for your devotion. I reach out to my family who waited patiently while I was away on studies and encouraged me through out. Thank you all for your support for you taught me everything that has a beginning must have an end.

Finally, I give all glory and honour to the Almighty Lord for the successful completion of the entire programme.

DEDICATION

This work is dedicated to my parents, the late Eng. Lawrence Munyiri Ruthuthi and Rose Nyaguthii Munyiri for their passion of impacting the love for knowledge in me. To my wife Judy Nyaguthii Kinyua for taking care of my family. Finally, to the lovely kids who look at me as their role model including Tess Nyaguthii for giving new meaning to life.

ABSTRACT

Olkaria geothermal field is a high temperature geothermal system located on the eastern arm of the East African Rift System. It is placed within the Central Kenya Rift Valley and is dominated by late Quaternary rhyolitic volcanism. Basalts, tuffs and trachytes occupy the subsurface with the latter forming the reservoir rock. Normal faulting mapped during this study is prominent in the Domes field with dips ranging from 20° to 80° to the west and the east. Fault strikes vary from north-south, northwest-southeast, northeast-southwest and east-west. The oldest faults strike northwest and coincide with the initiation of the Kenyan rift system while the youngest are the North striking and are thought to have formed during a distinct period of dyking that took place along the Ol Njorowa Gorge. East-west striking faults were discovered to the east of Domes field and are inferred to have been formed during a period of transform faulting. Thrust faulting is rare throughout the field but portrays brief periods of crustal compression. Geothermal manifestations were observed as key indicators of permeable zones that gave indication of faults and fractures which may have been obscured by recent pyroclastic deposits. Soil gas surveys indicate an E-W orientation of anomalies along the south of Domes field. Digital elevation models show step normal faulting to be dominant forming steep shoulder faults along the Central Kenyan rift. Regional faults exhibit near vertical dips to the east and west, forming a graben which is approximately 45km wide. Transform faulting is evidenced along the Central Kenyan rift and may have been responsible for sudden changes in the strike of the rift faults. A cauldron with four arcs was observed south of Lake Naivasha where Olkaria and Longonot calderas occur on its periphery while Suswa caldera is located at its centre. It forms a structure similar to a knee joint along the rift where all shoulder rift faults are arcuate. Magnetic data shows existence of a shallow anomaly which may signify presence of a shallow magma reservoir at a depth of about 15 km.

TABLE OF CONTENTS

Page

1. INTRODUCTION....1
   1.1 Morphology of the Kenyan Rift System....2
   1.2 Geographical setting of the study area....3
   1.3 History of geothermal development at Olkaria geothermal field....5
   1.4 Aim and scope of the research project....7

2. GEOLOGY AND STRUCTURAL PROVENANCE OF THE GREATER OLKARIA VOLCANIC COMPLEX....9
   2.1 Structural geology....10
   2.2 Tectonic activity....12
   2.3 Hydrogeology....12

3. METHODOLOGY....14
   3.1 Desktop studies....14
   3.2 Preliminary data analysis....14
   3.3 Reconnaissance studies....14
   3.4 Field work....15
   3.5 Data analysis and synthesis....15
   3.6 Geochemical soil gas surveys....16
      3.6.1 Measurement of carbon dioxide (CO_2)....16
      3.6.2 Radon gas measurements....17

4. RESULTS....18
   4.1 Surface Geology....18
      4.1.1 Lacustrine sediments (100 Ka)....18
      4.1.2 Longonot pyroclastics (0.2 – 400 Ka)....19
      4.1.3 Kinangop tuffs (3.4 – 3.7 Ma)....19
      4.1.4 Trachytes (0.1 Ka - 6.9 Ma)....20
   4.2 Structures in the Central Kenyan Rift segment....20
   4.3 Olkaria Domes field....24
      4.3.1 Fractures....24
      4.3.2 Faults....25
      4.3.3 Calderas....28
      4.3.4 Dykes....30
      4.3.5 Folds....32
      4.3.6 Altered Ground....32
      4.3.7 Hot springs....34
      4.3.8 Volcanic plugs and eruption centres....35
   4.4 Geochemical soil gas survey results....36
      4.4.1 CO_2 gas survey....36
      4.4.2 Radon gas survey....37

5. DISCUSSION....39
   5.1 Updated structural map of Olkaria Domes geothermal field....39
   5.2 Olkaria conceptual model....40
   5.3 The knee joint structure....42

6. CONCLUSION....44

7. RECOMMENDATIONS....45

REFERENCES....46

Page
APPENDIX I: Clay analysis data for selected samples 52

APPENDIX II: Sampling stations 61

APPENDIX III: Geochemical data 63

LIST OF FIGURES

1. Digital Elevation Model of northeast Africa, showing the plate boundaries 2
2. Simplified map of the Kenyan rift showing location of geothermal prospects and fields 3
3. Central Kenyan rift with location of Olkaria, Longonot and Suswa volcanoes 4
4. Map showing relative location of Olkaria geothermal sectors and the study area 5
5. Resource map showing numerous wells drilled in different geothermal sectors 7
6. Summarized representation of the upper Olkaria volcanic sequences 9
7. Map showing the surface geology and the structures in Olkaria 11
8. InSAR data from Mt. Longonot show vertical movement of up to 9 cm 12
9. Geodetic activity detected at volcanic centers in the Kenyan rift 13
10. Map showing the distribution of geochemical sampling points 16
11. Image of an Orsat apparatus used in measuring CO_2 17
12. Geological map of Kijabe area showing the dominant rock types and structural trends 19
13. Map showing the transform zones that led to the changes in rift orientations 21
14. DEM of the Kenyan Rift System showing the general orientation of the rift 22
15. Map showing variation in Curie Point depth (CPD) along the Kenyan rift system 23
16. Plate showing one of the NW-SE fractures located on the ridge 25
17. Map showing location and strike of mapped fractures 26
18. Normal faulting depicted by the white ash deposits 27
19. Plate showing normal faulting along Ol Njorowa gorge 27
20. Map showing structural trends in Olkaria Domes field 28
21. Image of a thrust fault observed along the ridge structure east of Domes field 28
22. Map showing Olkaria ring structure and both outer and inner Longonot caldera rims 29
23. Figure illustrating conditions for dyke propagation 30
24. Plate showing dykes extrusion along the Ol Njorowa gorge 31
25. Plate showing folding along the ring structure. 32
26. Map of the study area showing spatial distribution of altered grounds 33
27. Altered grounds showing different levels of alteration 34
28. Map showing location of hot springs along Ol Njorowa gorge 35
29. Map of the study area showing volcanic plugs and eruption centers 36
30. Soil gas map of CO_2 gas survey carried out in Domes field 37
31. Map of radon gas values measured in Domes field 38
32. Updated structural map of Olkaria Domes field 39
33. Schematic geological conceptual model of Olkaria 42
34. The schematic model of the knee joint structure located on the Central Kenyan rift 43

LIST OF TABLES

1. Current geothermal installed capacity for geothermal power in Kenya. 1
2. Work breakdown structure 8

ACRONYMS AND ABBREVIATIONS

AMMP	Africa Magnetic Mapping Project
Bp	Before present
CPD	Curie Point depth
EARS	East African Rift System
GOGA	Greater Olkaria geothermal area
GOVC	Greater Olkaria volcanic complex
ISOR	Iceland GeoSurvey
Ka	Thousand years
KenGen	Kenya Electricity Generating Company, Ltd.
km	kilometres
m	metres
Ma	Million years
m a.s.l.	metres above sea level
m b.g.l.	metres below ground level
MWe	Megawatt electric energy
MWt	Megawatt thermal energy
OW	Olkaria well
UNU-GTP	United Nations University Geothermal Training Programme
XRD	X-ray diffractometry

1. INTRODUCTION

Kenya's current installed geothermal electric power capacity is 658.3 MWe (Table 1) and an extra 560 MWe is being developed in Olkaria geothermal field (KenGen, 2015; Kenya Power, 2015; Ormat, 2015; Omenda and Simiyu, 2015). An additional 105 MWe is proposed for development in Menengai geothermal field (Omenda, 2014). The aim is to increase the renewable energy output to meet the current national peak demand of 1,468 MWe and ensure a base load reserve of close to 600 MWe (Kenya Power, 2015). The country has put a major focus on geothermal expansion in order to reduce over-reliance on non-renewable electricity resources. For the sake of environmental conservation, the Government has committed to develop cheaper, cleaner, more reliable and green energy, from renewable sources, mainly from geothermal, wind and solar (MOE, 2015).

TABLE 1: Current geothermal installed capacity versus effective capacity for all geothermal power plants in Kenya

Geothermal power plant	Installed capacity (MW)	Effective capacity (MW)	Data source
Olkaria I Units 1, 2 & 3	45	44	KenGen (2015), Kenya Power (2015)
Olkaria I Units 4 & 5	150.5	140	KenGen, 2015; Kenya Power, 2015
Olkaria II	105	101	KenGen, 2015; Kenya Power, 2015
Olkaria III	140	140	Ormat, 2015
Olkaria IV	149.8	140	KenGen, 2015; Kenya Power, 2015
Wellheads	64	64	KenGen, 2016
Oserian 1 & 2	4	3	Omenda and Simiyu, 2015
Total	**658.3**	**632**	

Although the Kenyan Rift system has an estimated geothermal capacity of approximately 10,000 MWe, less than 10% of the potential has been utilised (Omenda, 2014). To accelerate geothermal development, Government policies reforms have been initiated and fast tracked. Vision 2030 is an ambitious government policy geared towards developing Kenya to a middle level economy on the global stage by the year 2030. In this policy, energy is considered as one of the key pillars for economic growth. It is estimated that 33,000 MWe are required for powering Kenya's industrial and domestic sectors (Omenda *et al.*, 2014). The current Government has put in place 'the 40 months challenge' (extracted from Vision 2030), with the objective of fast tracking development of 5,000 MWe from alternative and renewable energy resources. Major consumers of this additional power generation will be smelting industries, The Lamu Port Southern Sudan-Ethiopia Transport project (LAPPSET) & ICT industrial Parks, which are estimated to consume 4,196 MWe of this new electrical power (Kenya Power, 2015 and KenGen, 2015).

The Kenya Electricity Generating Company Limited (KenGen) is the largest power producer in Kenya, with a market share of 73%. It has taken on the task of developing geothermal resources in Olkaria geothermal field (KenGen, 2015). An additional 280 MWe was commissioned between September 2014 and early 2015. KenGen is currently developing additional power plants with an installed capacity of 560 MWe. These will be constructed in two phases to be completed by the year 2030. The first phase runs from 2015 to 2019 where KenGen should install an additional 350 MWe of geothermal power to the national grid. The second phase runs from 2019 to 2030 with additional 210 MWe (KenGen, 2015).

To achieve these goals, KenGen has pledged to increase its human resource capacity and expand its knowledge base. This study program is one of the initiatives under the capacity development that is focused on structural geology of the less explored Olkaria Domes field and East of Domes field. This report presents results from the structural geology and surface mapping of geothermal manifestations in Olkaria domes field. Desktop studies of the Central Kenyan rift are also briefly described.

1.1 Morphology of the Kenyan Rift System

The Kenyan rift is part of the East African Rift System (EARS) which was formed due to continental breakup of the Nubian and Somalia plate boundaries (Figure 1). The rift extends from Ethiopia to Mozambique with rifting of relatively high-degree of tectonic maturity in the North that decreases southwards. The Western branch passes through Uganda, Democratic Republic of Congo and Rwanda (*Bonini et al., 2005*) (Figure 1).

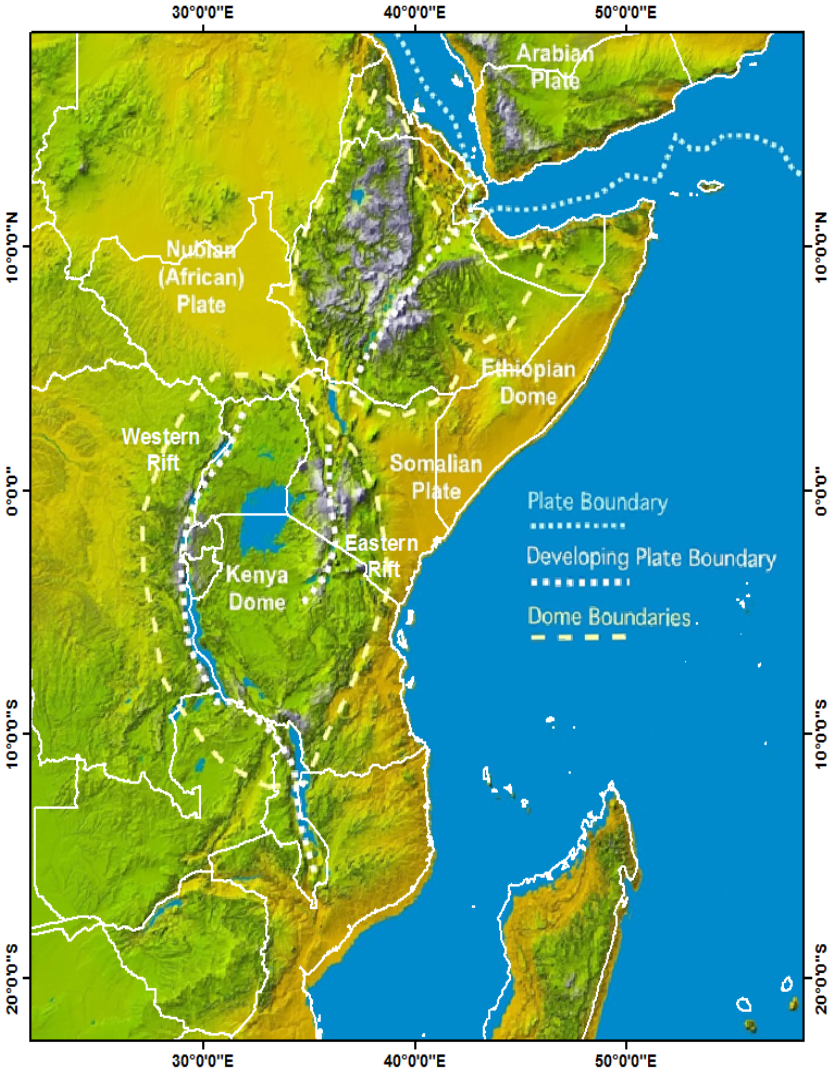

FIGURE 1: Digital Elevation Model of northeast Africa, showing the plate boundaries, and the dome-like regional structures associated with the EARS. The domes are interpreted to have been produced by upwelling mantle plumes. Also shown are the largest rift-related lakes in East Africa (Wood and Guth, 2015)

Suess (1891) came up with the concept of the East African rift fracture after a brief period of exploration. Gregory (1896) also named it the Great Rift Valley of East Africa and described it as a sunken graben system forming a basin that hosts the Red Sea and Dead Sea. Smith (1931), McCall (1957), McConnel (1959) and Harkin (1960) carried out geological mapping within selected parts of the rift and documented near vertical step faulting along the rift shoulders. Regional studies were later carried out by Mohr (1962), Harris (1969) and Wohlenberg (1969) who modelled the EARS as an active rift with the driving force being provided by convecting asthenospheric mantle, based on the fact that the regional volcanism preceded the major rift faulting events. The theory of upwelling magma plumes, namely, Afar and Kenyan plumes as the main sources of tectonic and volcanism was then born and has been continuously used to explain the constant pressure source Baker (1970), Mohr (1970), Baker *et al.,* (1971) and McKenzie *et al.,* (1972) (Figure 1). The Kenyan plume also resulted in up-doming effect forming three rift arms at the Nyanzian triple junction. The north and southern arms continued spreading while the third arm (Nyanzian rift) died out (Figure 2).

When the Ethiopian segment of the rift approaches Kenya, at the latitude 5° N, it bifurcates into the Eastern and Western branches as it bends around the Tanzania craton, following the Late Proterozoic sutures on either side of the craton (Smith and Mosley, 1993) (Figure 1). The Eastern branch of the rift is known as the Kenya rift and is older and has more active volcanicity than the Western branch, that contains the Albert–Tanganyika-Malawi rifts (Smith and Mosley, 1993). The Eastern Rift has also been subjected to more vigorous geothermal exploration, although the success rate has been highly variable Mungania (1999), Muchemi (2000), Simiyu (2010).

The Kenyan rift began its development during the late Oligocene at approximately 30 Ma. Magma resurgence created weak points in the crust which later transformed to major volcanic landforms (Baker *et al.*, 1971; Muchemi, 1992). The relatively shallow level of the lithosphere-asthenosphere boundary and Moho beneath the EARS is responsible for the high heat flow and geothermal gradient (200°C/km) within the rift (Wheildon *et al.,* 1994 and Simiyu and Keller, 1997). Quaternary volcanic activity was focused along the central axis of the rift and crustal thinning may have been responsible for formation of the key volcanic centres, including Eburru, Olkaria, Longonot and Suswa (Mohr, 1970; Mungania, 1999; Chorowicz, 2005). Explosive extrusions also created caldera volcanoes (Simiyu, 2010; Wood and Guth, 2015). Development of shallow magma chambers of intermediate to silicic composition formed the most important geothermal prospects (Figure 2). The volcanoes include Suswa, Longonot, Olkaria, Eburru, Menengai, Korosi, Paka, Silali, Emuruangogolak and Barrier (Clarke *et al.*, 1990; Muchemi, 2000; Omenda, 2014) (Figure 2). The Greater Olkaria geothermal complex is one of the resultant volcanic edifice showing highly evolved rock sequencing (Omenda *et al.*, 2014).

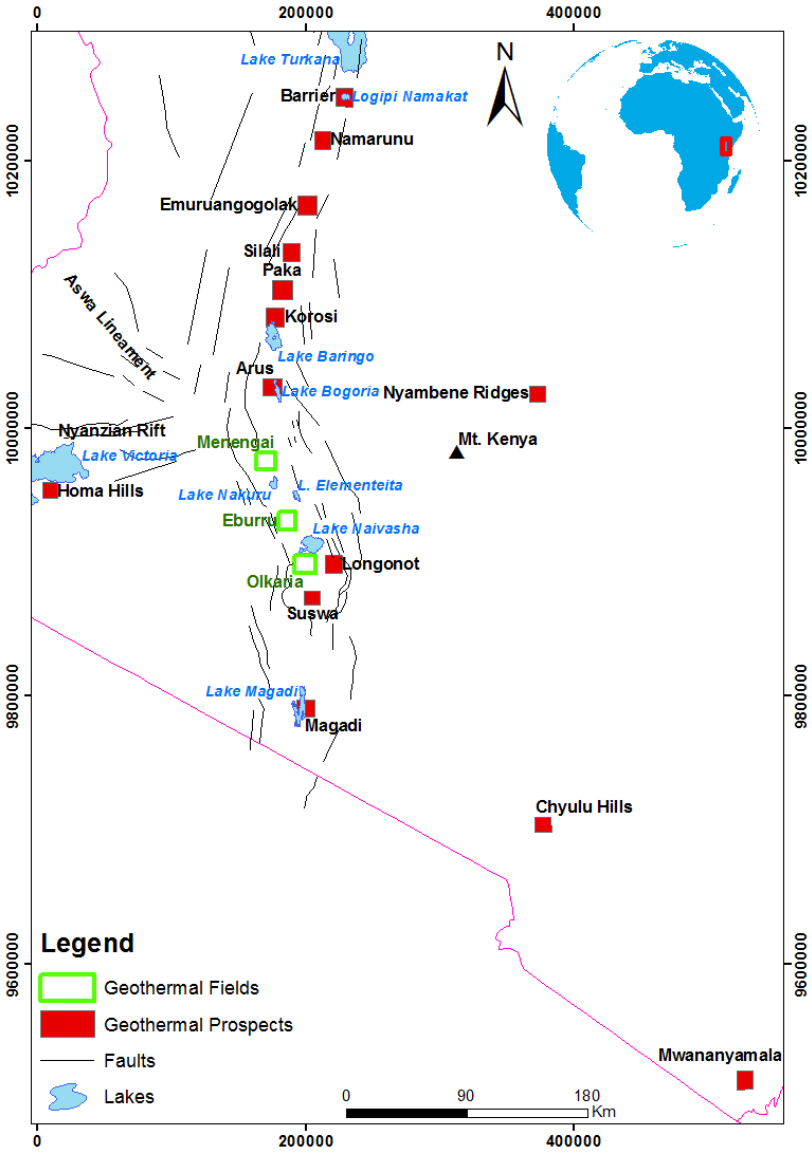

FIGURE 2: Simplified map of the Kenyan rift showing location of geothermal prospects and fields. The three arms of the Kenyan rift are shown at the Nyanzian tripple junction which caused segmentation of the rift. The North, Central and South rift segments are indicated by the dashed brown lines (modified from Clarke et al., 1990 and Simiyu 2010)

1.2 Geographical setting of the study area

The study area is approximately 1500 km^2 and runs from the southern tip of Lake Naivasha to Ndeiya area (Figure 3). The area is characterized by regional faulting with arcuate fault scarps that define a cauldron circular structure that measures approximately 50 by 30 km in diameter. The bounding fault scarps are up to 800 m high, implying a down faulting of similar magnitude. Olkaria, Longonot and Kijabe volcanoes are placed along the periphery of the circular structure (as if they form nested calderas), while Suswa volcano lies in its centre (Figure 3). The floor of the circular structure is relatively flat due to infill of lacustrine sediments formed by catastrophic floods from Lake Naivasha, which occurred at about 10-30 Ka Bp. Mt. Margaret is a trachytic volcanic cone located northeast of Suswa

volcano and has also been demarcated as a potential geothermal site (Clarke *et al.,* 1990). The eastern rift scarp hosts numerous geothermal manifestations around Kijabe area (Figure 3), which were studied during field work.

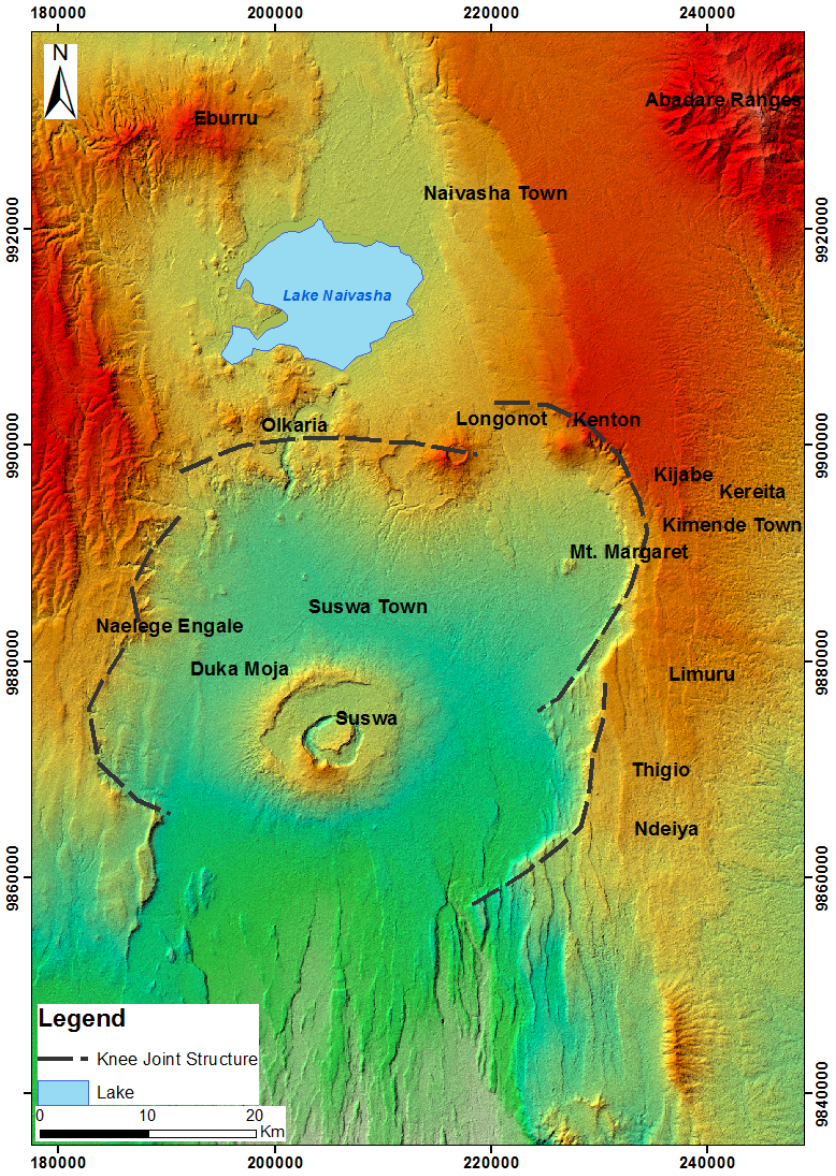

FIGURE 3: Figure showing the Central Kenyan rift with location of Olkaria, Longonot and Suswa volcanoes. Local place names are also shown

Thompson (1964) carried out geological studies in the study area and described the eastern scarp as complex systems of down faulted blocks that are variably tilted. Subsequent pyroclast-producing eruptions have modified and dampened the topographic relief, although the tectonic fabric is still evident. Kinangop tuffs are the dominant pyroclastic formation along the eastern margins, forming about 10 m thick strata extending throughout the central region towards Suswa volcano (Baker *et al.,* 1971). The Kinangop tuffs are quarried and sold as building stones to the local population. Trachytes mainly occur as extrusions at Longonot, Suswa and Mt. Margaret areas (Guth and Wood, 2013). En Echelon faulting is evident on the south of Suswa and the faults run sub-parallel to each other with a north-south orientation (Baker *et al.,* 1971). Numerous scoria cones occupy the basin forming topographic highs some of which are not discernible from the Digital Elevation Model (DEM).

Ignimbrite deposits are widespread in Suswa and Longonot region and especially in association with Kedong Valley tephra formation, which signifies a period of violent explosive eruption in an association with caldera formation. Basaltic dykes and lava flows have been identified along the eastern margin. Kijabe area hosts numerous basaltic dykes while Kijabe hill is a basaltic cone (Clarke *et al.,* 1990). The western arc of the circular structure exposes the approximately 0.6 Ma Mau Ashes formation, which is comenditic and blankets the western part of the structure (Guth and Wood, 2013). Steeply inclined shoulder faults forming co-linear ridges typify this region.

Olkaria Geothermal Field (OGF) sits within the Central Kenyan Rift and is one of the late Quaternary central volcanoes with proven geothermal potential (Mwangi, 1986; Clarke *et al.,* 1990; Muchemi, 1992; Ofwona, 2002; Lagat, 2004; Omenda *et al.*, 2014; Musonye, 2015). Olkaria geothermal field is located in Nakuru County, about 120 km North West of capital Nairobi (Figure 3). The surface geology is dominated by comenditic rhyolites which are present as scattered lava flow fields throughout the OGF

(Lagat, 2004). Volcanic ashes, pumaceous deposits, and trachytes are also present along with rare lacustrine sediments in the vicinity of Lake Naivasha. In the subsurface, the rocks consist of basalts, trachytes, rhyolites lavas and tuffs of ages ranging from Pliocene to Holocene.

The Olkaria geothermal license area is situated immediately south of Lake Naivasha. It´s divided into seven subfields for ease of geothermal development (Figure 4). These include; Olkaria Central, Olkaria East, Olkaria Northeast, Olkaria Northwest, Olkaria Southeast, Olkaria Domes field and Olkaria Southwest. Olkaria Domes field is located to the southeast of Olkaria hill and lies on the periphery of the fields licensed to KenGen (Figure 4). The field is bounded by the Ol Njorowa Gorge to the west, Olkaria ring structure to the east and the Gorge Farm fault to the North. Longonot caldera is located to the east of Domes field (Figure 4). It is also bounded by Northings 969380 to 99035 m and Eastings 201500 to 208500 m. This report largely focuses on the Olkaria Domes field and the area between Domes and Longonot caldera. The field work was carried out from September to December 2015.

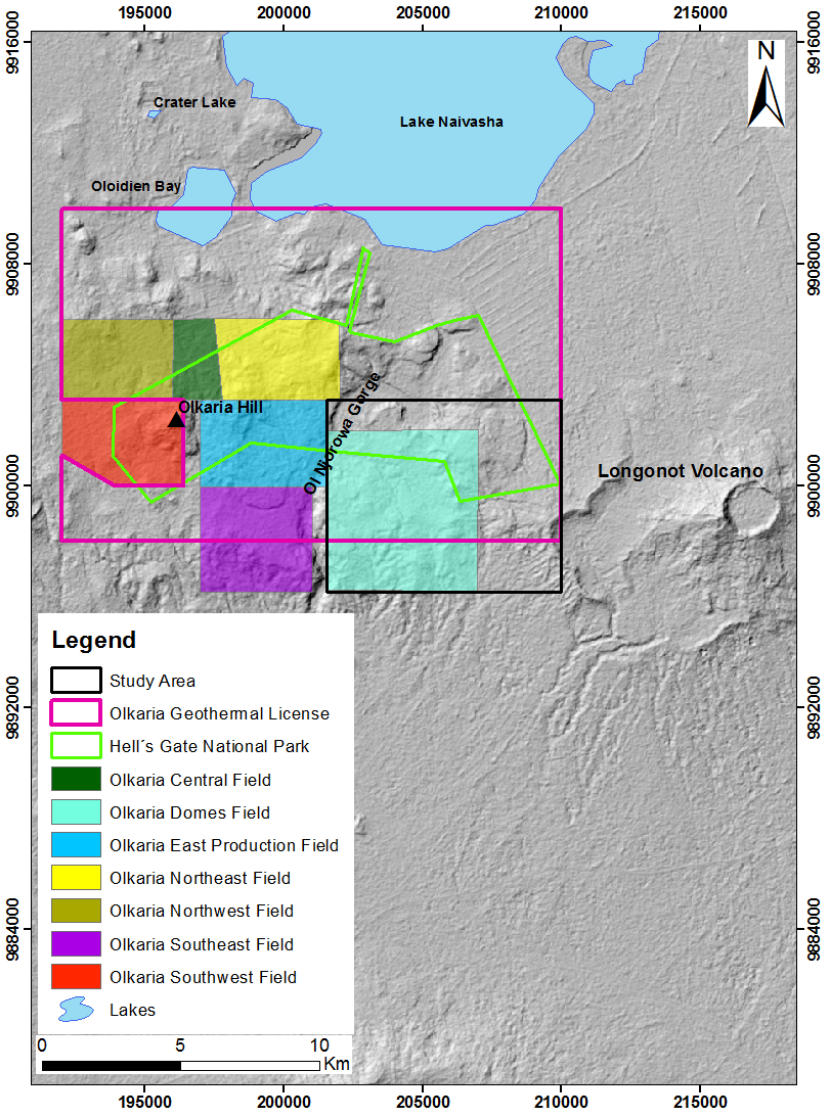

FIGURE 4: Map showing relative location of Olkaria geothermal sectors and the study area in Olkaria Geothermal field. Longonot caldera borders Olkaria Geothermal field to the East

1.3 History of geothermal development at Olkaria geothermal field

Geothermal exploration began in the 1950's with much emphasis being laid on Olkaria East, Central and West fields. Two exploration wells were drilled in Olkaria in 1956 which proved existence of a geothermal reservoir. Exploration work began in 1960 and was extended significantly by work carried out by Furgerson (1972), Sweco-Virkir (1976), VIRKIR Consulting Group (1980), Browne (1984), Odongo (1984), Mwangi (1986), Onacha (1989), Dimitrios (1989), Simiyu *et al.,* (1995), Onacha (1999), Lichoro (2009) and Wanjohi (2014). Most of the research was carried out between Lake Bogoria and Olkaria where several low resistivity zones were identified. However, results indicated Olkaria geothermal field to be the most promising of all detected anomalies (Muchemi, 1998).

Geological mapping of surface geothermal manifestations and other geological features was carried out in Olkaria geothermal field. Naylor (1972) identified the Olkaria ring structure marked by arcuate rhyolitic domes running from the east to the south eastern part of the volcanic complex and have been

used to invoke the presence of a buried caldera. Geothermal surface manifestations were mapped by Baker *et al.,* (1971). Intense fumarolic activities mostly follow linear trends which were presumed to indicate permeable fault zones. Temperature measurements collected showed boiling conditions in fumaroles in Olkaria East and Central fields.

This exploration culminated in drilling of production wells in most of the geothermal segments. The first geothermal power plant (Olkaria I) was set up in June 1981 with a capacity of 15 MWe (Ouma, 2009). The second was commissioned in November 1982 and the third in March 1985 totalling the capacity to 45 MWe. Browne (1984) and Odongo (1984) analysed cores and cuttings from initial wells and established that the litho-stratigraphic succession of the area featured at least 2600 m of sub-aerial rhyolitic, trachytic and basaltic lava and associated pyroclastic rocks.

After proving the geothermal potential in Olkaria, the Government of Kenya through the Ministry of Energy (MOE) contracted the British Geological Survey (BGS), to undertake more exploration in the region (Clarke *et al.*, 1990). BGS carried out extensive regional exploration of geothermal energy in the Kenyan rift. This included geological mapping of Longonot Volcano, Greater Olkaria Volcanic Complex (GOVC) and the adjacent areas. Their findings identified several potential areas for harnessing geothermal energy. Among them was the Domes field, which was to be considered for further exploration. Mt. Margaret was also delineated as a potential geothermal prospect (Clarke *et al.,* 1990).

Exploration drilling in Olkaria Domes field began at the turn of the 20th Century when three exploration wells were drilled i.e. OW-901, OW-902 and OW-903. Lagat (2004) carried out detailed lithological and alteration mineralogy analysis and found alteration zoning to depict high temperature geothermal reservoir conditions. Further geological work in Domes field was carried out by Omenda (1998) and geophysical analysis was done by Lichoro (2009). They identified structural controls and potential upflow zones controlling geothermal fluid movement at the central part of Domes field which formed drilling targets. Several appraisal wells were later drilled in the upflow zones and were quite productive.

The exploration company West-JEC (2009) carried out optimisation studies and advised on the best drilling practises for both production and re-injection wells for Olkaria geothermal field. Domes field was considered a prime area for production drilling and recommendations for intensive drilling issued. A geothermal well drilling contract was signed between KenGen and Great Wall Drilling Company (GWDC) of China and saw accelerated drilling of 80 wells in Domes field and subsequent steam production that culminated in the construction of Olkaria IV power plant in 2014. MANNVIT/ÍSOR/Vatnaskil/Verkís Consortium (2011) have been carrying out field monitoring exploration and optimisation studies. They identified four major heat sources in Olkaria geothermal field based on geophysical and reservoir data. The research has updated the conceptual model and recommended several measures to ensure sustainable steam production.

By December, 2015, KenGen had drilled 281 wells in Olkaria Geothermal field with an estimated geothermal output of more than 600 MWe (KenGen, 2015) (Figure 5). Domes field with more than 70 wells, has an estimated total production capacity of more than 350 MWe. Most of the geothermal fields have also been explored and their potential proven. Olkaria Domes is one of the most recently drilled fields where work is still ongoing. A single flash geothermal power plant known as Olkaria IV was commissioned in November 2014. It has a peak production of 140 MWe from its two turbines. A second power plant, Olkaria I Additional Unit (AU) with a capacity of 140 MWe was also constructed in the East field to cater for excess steam produced (Figure 5).

The area East of Domes only has a single well, OW-922, which was drilled in August 2014 (Figure 5). The South East field has not been fully explored although several wells have been drilled, showing different degrees of success. More research will be carried out in future to prove its productive potential. Olkaria Central and North West fields were explored and show significant geothermal potential.

1.4 Aim and scope of the research project

The current structural map of Olkaria Domes (Figure 7) puts strong emphasis on the Olkaria Ring Structure and the Ol Njorowa Gorge as being the prominent structures for subsurface movement of geothermal fluids (Karingithi 1999; Ouma 2009; Wamalwa 2014). However, it is likely that other, yet to be discovered, structures may act as strong water passage zones and hence would be potential drill targets. For example, the area east of the Ring Structure has not yet been explored comprehensively compared to areas west of Ol Njorowa Gorge and the stand-alone exploration well OW-922, drilled in 2014, unfortunately did not reveal as much information as was expected.

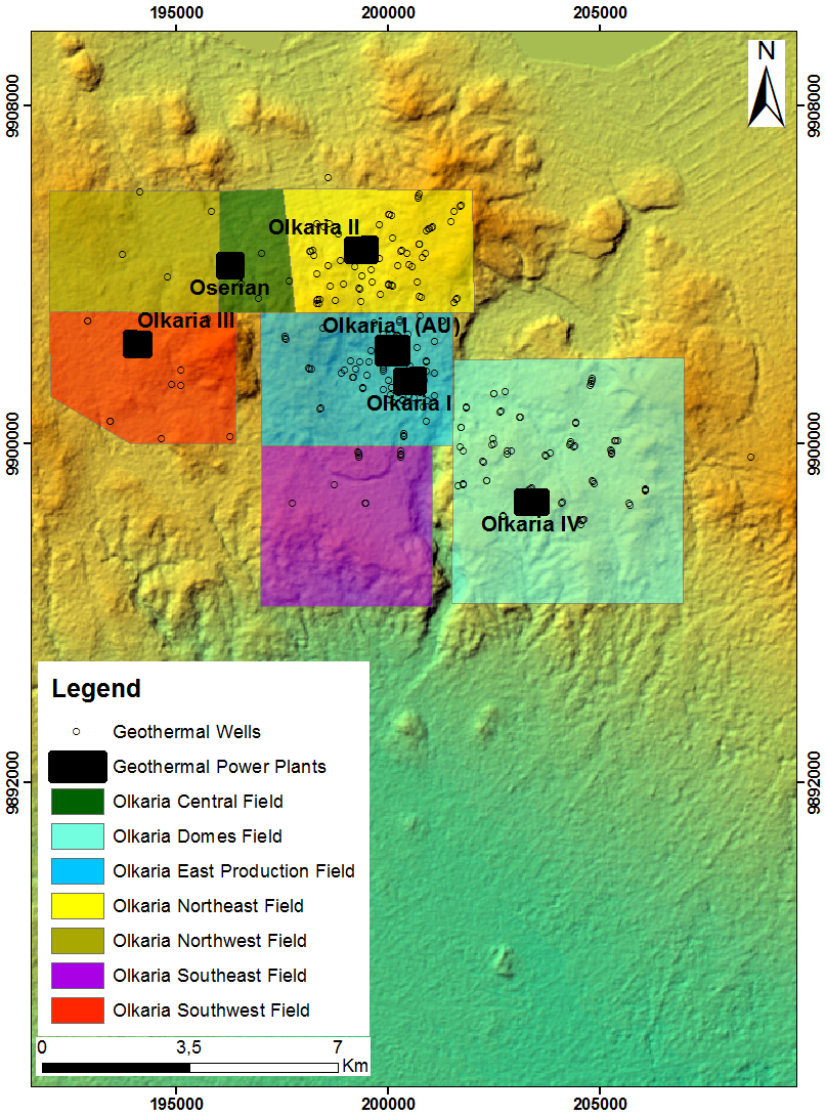

FIGURE 5: Resource map showing numerous wells drilled in different geothermal sectors of Olkaria Geothermal License by December, 2015. Olkaria I (AU) and Olkaria IV Geothermal power stations are the newly commissioned plants

The aim of this study is to improve our understanding of the geology and geothermal prospects of Olkaria Domes area through geological mapping and soil gas geochemical survey. This project is carried out in partial fulfilment of a Master's Degree in geology at the University of Iceland. To achieve the full expectations of this project, the following key objectives are identified:

- To identify the major structural patterns controlling fluid movement in the Olkaria Domes geothermal field.
- To establish the localities, strikes and dips of geological structures in the Olkaria Domes geothermal field.
- To map all geothermal surface manifestations and relate their occurrence to the fault systems.
- To collect soil gas geochemistry data that will assist in determining the structural controls in the study area.

To achieve these objectives within the given scope, the work was divided into several tasks each with specific deadlines (Table 2). A preview of existing geothermal data was also done and knowledge gaps established. These gaps would be addressed in the report during compilation.

The implementation of the project aims was focused on mapping geological structures within central Kenyan rift and Olkaria Domes field, which in part have surface manifestation via geothermal activity.

Remote sensing and GIS were used in preparatory desktop studies. The structural mapping in the field was carried out from August to November 2015 and was largely focused on the Domes field. Field work also involving geochemical soil gas surveys was carried out in Domes field, where geothermal surface manifestations and bed rock exposures are poor due to thick pyroclastic overburden. The gas surveys were carried out to determine surface permeability of the Domes Field. Laboratory-based analysis and synthesis of field data and samples was subsequently carried out in the period December 2015 to May 2016. The results of this work are presented in this report.

TABLE 2: Work breakdown structure

Time frame 2015 / **Activity**	**February**	**March**	**April**	**May**	**June**	**July**	**August**	**September to November**
Planning								
Desktop studies								
Reconnaissance								
Field mapping and geochemical survey								

2. GEOLOGY AND STRUCTURAL PROVENANCE OF THE GREATER OLKARIA VOLCANIC COMPLEX

The Greater Olkaria Volcanic Complex (GOVC) was formed about 22-20 Ka Bp. It occurs along the East African rift which was formed due to tectonism involving lithospheric spreading, fracturing and eventually faulting (Bonini *et al.*, 2005; Biggs *et al.,* 2009; Corti *et al.*, 2007; Corti, 2012). The continental spreading was initiated by the collision between the Archean Tanzania craton and Proterozoic orogenic belts. Volcanic uplift resulted from upwelling of two upper mantle plumes in Afar and Kenya with dimensions of thousands of kilometres (MacDonald *et al.*, 2008; Smith and Mosley, 1993). Both plumes are characterised by extrusion of flood basalts whose isotopic analysis indicate a deep mantle origin for the Afar plume and a shallow origin for the Kenyan plume (Baker *et al.*, 1971). It has been suggested that the upper mantle immediately beneath the rift may contain reservoirs of magma generated at greater depth (Marshall *et al.,* 2009). Crustal thicknesses along the rift axis decrease from 35 km in the Naivasha-Nakuru area to 20 km in the north near Lake Turkana (KRISP, 1991).

GOVC hosts numerous volcanic centres of Quaternary age, most of which contain comenditic lavas (Baker and Wohlenberg, 1971 and Lagat, 2004). The volcanic edifice hosts an inferred caldera rim which is not very conspicuous. It is characterised by numerous domes and craters which are rhyolitic in composition with their relative positions forming a loci to the east, south and southwestern parts (Omenda, 1998). These domes have been interpreted to be remnants of the buried caldera and have been obscured by recent pyroclastic ash falls from neighbouring Longonot volcano (Naylor, 1972 and Omenda, 2000).

Omenda (1998) carried out extensive petrological research to identify the lithological succession in the GOVC and identified six lithological sequences based on deep drilling rock sampling, namely;

(1) The upper Olkaria volcanics (comenditic lavas and pyroclastics, basalts and trachytic intercalations, volcanic ashes from Longonot and Suswa). Most of these rocks have surface exposures and their relative lithology is summarised based on carbon dating (Figure 6),

(2) Olkaria basalts occurring from 500 to approximately 1000 m below ground level (b.g.l.). This rock suit is dominated by basaltic flows with

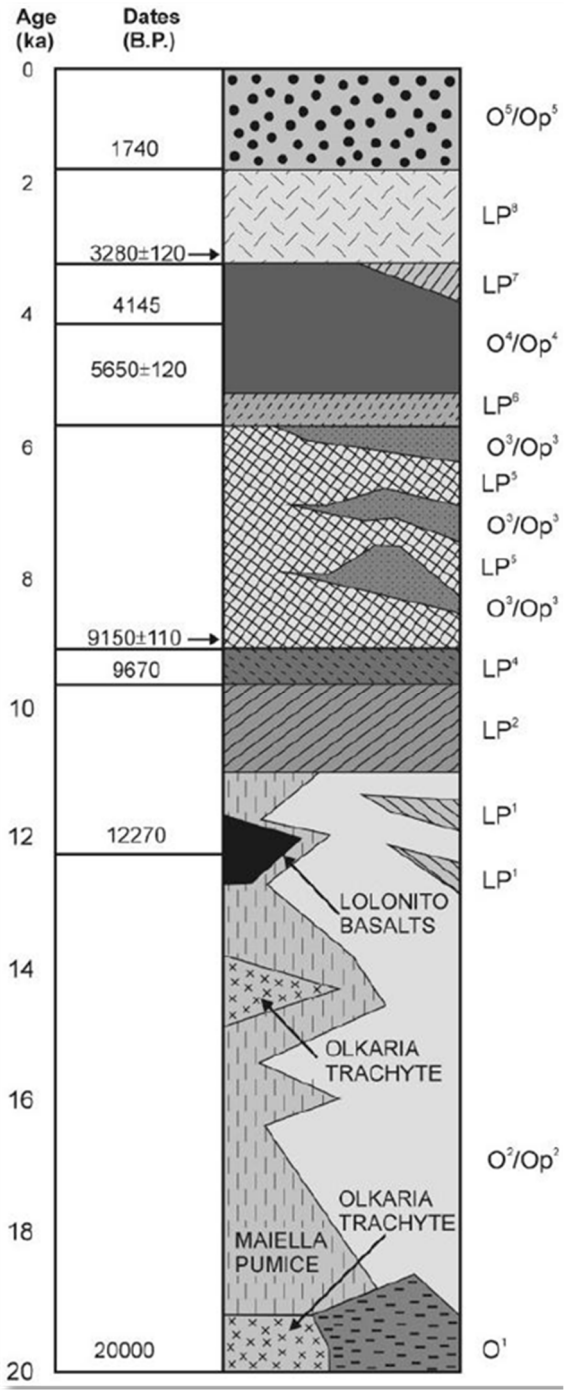

FIGURE 6: Summarised representation of the upper Olkaria volcanic sequences showing the stratigraphic column of the GOGA. Units O1 to O5/Op5 and the Olkaria trachyte are from the Olkaria complex; LP1 to LP8 units are Longonot pumice falls. The arrowed 14C dates come from palaeosols immediately beneath the LP5 and LP8 units (Marshall et al., 2009)

trachytes and minor pyroclastics and hosts the geothermal cap rock in Olkaria geothermal field (Ambusso and Ouma, 1991).

(3) The plateau trachytes are the third succession occurring from 1000 m to approximately 2600 m b.g.l. This series is dominated by trachytes and minor encounters of basalts, tuffs and rhyolites. Thickness varies throughout the field but they are deepest in the East field where they form the geothermal reservoir (Omenda, 1998). These rocks are believed to be related to fissure eruptions along the rift,

(4) Mau tuffs occur in this zone and are mostly widespread in the Olkaria west field beyond the Olkaria caldera (MacDonald *et al.,* 2008). They are believed to be the oldest exposed rock units in Olkaria. The tuffs have been well consolidated by the rock overburden and have an ignimbritic texture,

(5 & 6) The other two units may be very deep beneath hence not encountered during drilling. They are however encountered along the southern flanks of the Kenyan rift and are mostly composed of trachytes (Musonye, 2015).

The upper Olkaria volcanics exposed in surface outcrops were mapped and dated by Baker *et al.,* (1971), Clarke *et al.,* (1990) and Marshall *et al.,* (2009) using the ^{14}C method and showed that the volcanic suit must have been formed during different time periods and stages which have been summarised below (Figure 6);

Stage 1; The extrusion of Olkaria trachytes and Maiella pumice during the initial pre-caldera formation (20-12±120 Ka) (Baker *et al.,* 1971; Marshall *et al.,* 2009).

Stage 2; Olkaria caldera collapse forming a depression of 11 km x 7.5 km across (Clarke *et al..,* 1990). The collapsed caldera initiated plinian like eruptions of welded pyroclastics of the Ol Njorowa Pantellerite Formation (O^1), the Lower Comendite Formation (O^2) signifies further eruption that occurred during the post-caldera activity linked to the eruption of peralkaline rhyolitic lavas and pyroclastic rocks (Op^2) (MacDonald *et al.,* 2008; Clarke *et al.,* 1990).

Stage 3; The Lower Comendite Member of the Olkaria Comendite Formation (O^2/Op^2) were extruded after the caldera collapse. Rhyolite lavas and pyroclastics, dated at >9150±110 BP by the ^{14}C method dominate this stage (MacDonald *et al.,* 2008).

Stage 4; Further extrusion of the Middle Comendite Member (O^3/Op^3) mainly composed of rhyolites formed ring domes. Thick pyroclastic deposits were also produced between >9150±110 and >3280±120 BP (MacDonald *et al.,* 2008).

Stage 5; The collapse of the caldera floor and the formation of thick lava flows that resulted in the Upper Comendite Member (O^4/Op^4) was experienced in the fifth stage (5650 – 3280 ± 120) (MacDonald *et al.,* 2008).

Stage 6; Stage six signified the last flows of very thick comendite lava from a north–south fissure system. The youngest lava flow, Ololbutot Comendite (O^5/Op^5) was date 180±50 BP (MacDonald *et al.,* 2008; Marshall *et al.,* 2009; Clarke *et al.,* 1990) (Figure 6).

2.1 Structural geology

Geothermal fluid flow along the Kenyan rift system is greatly influenced by the system of normal faulting, En echelon rift shoulder faulting and the rift floor basin. The faults may facilitate geothermal fluid flow by providing channels of high permeability or they may create barriers to flow by offsetting areas of high permeability (Muchemi, 2000 and Chorowicz, 2005). The domal uplift caused by the Kenyan dome also created high hydraulic gradient from recharge areas to the rift floor where most of the geothermal fields are located. The formation of water catchment areas in Aberdare Ranges and Mau escarpments has ensured a constant fluid supply to the geothermal areas. GOVC is characterised by a series of structural controls which depict different tectonic successions (Figure 7). The most dominant faults include; N-S, NW-SE, NE-SW, ENE-WSW and a loci of rhyolitic domes which are distinctly visible in satellite images (Muchemi, 2000; Omenda, 1998).

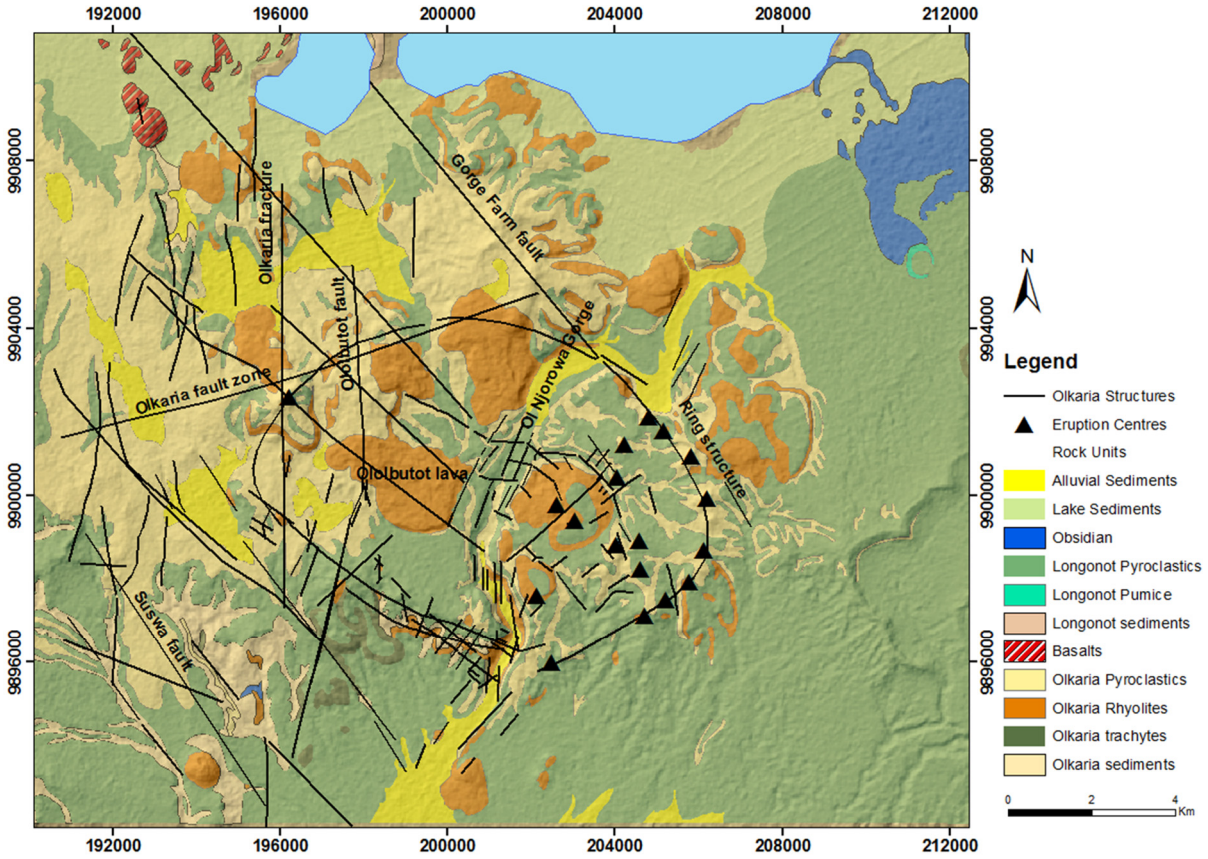

FIGURE 7: Map showing the surface geology and the structures in the Greater Olkaria geothermal area (modified from Clarke et al., 1990)

The young N-S oriented faults represent the most recent tectonic activity on the rift floor. Although most of the faults are buried by recent lava flows, their outlines are signalled by fracturing of the lavas in a E-W direction due to minimum stress action (Muchemi 1998). Fumerolic activities are also magnified along their profiles. The Ololbutot fracture zone (Figure 7) is one of the best examples with fumaroles enriched with high sulphur depositions and temperatures indicative of boiling conditions. According to MANNVIT/ÍSOR/Vatnaskil/Verkís Consortium (2011), the Ololbutot fault presents an outflow channel that separates the eastern and the western parts of the geothermal system. Isotope studies from Olkaria fluids show two types of flows; 50% or more of the fluids originate from deep Rift Valley water oriented N-S, while shallower cold fluids flow from the western flanks of the escarpment (Wambugu, 1995 and 1996; Karingithi, 1999).

The Olkaria fault zone signifies another set of faulting that runs ENE-WSW from north of Olkaria hill but is buried by the Quaternary volcanics. The surface manifestations along this old rejuvenated fault are very distinct and seem to cover a width of about 50-100 m where intense sulphur encrustation and silicification is present. Its estimated surface displacement is about 5 m with a downthrow to the north (Omenda, 1998). Suswa fault has a NE-SW orientation and occurs on the SW part of the Olkaria geothermal license. It cuts through the Pleistocene Plateau Trachytes and is visible at its intersection with the NNW regional rift faults and on the area SE of Suswa volcano (Omenda, 1994).

The ring structure which marks the outer caldera rim of Olkaria is also an important structure in Olkaria. It is outlined by arcuate alignment of rhyolitic domes which may have been formed by resurgence of magma due to overpressurised magma chamber after piston collapse (Naylor, 1972; Clarke *et al.,* 1990; Mungania, 1999). Temperature measurements from fumaroles and altered grounds indicate high temperature zones to the western segment, along the Ol Njorowa Gorge and to the South West of Olkaria. The distribution of surface geothermal manifestations trending in the same direction as the main fault systems suggests that the geothermal system is structurally controlled, as a result indicating permeability and a possible connection to a heat source (Otieno *et al.*, 2014).

2.2 Tectonic activity

The East African rift is a mobile volcanic belt under constant motion. The movement causes deformation of the lithosphere resulting in propagation of fractures and faults, reactivation of buried inactive faults and in some cases, arrest or closure of previously active geological structures. The deviatoric stress causes strain and deformation along crustal discontinuities and this has direct effect on groundwater movement (Dzurisin, 2007). This effect may have partial influences in Lake Naivasha water levels and may be contributing to observed fluctuations (Awange *et al.,* 2013).

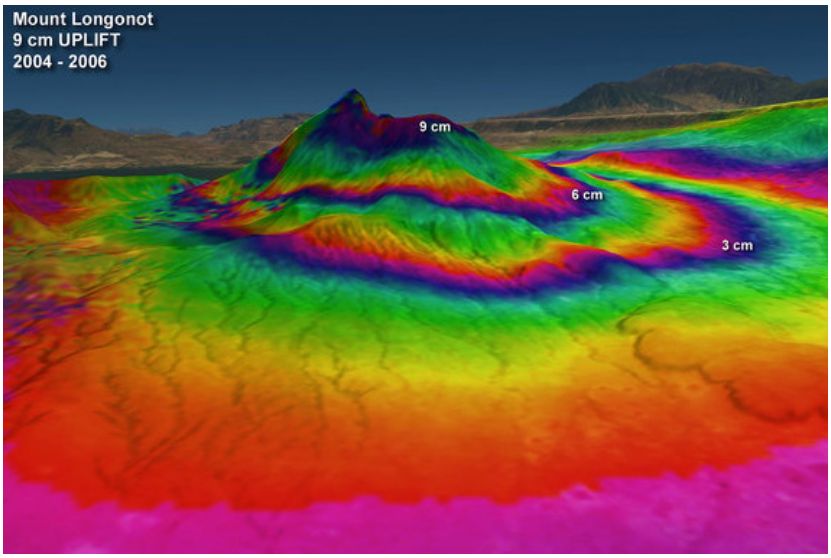

FIGURE 8: InSAR data from Mt. Longonot show vertical movement of up to 9 cm between 2004 to 2006. This is attributed to magma convection in the magma chamber (ESA, 2010)

Using Advanced Synthetic Aperture Radar (ASAR) obtained from the European Space Agency's Envisat (Environmental Satellite), it has been possible to monitor slight changes in elevation along different active volcanic centres in the rift. These measurements have shown an average movement of up to 9 cm in Mt. Longonot (Figure 8). The shear and tensile stress produced by the magma chamber convective currents in these volcanic centres is immense and leads to crustal strain and deformation. The interferograms appear as rainbow-coloured interference patterns denoting magnitudes in deformation (Figure 8). A complete set of coloured bands, called 'fringes', represents ground movement relative to the spacecraft of half a wavelength, which is 2.8 cm in the case of Envisat's ASAR (ESA, 2010).

This Envisat Advanced Synthetic Aperture Radar interferogram over the Kenyan rift shows small surface displacements of Longonot volcano (Figure 8). In the background is Suswa volcano, which was not deforming at the time these measurements were being collected. Using Interferometric Synthetic Aperture Radar (InSAR), a group of scientists discovered that from 1997–2000 the volcanoes at Suswa, Menengai and Paka subsided with a range 2–5 cm (Figure 9). The volcanic uplifts due to convective movement of magma beneath shows evidence of constant faulting and fracturing along the rift (Biggs *et al.,* 2009). This phenomenon may explain the causes of young faults discovered during field work.

2.3 Hydrogeology

Groundwater flux ensures steady steam supply to maintain geothermal production in any geothermal field. It is therefore very important to understand mechanisms enabling movement of groundwater from the recharge zone to and out of the reservoir system. Geothermal fluids originate from groundwater which moves through complex geological structural channels to reach the hot reservoir rocks (Awange *et al., 2013*). However, the modes and mechanisms of flow of both steam and groundwater are different due to their changes in physical state and pressure (Todd and Larry, 2005).

Groundwater flow is dependent on hydraulic gradient and intrinsic permeability of the transmitting medium, assuming uniform viscosity. Groundwater moves through rocks which contain different transmissivity and porosity values that directly affect their water retention and transmission capacities

respectively. Many faults and fractures have been buried by either clastic sedimentary material or have been filled up during subsequent eruptions, reducing their transmissivities. The burying material always reduces the hydraulic conductivity causing ground water to move very slowly as compared to surface water. Aquifereous strata may be offset by fault systems making them barriers or channels of groundwater flow (Heath, 1983).

The Aberdare Ranges located to the east of Central Kenya rift form the main recharge channels to the floor of the rift. Additional groundwater is received from the Mau catchment region to the west of the rift. Water movement is mainly through underground channels formed by enhanced permeability of the regional faults. The main source of fluids in Olkaria geothermal system is therefore considered to be meteoric in origin (Karingithi, 1999).

Movement of groundwater along the rift basin varies considerably since the lake waters range from fresh to highly alkaline in their chemistry. Two main flow regimes affecting the Naivasha basin were identified, namely (1) the fresh underground discharge flow of Lake Naivasha surrounded by the cold and shallow groundwater table; and (2) the deep, highly alkaline brines of geothermal origin emanating from deep geothermal reservoirs. Further piezometric and isotopic studies show that deep groundwater flux occurs both axially along the rift and laterally from the bordering highlands into the rift. The main outflow of the shallow groundwater is to the south towards Suswa where these shallow aquifers form a significant conduit for the southerly flow (Darling *et al.,* 1995).

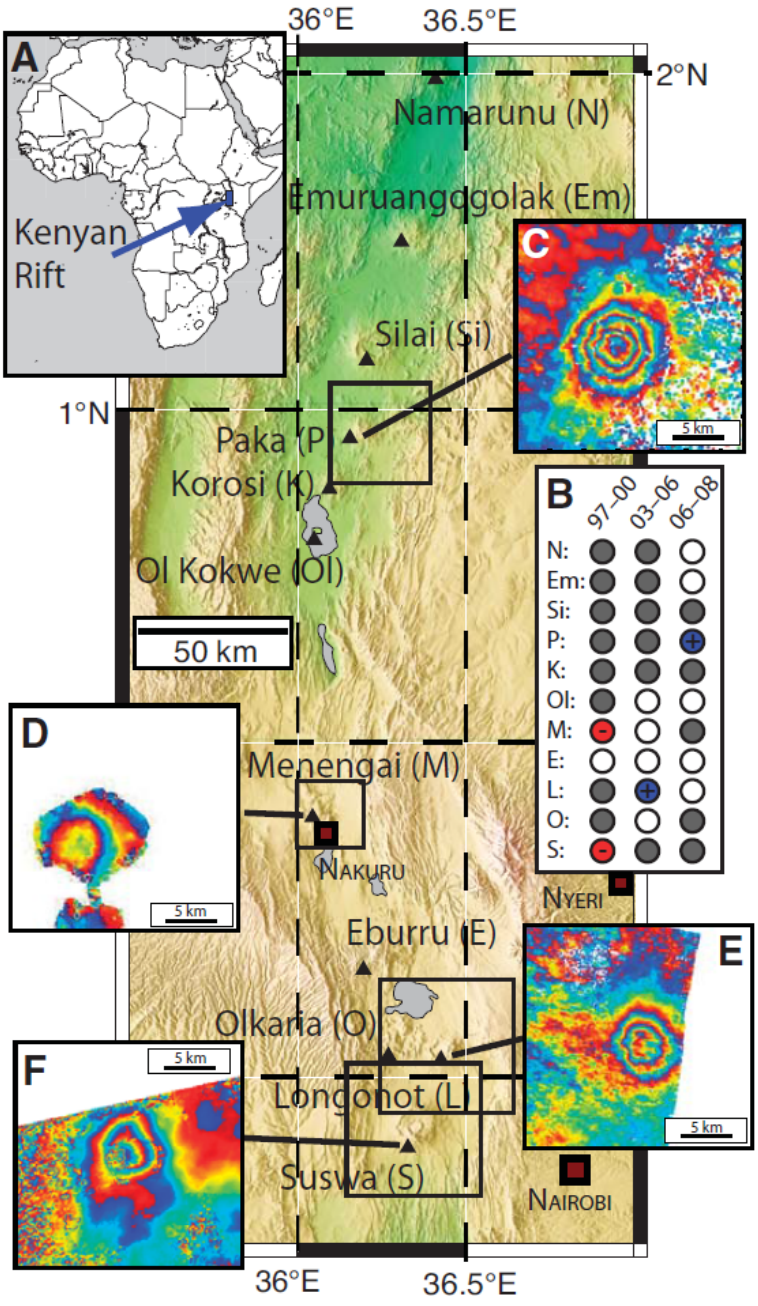

FIGURE 9: Geodetic activity detected at volcanic centres in the Kenyan rift. A: Location map. B: Chart summarizing the observations at each volcano during each of the three time periods initially surveyed (1997–2000, 2003–2006, 2006–2008). Red circles—subsidence; blue circles—uplift; grey circles—no displacement; empty circles—no observation due to data gaps or lack of coherence. C: Paka in 2006–2008 (stack of three interferograms). D: Menengai in 1997–2000. E: Longonot in 2003–2006 (stack of seven interferograms). F: Suswa in 1997–2000. Footprint of geodetic signature for all four volcanoes is the diameter of the trachytic shields, rather than the smaller caldera and postcaldera morphology. (Biggs et al., 2009)

3. METHODOLOGY

GIS and remote sensing were integrated in this study and aided in identifying the prospect areas through a combination of digital data analysis methods. This is due to their capacity to display various spatial data in one platform for easier correlation. Establishment of relationships between neighbouring features is key in geothermal mapping. Therefore, by using these tools, it was possible to overlay data from different exploration methods to create maps of desired features.

3.1 Desktop studies

The desktop studies were carried out as part of course work for the MSc degree in Geology at the University of Iceland beginning from September 2014. Courses in Remote Sensing and GIS were completed under the program with end of semester reports focusing on preliminary studies of Central Kenyan rift segment and Olkaria Domes field. The work involved downloading satellite images from different open source sites and basic image processing to extract meaningful data. It also entailed compilation of previous geological work done in the study area and determination of knowledge gaps that needed to be addressed. Older maps were georeferenced and geological and structural features digitised using ArcGIS. A geodatabase was created comprising of all feature classes and raster data obtained from previous maps.

3.2 Preliminary data analysis

The remote sensing tool involves use of spatial data obtained by space orbiting vessels that record radiation properties of different features on the Earth's surface without being in physical contact (Liu and Mason, 2009; Abrams *et al.,* 2015). The features are distinguished by their backscattering properties which vary depending on abilities to absorb, reflect or transmit radiation at different wavelengths of the electromagnetic spectrum (Lillesand and Kiefer, 2004).

Remote sensing and GIS were used to analyse and interpret some of the surface geology features with surface footprint with considerable lateral extent to be visible on the satellite images. Image analysis and enhancement was carried out using ArcGIS software. Mapping of the volcanic and tectonic landforms was carried out using open source satellite imagery, complemented by ground truthing during field mapping. Satellite images used in the report were downloaded from ASTER Global Digital Elevation Models (GDEM), Landsat, Sentinel Data hub and ASTER Volcanic Archives (AVA) were used to infer other surface features on the ground. One SPOT 5 high resolution image obtained from KenGen was used to analyse parts of the Ol Njorowa Gorge since it had limited lateral extent east of the gorge. The images used in preliminary studies were acquired from May, 1987 to April, 2015. The work was carried out between January to April, 2015 at the University of Iceland, Department of Earth Sciences laboratories. Based on the initial findings from these preliminary studies, field work was divided into two phases. One of the areas of interest was demarcated in the Central Kenyan rift, while the second part was focused in Domes field extending to the area east of the Olkaria ring structure to the outer caldera rim of Mt. Longonot.

3.3 Reconnaissance studies

Reconnaissance studies were divided into two phases in line with desktop studies. The first phase was concentrated on the Central Kenyan Rift and while the second phase was in Olkaria Domes field. Due to lack of enough time and fiscal resources, the former area was only studied during reconnaissance. During field visit in phase one, emphasis was laid on the Kijabe-Limuru area (Figure 3) due to numerous geothermal manifestations identified during preliminary investigations. Poor road networks and local communities' hostilities prevented exploration of the western part. Field work in Central rift was carried out during the month of August 2015. The main aim of the reconnaissance was to map the knee joint structure (Figure 3).

Olkaria Domes field and the area adjacent to the east were explored from September 2015. The area east of Olkaria Domes field was of particular interest due to lack of surface geological data which necessitated further exploration in this part of the license. Although one exploration well (OW-922) was drilled east of Domes field, there was little success during its discharge testing. This study aimed at determining the potential of the area. Reconnaissance studies begun on 15th September, 2015 and ran for a week. The main aim of the study was to get acquainted with the study area, plan for proper traverse routes, assessing the situation of the existing road networks as well as checking the potential hazards in the operation area. Since most parts of the Domes field is under the KenGen geothermal licensed area, approval was granted by the Geothermal Development Director. The Kenya Wildlife Services (KWS) were also consulted since part of the study area lies in the Hell's Gate National Park.

3.4 Field work

Detailed structural geology mapping in Olkaria Domes field begun from 21st September, 2015 and ran to 24th November 2015 where 213 stations were visited and recorded. Target features included; surface geothermal manifestations, rock outcrops, faults, fractures, eruption centres, fissures and dykes. To be able to plot these features on a map, it was crucial to record their geographical location using hand held GPS. Other auxiliary equipment such as geological hammers, camera, thermocouple thermometer, compass, clinometers, field note book, base maps and sample bags were used to assist in accurate data collection and recording.

To ensure satisfactory coverage of the study area, some of the traverses were designed in erosional gullies that were free of vegetation and showing good lithological exposures. Areas of interest suspected to host geothermal surface manifestation delineated during preliminary remote sensing studies were visited and verified during field work. In areas where access was impossible due to terrain challenges, binocular lenses were used to attempt closer view of any surface features present.

All features encountered in the field were studied in detail, with all information recorded in the field note book. Where necessary, samples were collected and taken to the lab for further tests. Most stations involved collection of data such as strike, dip, dip directions in cases of fractures, faults and folds; while in altered grounds, on site descriptions of rock type, colour, grain sizes, level of alteration as well as alteration minerals identified where possible. Samples were then collected, well labelled and further XRD analysis carried out in the laboratory for those samples suspected to be altered to clays (see Appendix I). Where rock outcrops were encountered, physical rock description was carried out and in-situ samples collected for further petrographic analysis. Hot grounds, hot springs and fumarole temperatures were measured using thermocouple thermometer and readings recorded in the field note book. Geographical coordinates of all stations studied and points of sampling were also marked and recorded using the hand held GPS (see maps in Appendix II). For purposes of conformity, the reference datum used in making all maps in this study was Arc 1960 UTM Zone 37S.

3.5 Data analysis and synthesis

Field data was processed to observe correlation and produce structural maps. Shape files of faults, fractures, dykes, volcanic centres, volcanic plugs, hot springs, caldera rims and dykes were created using the strike and dips obtained in the field. The features were either lines, polygons or points depending on their occurrences. Rose diagrams for all fractures, faults and dykes were projected using the Online Rose Diagram software (Yong Technology Inc., 2016).

Rock samples collected in the field were polished to thin sections that were analysed using a petrographic microscope. Clay samples were analysed using the XRD Shimadzu equipment. First they were crushed to fine powder and each rock sample powder was mounted on three different slides that were treated as either air dried, glycolated or heated. The samples were then illuminated by the X-Rays at a maximum incident angle of 35° to ensure detection of all wave reflections by the clays. The output curves were then loaded to a desktop computer with installed Shimadzu software. The data were then

converted from RAW files to Brucker format using PowDLL software. The new format was compatible with the Diffract Plus EVA software which was used to analyse the clay peaks. Each clay type exhibits its own characteristic peak values depending on its Van Der Waals bonding structure. These bonds which form flat interbedded layers are responsible for reflecting the X-Ray waves. The synthesised data is discussed in the next chapter and the clay graphs with the peaks are displayed in Appendix I.

3.6 Geochemical soil gas surveys

The soil gas surveys were carried out in this study to identify areas of anomalously high gas concentrations in the soil. The main objective of the soil gas survey in this study was to determine the existence of buried geological structures in areas with thick pyroclastic overburden. It is highly recommended in areas with poor surface geothermal manifestations like the area east of Olkaria Domes field. CO_2 and radon gas sampling were carried out along grid lines with a separation distance of 500 m and stations placed in each sampling point (Figure 10). Magmatic intrusions are known to release gases from craters, fumaroles or flanks by diffuse degassing of gaseous species such as carbon dioxide, radon and helium. The gases move through the easiest routes where rock strata have experienced fracturing and faulting. It is the distribution and concentration of such gases that information on permeability can be obtained. It is their high mobility that makes them the best pathfinders for hidden geothermal resources.

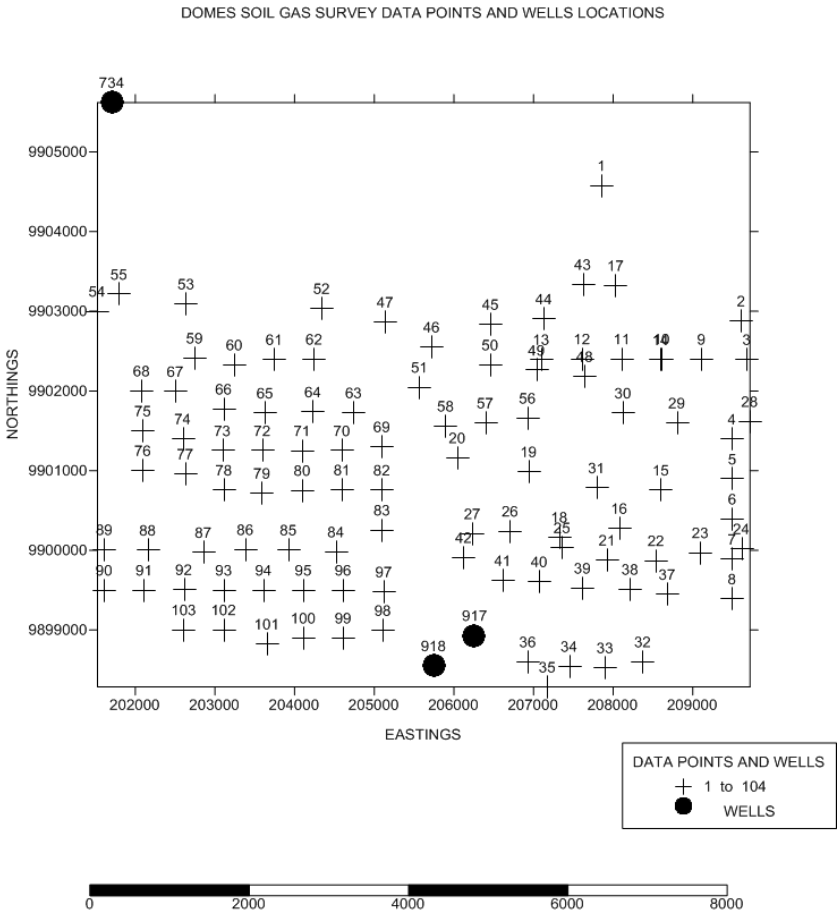

FIGURE 10: Map showing the distribution of geochemical sampling points and their respective station numbers where soil gas sampling was carried out. The wells are used as references for ease of navigating the map

3.6.1 Measurement of carbon dioxide (CO_2)

Soil gas CO_2 measurements were also carried out in this study using a Fischer Type Orsat apparatus (Figure 11). The soil gas was hand pumped from a depth of about 1m below ground surface via a hole made using a steel spike with jacket. Once the spike was removed, the outer jacket was left inside the hole to allow for sampling by fixing a stopper and a horse pipe onto the mouth of the jacket. The hand pump was used to drive the soil gas from the ground, to the absorbing pipettes of the Orsat apparatus. These vessels measured 100cm^3 of gas and contained 40% potassium hydroxide (KOH) solution that absorbed the acidic carbon dioxide gas. The corresponding changes in volume in the absorption vessels represented the amount of CO_2 gas as a percentage volume of the total gas. Therefore, by quantitative analysis, the volume of CO_2 dissolved was determined. This method assumed that no other gas apart from CO_2 was dissolved or lost during the measurement.

3.6.2 Radon gas measurements

The radon radioactivity levels were measured using a portable radon detector also known as the emanometer. The measurements were done using the spike as used for CO_2 sampling above where a stopper attached to a flexible tube was fixed to the mouth of the outer jacket and gas sniffed by a radon detector using an inbuilt meter pump. The soil gas sample hosting radon gas was pumped into a decay chamber of the emanometer consisting of a cylindrical copper can, whose walls were coated with zinc sulphide where the radon decays into other radio-nuclides by emitting alpha particles. The readings were recorded in real time as counts per minutes (cpm). Three background readings were taken at three minute intervals prior to the introduction of the sample into the emanometer. Once the sample was introduced, three more readings were taken at three minute intervals to give the total radon count.

All the data was recorded in a field note book together with GPS waypoints to enable plotting it on a map. Soil temperature in every station was also recorded.

FIGURE 11: Image of an Orsat aparatus used in measuring relative CO2 abundance in soil. (courtesy of EEE Ltd, 2016)

4. RESULTS

When rocks are subjected to hydrothermal alteration in geothermal areas, changes in mineralogy occur as a result of hot fluid and rock interaction. In some instances, the mineral alteration reaches the surface due to enhanced permeability caused by structures such as faults and fractures. These fluids alter the ground surface to show evidence of geothermal activity beneath. Hydrothermal fluids also form secondary minerals which are precipitated on the surface due to reduction in pressure and temperature conditions (Tole, 1996).

Van der Meer *et al.,* (2014) classified the above changes either as direct or indirect. The direct changes are those affected and linked directly to geothermal activities while indirect changes are those that require further inferencing and interpretation leading to effects of geothermal activities. Direct changes may include formation of features such as calderas, faults, hot springs, steaming grounds, and fumaroles. Surface manifestations mostly occur in a structurally controlled manner to depict preferred permeability zones. This linearity was easily detected during this study by use of remote sensing techniques.

Indirect changes are those interpreted changes based on scientific observations and testing of crustal materials. For example, zones with elevated CO_2 soil gas may be as a result of shallow seated intrusions which are degassing during periods of cooling. Radon gas may be a product or radioactive decay of Uranium from magmatic sources. Due to its short half-life, its detection near the surface would signify high speed transient times, likely to signify movement in fractured or faulted paths. Presence of geothermal grass on the surface maybe interpreted to be caused by hydrothermal alteration.

Fractures, faults, surface temperature, soil gas variations and alteration mineralogy can therefore be directly or indirectly linked to geothermal activities on the surface of a geothermal field. Using ArcGIS, it was possible to place these features on a map and analyse their trends.

4.1 Surface geology

The main rock types encountered throughout the Central rift region and Olkaria Domes were; volcanic ashes, trachytes, rhyolites, basalts, tuffs brecciated materials and lacustrine deposits. Rhyolites are predominant in Olkaria volcanic complex while basalts lava flows occur at the south western side of Olkaria, immediately outside the caldera rim. Basalts dominate Kijabe hill and are also observed in dykes around Kijabe town. Lacustrine deposits are dominant in low elevation areas whose source is lake deposition during the Lake Naivasha flood period (10-30Ka) (Clarke *et al.,* 1990). Longonot pyroclastics extend to the northeast covering most parts of Naivasha, Longonot and Kijabe areas. They are also encountered in Domes field where they form thick deposits. They seem to have been deposited as pyroclastic flows close to the caldera while the ones further away may have been blown by wind. Mt. Margaret is dominated by trachytic lava flows which have limited extent. Suswa volcano is mainly covered by trachytes which are evident in outcrops adjacent to Suswa Town (Figure 12). Volcanic cones of trachytic and pumaceous composition are present at the Suswa caldera floor. Some of the most dominant rocks encountered are described below.

4.1.1 Lacustrine sediments (100 Ka)

The sediments form the most recent cover of the Kedong Basin and Ol Tepesi plain to the south (Guth and Wood, 2013) (Figure 12). It is envisaged that the formation resulted from deposition of reworked lake sediments when the flooded Lake Naivasha was suddenly emptied. In hand specimen, the formation is cream to pale yellow in colour, fine grained, non-porphyritic clastic material derived from different rock types and organic material. In situ encounters show well graded and good sorting of strata signifying different water flow patterns during deposition. The formation produces very fine dust in areas with scarce vegetation and is prone to rapid erosion forming deep gullies. Sand sized deposits are observed with thicknesses of up to 10 m. The numerous deposits are harnessed for building sand. Baker *et al.,* (1972) named this formation as the Kedong Flood formation which is comprised of sand and fine gravel.

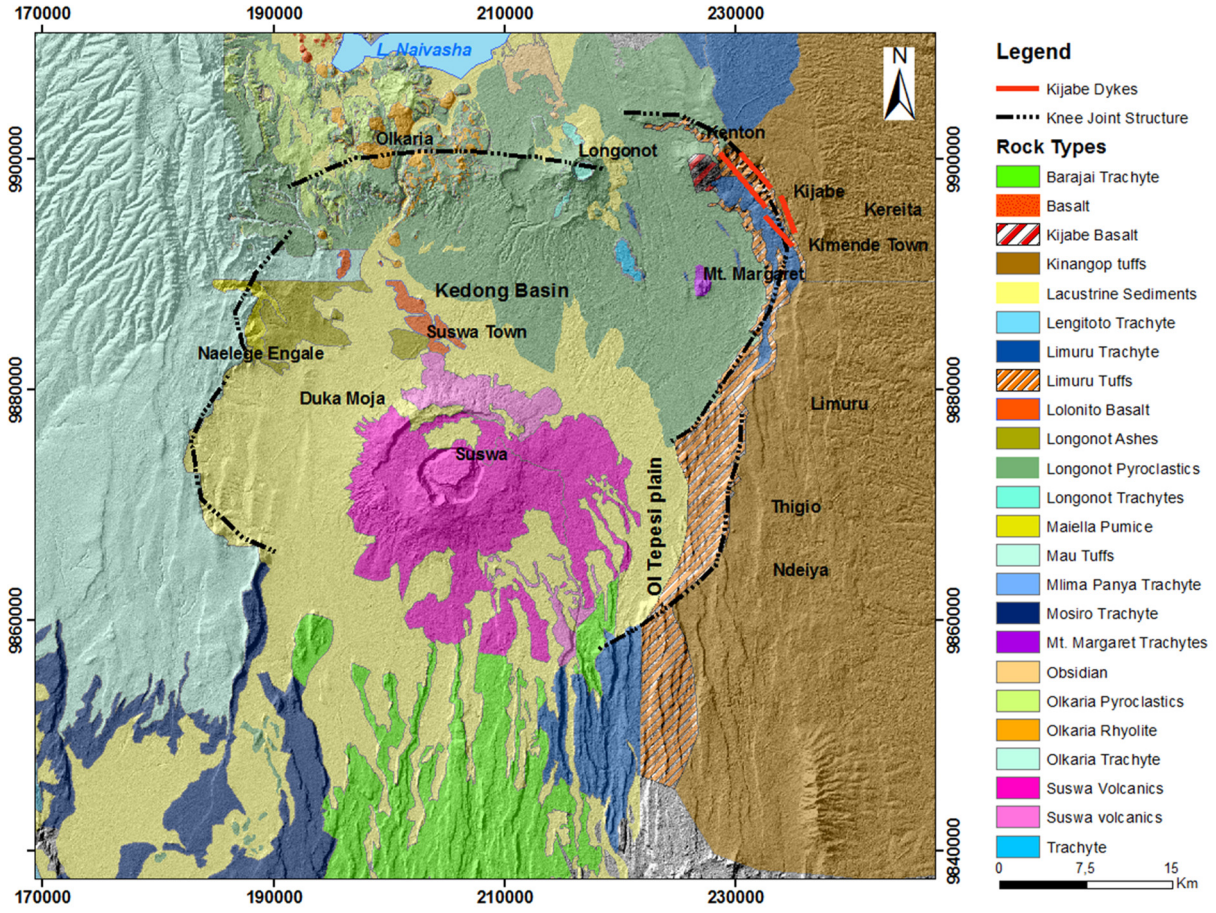

FIGURE 12: Geological map of Kijabe area showing the dominant rock types and structural trends. (modified from Thompson, 1964; Guth and Wood, 2013)

4.1.2 Longonot pyroclastics (0.2 – 400 Ka)

They form the most recent plinian eruption material from Longonot volcano which are dominant on the eastern escarpment and north of Naivasha town (Figure 12). Thin ash fall deposits are encountered in Karati area, north east of Naivasha town. In hand specimen, the pyroclastics appear light grey to brown, unconsolidated clastics composed of tuffaceous and pumiceous fragments. Also noted are obsidian, and volcanic glass fragments. Minimal hydrothermal alteration is noted on the formation except in parts of Olkaria Domes field where argillic alteration to smectite and kaolinite clays were noted (see section 4.2.6 below). Thick deposits are encountered in Domes field where average thickness is estimated to be up to 350 m. The deposits are intercalated with pale grey pumice intermittent layers which are also observed east of Longonot town. These pumice deposits are mined and sold to flower farmers since they are rich in phosphorous which accelerates plant growth. These deposits are also intercalated with Olkaria volcanic ashes which are dominantly reddish brown and Suswa ashes which are light grey to cream in colour.

4.1.3 Kinangop tuffs (3.4 – 3.7 Ma)

The tuffs originated from Kinangop flank eruptions during formation of Aberdare Ranges. They are exposed in most parts of the eastern escarpment where various artisan quarrying is ongoing (Figure 12). The deposits are between 20 and 40 m thick. The tuffs were formed by consolidation of ash and volcanic material that was airlifted, transported away from the vent and deposited. The tuffs can also be categorised to three distinct series which are distinguishable by their physical properties as follows below.

Non homogeneous tuff being the most recent, appears as dark grey, poorly consolidated, non-porphyritic rock composed of ash matrix cementing different light grey to brown clastic sediments composed of volcanic bombs and gravels. They are locally known as *Githunju* and forms the upper parts of most quarries along the eastern flanks of the Central rift.

Homogeneous tuff is also grey in colour but moderately consolidated. It is composed of volcanic material including pumice which are cemented by fine grained ash. This is more preferred by masons since its compact and easier to shape. It is locally known as *Grey*.

Lithic tuffs are widely variant in colour from light grey to brown and cream colour. They are well sorted, fine grained highly consolidated with no crystallinity in their structure. The rock is highly compact and is a nightmare to masons due to its heavy weight compared to the previous two but its only advantage is that it exhibits near perfect brittle fracture. This makes it easy to blast the outcrops with explosives. This formation is locally known as *Curve* since they produce straight face blocks after curving.

4.1.4 Trachytes (0.1 Ka - 6.9 Ma)

The rocks are characterised by a dark grey to black colour, fine grained, moderately porphyritic with euhedral crystals of sanidine feldspar. In thin section, the rocks are fine grained, porphyritic with abundant sanidines, pyroxenes, biotite and mafic minerals observed. Sanidines are distinguished by the prismatic shape, simple twinning and euhedral perfect crystal faces along 001. Pyroxene group is divided into ortho and clinopyroxenes which can be optically distinguished since orthopyroxenes have maximum interference colours of upper first order, while clinopyroxenes range to upper second order colours. Extinction angle were also used to differentiate between the two pyroxenes, as orthopyroxenes have parallel extinction and clinopyroxenes have inclined extinction. Both types were found to exhibit good cleavage intersections of 90°.

The rock is relatively fresh in most encountered outcrops but slight to moderate weathering and oxidation phenomena are rarely observed. Trachytes are a common and characteristic occurrence in high altitude areas. This may be due to their erosion resistance nature compared to the more prone pyroclastic and tuff counterparts. In some parts, they are exposed along deeply eroded rift shoulder faults while in other circumstances, they form volcanic cones as well as recent episodes of extrusions in edifice geometries.

Trachytes were encountered in Mt. Longonot, southwest of Olkaria caldera, Kamuyu hills located along the east rift escarpment in Mirera area, along the eastern rift scarp near Kijabe where the rocks are exposed along a stream profile, at view point section along Kamandura – Mai Mahiu road, Mt. Longonot trachyte flows observed on the flanks and summit of this hill and in Suswa volcano (Figure 12). Numerous cinder cones around Suswa and Duka moja area are trachytic in composition.

4.2 Structures in the central Kenyan rift segment

Structural analysis from Digital Elevation models (DEMs) images show a southern change in the Kenyan rift strike direction from NE-SW to NW-SE, then trending back to NE-SW (Figure 2). This sudden change in orientation is related to a triple junction near the summit of the Kenya dome with a third arm (Nyanzian rift) splitting off and dying out but the other two developing towards a plate boundary. The Aswa transform appears to connect the Eastern and Western branches of the East African rift (Figure 13). Chorowicz *et al.,* (1987) and Smith and Mosley (1993) attributed this sudden change in direction to the Aswa lineament which caused lateral shift. Chorowicz (2005) came up with a model of the EARS affected by vast transform faults oriented NW-SE (Figure 13).

Transform faults form along plate boundaries with accretionary motion which in many circumstances is caused by magmatic upwelling. The EARS is a lithospheric brittle failure caused by extension. A closer study of structural geology on the Northern part of the Kenyan rift shows sudden changes in regional fault orientations from NE-SW to NW-SE (Figure 13). The change may have been caused by crustal

inhomogeneities and variations in extensional force tensors due to transform faulting. Deformation models show differences in movements on the Kenyan rift system varying from E–W to ENE–WSW and NE–SW direction between 12 and 0.6 Ma, to turn since 0.6 Ma to the NW–SE direction (Bosworth and Strecker, 1997). The constant changes in direction is caused by changes in kinematic regimes being attributed to volcanic activities on both local and regional scales. Delvaux *et al.*, (1992) even found evidences of compressional forces on the East African rift during the Cenozoic period.

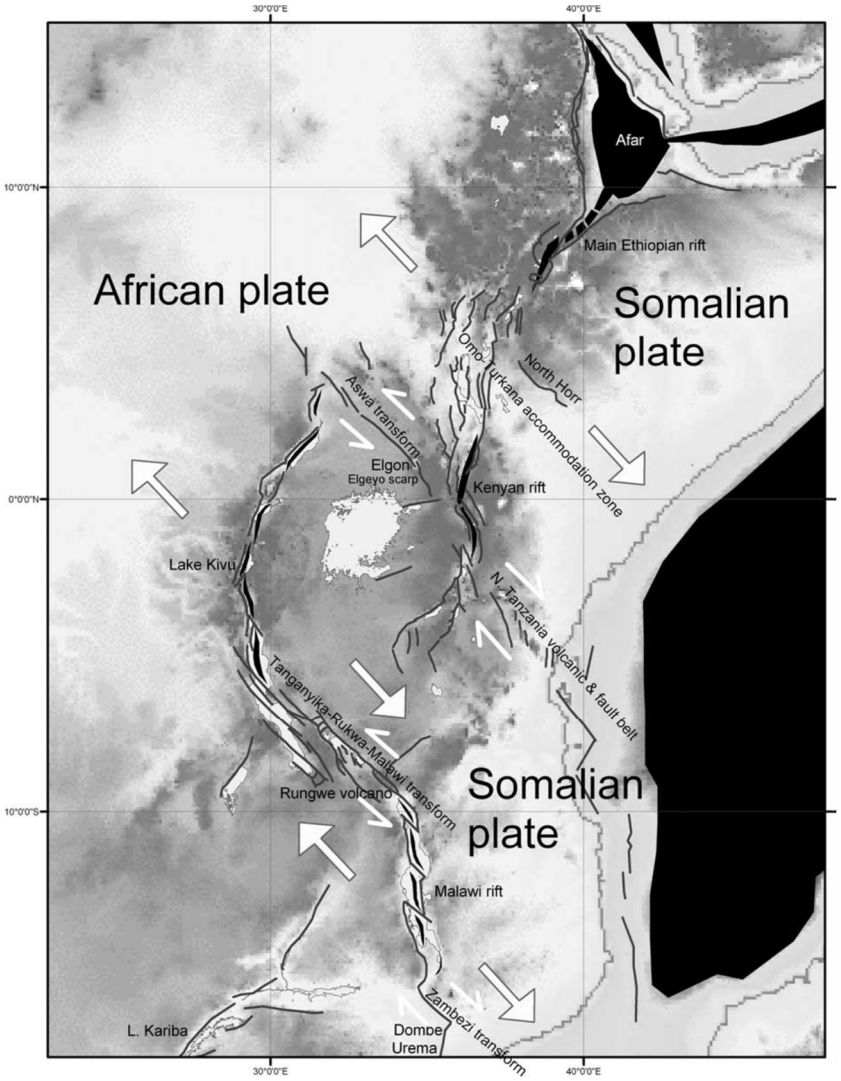

FIGURE 13: Map showing the transform zones that led to the changes in rift orientations. The Aswa transform zone is located west of the Kenyan rift and is believed to be the host of the Aswa lineament. Lateral spreading has formed the Victoria micro-plate. Black lines indicate existing major rift faults while the white arrows represent the direction of relative crustal movement (Chorowicz, 2005)

According to Chorowicz (2005), the Aswa lineament is one of the major transform zones with several large left-lateral NW-SE striking faults. These faults host some of the major volcanic centres on the EARS and produce major earthquakes in Africa. The lineament is located along Mt. Elgon moving south eastwards towards Elgayo fault scarp and is believed to have affected parts of the Central Kenyan rift segment (Figure 13). Further southeast, it intersects with the Kenyan rift and causes a major change in rift orientation from NNE-SSW to NW-SE. When it approaches the Central Kenyan rift, it further changes to the SW to form the southern Kenyan rift segment which is characterised by high geothermal activity. Further southwards towards northern Tanzania, there is seismicity and faulting resulting from early stages of right lateral transform faulting. The later opening up of the lithosphere through en echelon faulting and fissuring resulted in lava flowing to the Earth's surface. The Victoria micro-plate is also developing due to the continuous deformation caused by transform faults (Figure 13).

Analysis of DEMs show evidence of lateral shift of faults along the Central Kenyan rift shoulders (Figure 14 where left lateral movement was observed. Transforms of regional scale can be noted from the Nyanzian triple junction to Olkaria-Longonot axis where the rift orientation temporarily changes to NW-SE but later reverts to its normal NE-SW course (Figure 14). There is significant lateral shift resulting to formation of E-W loading zones and subsequent displacement of the N-S regional rifting. The E-W oriented faults have been previously observed in Eburru where dyke systems may have been extruded to form volcanic edifice (Mwania *et al.*, 2014). The Eburru massif is also oriented in the E-W direction depicting great influence of these structures in its plumbing system.

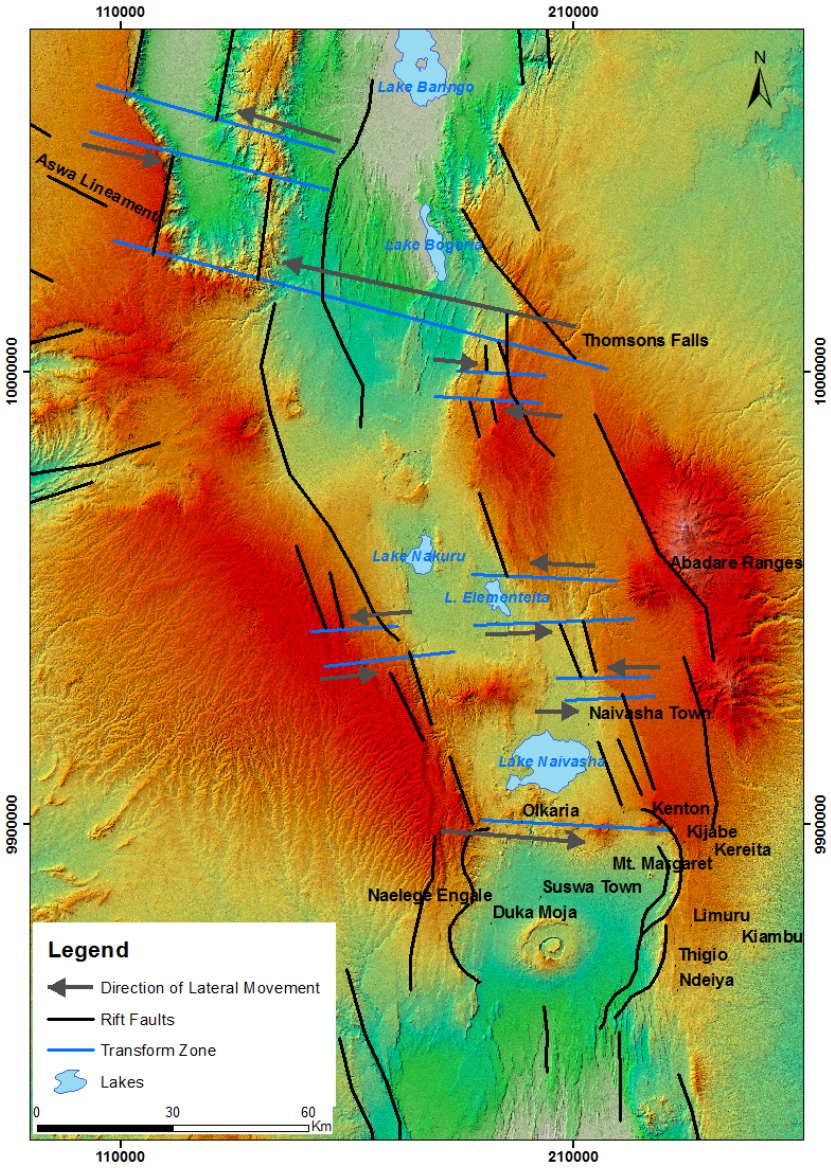

FIGURE 14: DEM of the Kenyan Rift System with the black lines showing the general orientation of the rift. The blue lines are indicative of areas affected by transform faulting while the black arrows show direction of lateral movement

Local transform faulting is also suspected in the area between Domes field and the outer caldera rim of Mt. Longonot where similar E-W fault trends were observed. The zone has characteristic ridges aligned in an E-W direction. The ridges show recent tectonic movements imprinted by folding and normal faulting on younger pyroclastics. Structural mapping results also show changes in fault orientations from the general N-S strikes to E-W trends further supporting the theory of transform faulting. The detailed account of these findings is documented in the next section. This transform zone may be connected to the Aswa transform zone (Figure 20).

The Central Kenyan rift hosts an arc like axial rift scarp south of Lake Naivasha forming a circular structure (referred as cauldron or knee joint structure) with Suswa volcano being at its centre (Figure 14). These arcs may have been a result of subsidence caused by panache ductile failure of the lithosphere during a period of low pressure in a magma chamber beneath the circular structure. Circular subsidence patterns have been modelled using the Mogi point source model and proven that surface deformation patterns are influenced by subsurface pressure changes caused by magma movement (Kiyoo, 1958; Dzurisin 2007). Magma chambers are assumed to be fluid-pressurized ellipsoidal cavities in an elastic crust of infinite length and uniform elasticity (elastic half-space). Considering any particular source depth and geometry, the surface deformation is proportional to the ratio of the cavity pressure change to the half-space elastic modulus (6.P/G), and to a lesser extent with Poisson's ratio (elastic properties of the crust) (Dzurisin, 2007). Emptying of a magma chamber results in spheroidal surface deformation, whose magnitude of deformation depends on the size of the magma cavity. The size of the cavity is the key factor between the pressure and volume change. Large eruptions that are within the elastic limit of the crust require large magma cavities (Dzurisin, 2007).

Kuria *et al.* (2010) showed evidence of a shallow magma source in the circular structure from magnetic surveys carried out along the Kenyan Rift. He used aeromagnetic data acquired using the African Magnetic Mapping Project (AMMP) to estimate the Curie Point Depth (CPD) of subsurface rocks. The main aim was to study the crustal thermal regime of the Kenyan rift and identify it´s potential for

geothermal resources. The data has a spatial resolution of 2 km and flight direction of 90° running in W-E direction at a flight height of 2896 m above mean sea level. His results discovered a shallow CPD with dimensions of 52 km by 37 km coinciding with the knee joint structure with an estimated diameter of 50km by 30km. Other smaller and shallow CPDs throughout the Kenyan rift also correlate very well to the known central volcanoes with shallow magma chambers which hold geothermal potential. (Kuria *et al.*, 2010) (Figure 15).

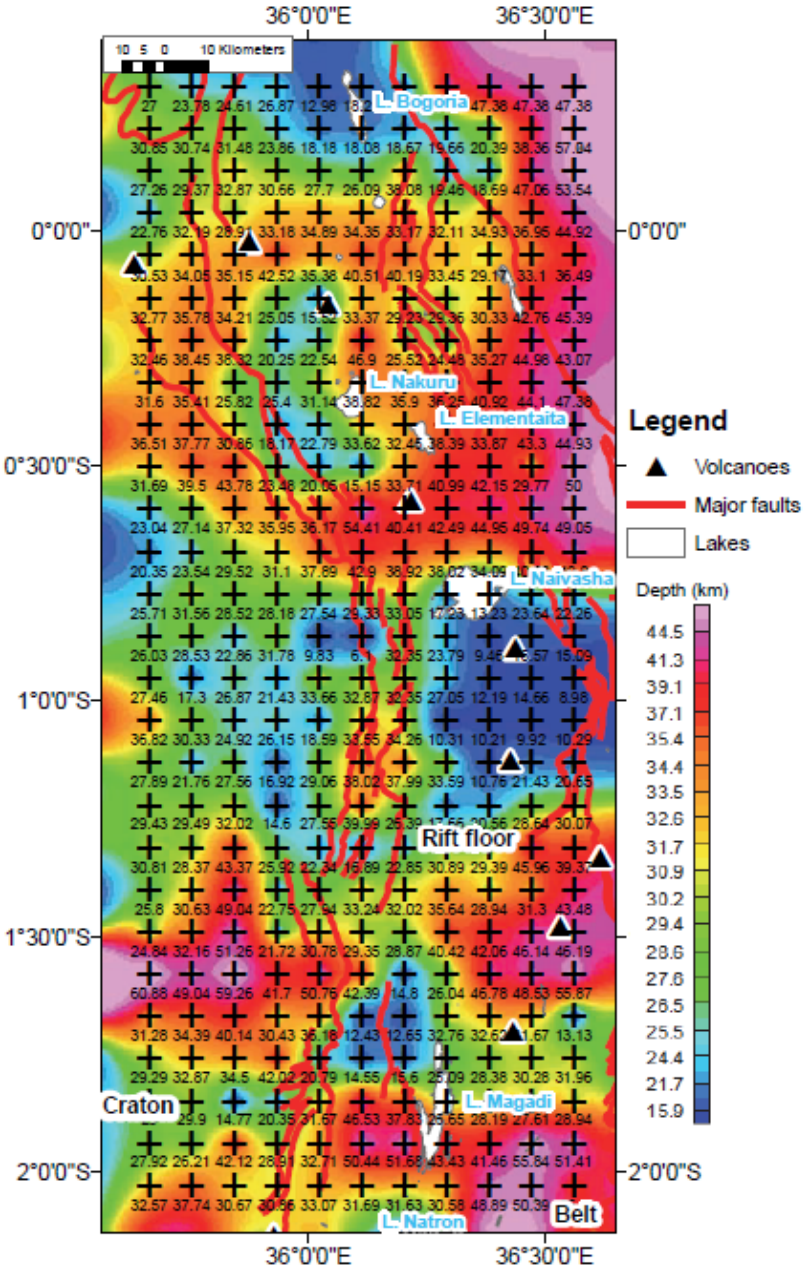

FIGURE 15: Map showing variation in Curie point depth (CPD) along the Kenyan rift system. The red bold lines show the regional fault systems which also mark the rift boundary. The map shows a local shallow CPD around Suswa, Longonot and Olkaria, south of Lake Naivasha which is marked by a dark blue colour (Kuria et al., 2010)

Kuria *et al.,* (2010) attributed occurrence of part of the shallow CPD to Olkaria geothermal field and validated his assumption using temperature logs from deep drilled wells in Olkaria geothermal field but did not envisage presence of the knee joint structure. However, according to previous geophysical studies carried out in Olkaria geothermal field, it is apparent that the shallow magma chamber which forms the main heat source does not extend outside the Olkaria caldera (Simiyu and Keller 1997, Simiyu *et al.,* 1995). The depth of Olkaria magma chamber has been estimated to be 6 km deep, which is much shallower than the estimated CPD of 15 km. This data was therefore used to infer presence of a larger magma source for the c. The magma cavity may have formed shallow magma chambers that supply Olkaria, Longonot and Suswa volcanoes. This theory is still in its infancy and requires more research.

Numerous basaltic dykes observed along the eastern escarpment from Kijabe area may have also originated from the big magma chamber. The dykes have a N-S orientation and depict recent volcanic activity. They may be heating shallow groundwater to form hot springs at Kinari forest with temperatures of 44.5°C (Clarke *et al.,* 1990). The dykes indicate presence of a shallow heat source in contact with the groundwater table or a mix of up flowing hydrothermal fluids with meteoric waters. Fumerolic activities were also observed in Mt. Margret with temperatures ranging from 65°C to 89°C (Clarke *et al.,* 1990).

The shallow magma chamber may further be responsible for elevated CO_2 gas around Kerita area (Darling *et al.,* 1995). The gas has been harnessed by Carbacid Ltd for more than five decades. The company has drilled several wells about 2 km east of Kimende Township where the gas is collected, purified and sold to beverage industries as a preservative. According to previous sampling done by Darling *et al.,* (1995), the wells appear to derive most of their CO_2 from a gas spring of inorganic crustal source. However, there is need to carry out detailed petrochemical and geophysical research to determine the paragenesis of this feature and determine its mode of formation.

4.3 Olkaria Domes field

Phase two of the study was concentrated in Olkaria Domes field and the area East of Domes. The total area of study is approximately 60 km^2. Vegetation cover and rough terrain in some parts were serious hindrances to the mapping exercise. Dense vegetation made it very difficult to delineate geological features from satellite images and necessitated field excursions. Most of the structures observed are detailed below;

4.3.1 Fractures

Fracture formation precedes faulting in an extensional stress field. During periods of volcanic unrest, they are initiated by magma resurgence and are driven open to the Earth's surface (Galland *et al.,* 2014). Rock fractures were the most common stress indicators in the field. Fracture sizes varying from micro-cracks that dissect small rock grains to veins and huge cracks. Veins and veinlets are micro-fractures infilled with hydrothermal fluid precipitates. These have been identified in numerous drill cuttings from wells drilled in Olkaria geothermal field. When rocks are subjected to pressure, displacement also occurs resulting to varying degrees of openings. In an active rift zone, the displacement is mostly heterogeneous and discontinuous.

Formation of fractures is mainly attributed to increased stress along areas of weakness in the crust. When fractures are subjected to vertical displacements in active tectonic environments, they form normal, reverse, thrust or strike slip faults. The stress which is a driving force may originate from over pressurized magma chambers or due to other plate tectonic forces. Some rocks may behave as plastics when critical stress is reached and result in formation of folds. Since the resultant plastic deformation is permanent, the rock strata do not regain their original shape even after the removal of the stress. Other rocks easily fracture when subjected to an external force. These rocks are said to exhibit brittle properties (Giordano *et al.*, 2013).

Fractures are the main avenues of fluid movement in Olkaria geothermal reservoir. They may be responsible for bulk fluid transport, especially where they form a system of interconnected clusters. This condition of cluster existence is commonly known as the percolation threshold (Tsang and Neretnieks, 1998). The permeability associated with this threshold is dependent on regional and local fracture trends.

Fractures were dominantly found in consolidated pyroclastics that lie beneath volcanic ashes and pumice deposits (Figure 16). The fracture patterns showed varying orientation, but mainly NW-SE, NE-SW and NNW-SSE directions (Rose diagram Figure 17). Some of the fractures conform to the general rift orientation, although they might be significantly younger than the rifting process. This may be a clear indication of continued stress conditions, probably due to continued rifting processes or caused by subsequent recent volcanic re-activation. Most of the fracture systems with NW-SE strike were mostly noted along the Ol Njorowa gorge (Figure 17). They may have been formed during the dyke extrusion period, where rhyolitic material was extruded to the surface and later erosion led to exposure of volcanic plugs that formed along the gorge.

An opposite fracture system was also noted with an orientation of NE-SW and ENE-WSW (Figure 17). This system is poorly distributed in the mapped area. The fracture propagation may also be attributed to tensile stress that causes rifting or due to magma resurgence. In addition, hydraulic pressure cannot be ignored in formation of vein filled fractures. Fluid infilling was observed in some fractures which may

have been caused by fluid overpressure leading to propagation of these openings. When fractures are infilled with fluid or other clastic material, the tensile strength of the fractures may approach that of the infilling material. However, due to differences in stiffness between the infilling material and the host rock, the stress build up at their contacts encourages further displacement and fracture propagation at the fracture tip. These tensional fractures are however believed to be shallow crustal deformations with the deepest reaching up to 1 km depth below ground level.

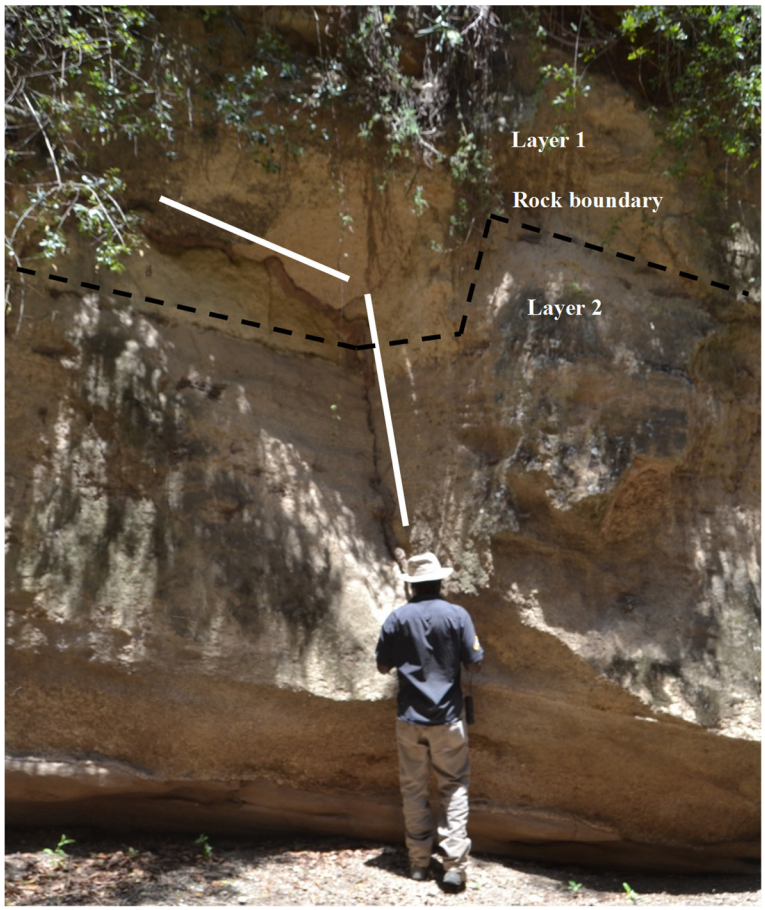

FIGURE 16: Plate showing one of the NW-SE fractures located on the ridge. Fracture deflection, shown by the white line while the black dotted line shows layer contacts with a displacement of a few centimetres

Most fracture systems were also found concentrated in close proximity to volcanic centres and volcanic plugs (Figure 17). The energy source of their propagation may have been the principle stress from magmatic activity and lithospheric extension caused by rising magma through vents. Rhyolitic outcrops also have fracture systems which may have been formed due to cooling, although these are not considered to be tectonic. Most of the fractures were also found affecting the young pyroclastic material, further proving existence of recent tectonism. An E-W trending set of fractures was identified on the ridged part East of Domes field where most of the rock strata showed moderate folding, which occurred during a brief period of rift compression. This unique set was only observed east of Domes field and may have been formed during the ridge formation process connecting Olkaria and Longonot calderas.

During geothermal drilling in Olkaria, fractures have always been observed in rock cuttings where most infilling minerals are secondary in origin. They are sometimes referred to as mineral veins, micro fractures or veins. Most of the productive wells have recorded high numbers of fractured strata at depth. These veins are partly or completely filled with secondary quartz, calcite, zeolites, clays, epidote, prehnite, actinolite among others. The alteration minerals are useful indicators of formation temperature and reservoir conditions during drilling. Fractures completely filled with secondary minerals like calcite, may sometimes form barriers to fluid flow. Some of them are tips of bigger fracture or fault zones that may be located much deeper where geothermal fluids formed pathways (Saemundsson, 2007). However, due to their small sizes and reduced fluid velocities, saturated fluids tend to settle in and precipitate the secondary minerals depending on temperature and pressure conditions in the reservoir. Where the network of fractures is well connected, they form fracture-parallel permeability, which may be enhanced by alteration of minerals in the host rock.

4.3.2 Faults

Formation of faults requires two types of forces that act on a plane in a rock; they include body forces and surface forces. Body forces act directly on the particles of the rock and are given as force per unit mass or per unit volume and a good example is gravitational force. Surface forces act across crustal

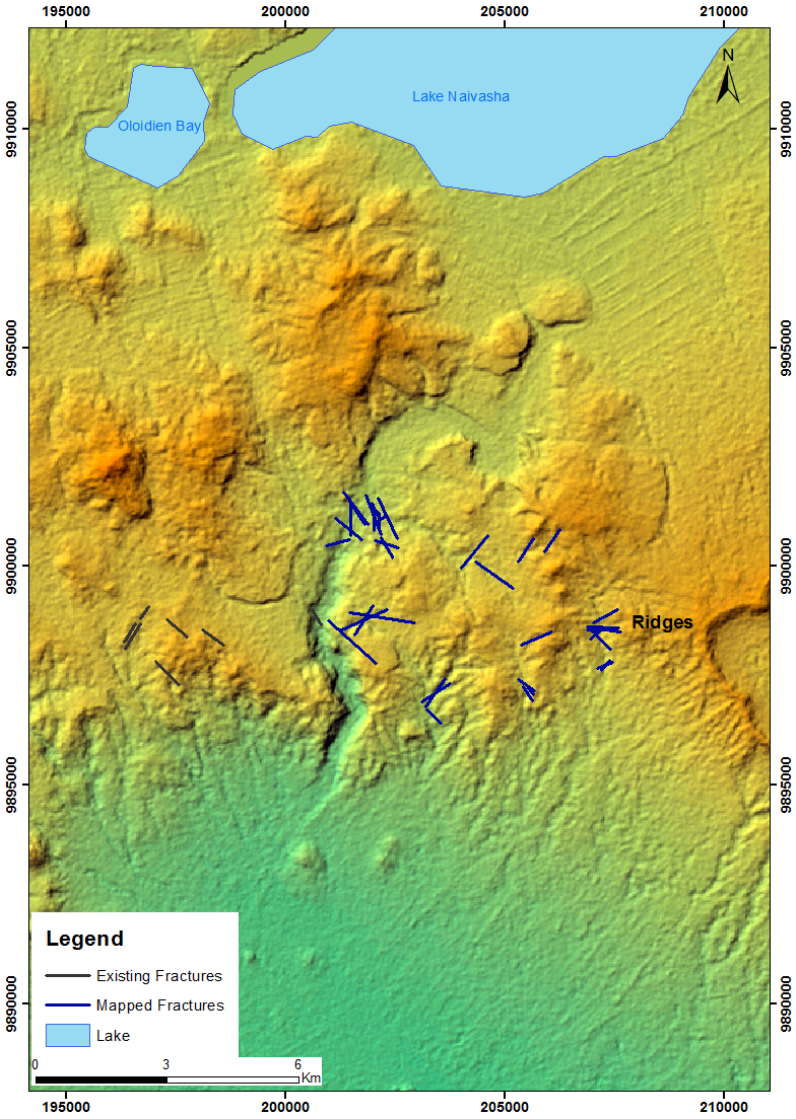

FIGURE 17: Map showing location and strike of mapped fractures as observed in the field with varying orientations as shown by the rose diagram on the lower right. The black lines labelled as existing fractures show previously mapped fractures on the Southeast field while the blue lines show the fractures mapped during this study

surfaces and can further be categorized as compressive or tensile forces; a good example is tectonic forces associated with plate movements (Peacock *et al.*, 1999). In rift systems, the most common surface force is tensile stress. Existing fault systems are very significant bulk fluid transport channels. They create high permeable zones for fluid movement, hydrothermal mineralisation and tectonic activity avenues (Hutchinson *et al.,* 2015). Understanding regional rift faults gives insight to evolution of rift zones and magma movement. Faults also act as important carriers for gases from magmatic sources and bring them to the surface. They may however be affected by near surface permeability variations due to changes in lithology and topography.

In the current study, extensional deformation patterns were mainly identified and gave some background information regarding the recent tectonic activity in the area. Although most extensional faults in a rift environment are believed not to be more than 1 km deep (Gudmundsson, 2011), their presence, especially in geothermal areas, is vital for fluid movement. They are good channels for infiltrating meteoric water to the deeper geothermal reservoirs, especially where magmatic activities have caused rejuvenation of older faults. They are responsible for increasing the surface area to volume ratio for fluid to interact with hot rocks. Different types of faults were encountered in the study area depicting different modes of formation.

a. Normal faults

In most cases, normal faulting dominated the study area. The faults were observed along erosional gullies as lithological displacements. From the plotted Rose diagram, most faults were oriented NW-SE, NNW-SSE, ENE-WSW and NE-SW while a few of the faults had E-W and N-S orientations (Figures 18 and 20). Others appear on the surface greatly influencing the topography with their throws ranging from 5 to 50 m and dips from 40 to 90°. Dip directions range from NE to NW. Faults with the highest displacements were mostly located along the Ol Njorowa Gorge and are clearly observed in satellite images. Their strike ranges from NW-SE to NE-SW and have highly influenced the orientation of the gorge. Normal faulting is believed to have shaped the erosion pattern of the Gorge. Wide basins of up to 300 m were created during the high stands of Lake Naivasha due to the erosion (Figure 19).

Other extensional faults were encountered east of Domes with their orientations ranging from NE-SW, SW-NE, WNW-ESE and ENE-WSW (Figure 20). Their orientation is in line with the general rift direction and may have formed during the continuous rifting process. The N-S faults are the most recent with resultant dyke emplacements mainly along the gorge. These faults have undifferentiated pyroclastic and tuff material that is brecciated and deposited along the fault planes (Figure 20).

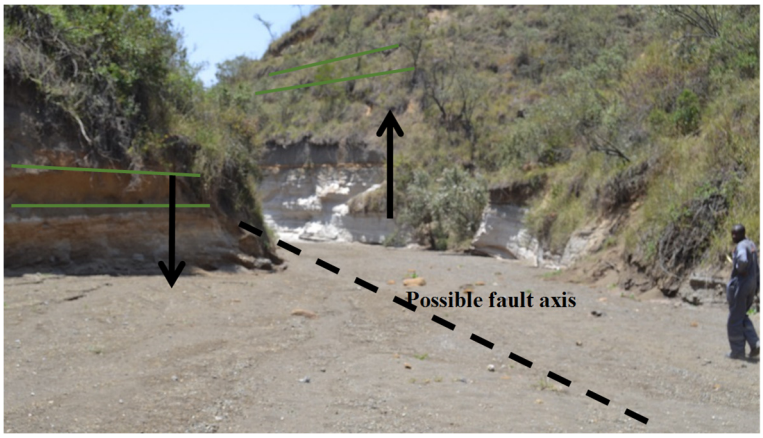

FIGURE 18: Normal faulting depicted by the white ash deposits exposed on the right side of the valley with no trace of the deposit on the left, a clear indication of displacement

The E-W features are limited in extent and may be attributed to transform faulting that formed the E-W oriented ridges between Longonot outer caldera and Olkaria caldera rim (Figure 20). A clear relationship could not be conceived at this stage due to deficient subsurface data which is required to understand the stratigraphic sequence of this area. They range in displacement from 2 to 10 m. These faults acted on the recent pumaceous and pyroclastic deposits. The faults are therefore presumed to be younger than the thick pyroclastic deposits from Mt. Longonot by relative dating. This is further evidence of constant crustal deformation caused by volcanic and tectonic activities in an active rift system.

FIGURE 19: Plate showing an erosion bevel along Ol Njorowa Gorge. The "stand-alone" rock column in the basin is the Fischer's Tower which is a remnant of erosion

Some gullies have been formed by the process of erosion along fault planes which are crustal weak point. Continued erosion continuously deepens the gullies and sometimes form seasonal stream channels and flash flood channels. Deep gullies along these fault lines expose lithological sequences displaying lithological displacement between the valley walls (Figure 18) with the brown volcanic ash layer showing a relative throw of about 5 m. The white ash was only visible on the right hand side of the photo but it's buried to the left. In these circumstances, it was difficult to determine the dip of the fault but the general orientation was identified to be NW-SE. The grey ash that has covered the valley walls was deposited by wind or water erosion reducing the exposure.

b. Thrust faults

Thrust faulting dominates deep buried weak rocks which propagate to the surface along planes of weaker rock overburden. Their occurrence resembles staircase trajectories due to reduced shear strength as they approach the surface. They result from compressional forces created by horizontal compressive stresses and so cause shortening of the crust. Few thrust faults were observed in the current study since most of the areas have experienced tensional stress. Field observations show displacement of pumice deposits of approximately 1m. The fault plane lies at an angle of 30° to the west (Figure 21). They indicate a period of compression probably during the formation of rhyolitic domes.

4.3.3 Calderas

The Greater Olkaria Volcanic Complex is bounded by a ring structure which is presumed to be remnants of a buried caldera system that is marked by volcanic domes to the east, south and southwest (Omenda, 1998). The ring structure is slightly elliptical in plain view (Figure 22), with unknown vertical displacement. The accurate displacement of the piston has not been ascertained since no stratigraphic correlation has been done outside the ring structure. The volcanic domes present on the eastern part of the complex were erupted from a ring fracture, probably related to a ring dyke during caldera collapse or an inclined sheet during magmatic inflation. Rhyolitic intrusions encountered during directional drilling intersecting the ring structure may therefore indicate presence of ring dykes or cone sheets.

Numerical and analogue models combined with laboratory testing on field data have proven that ring faults and dykes are generated by shallow sill-like magma chambers in a volcanic field subject to doming, tension or both (Gudmundsson and Nielsen, 2006). The presence of a shallow magma chamber is evident from

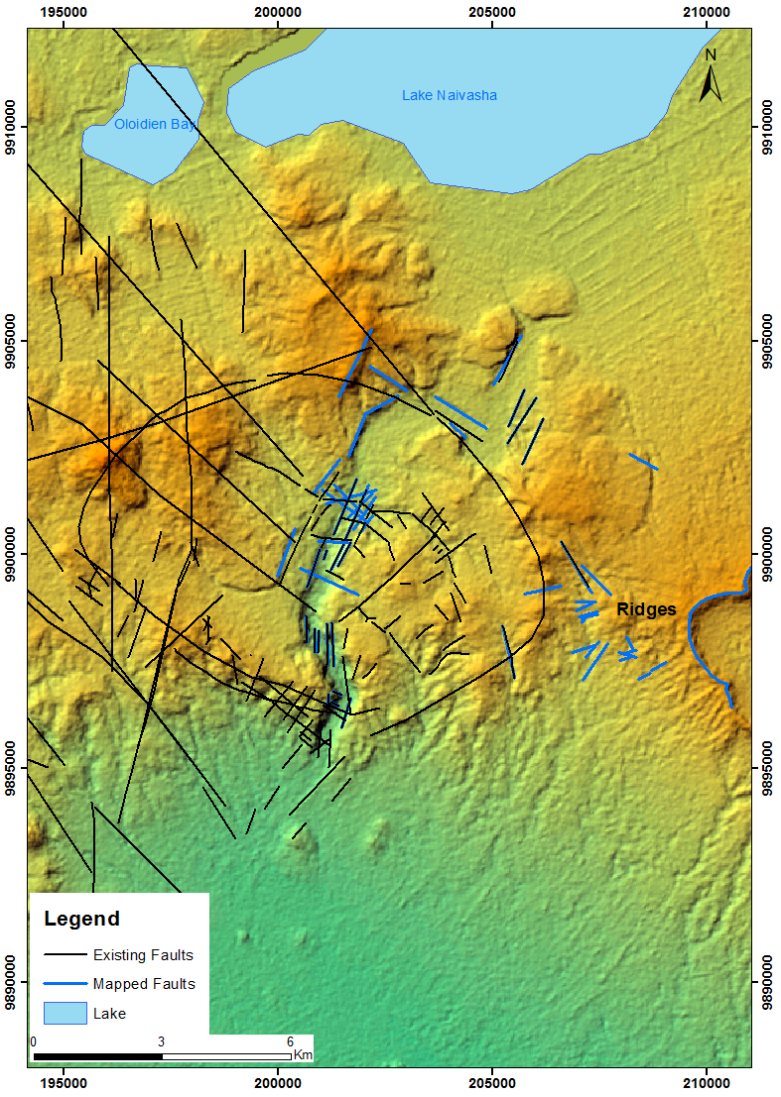

FIGURE 20: Map showing structural trends in Olkaria Domes field. The blue lines indicate the mapped faults while the black ones show the existing faults mapped through previous exploration and from stratigraphic correlation. The rose diagram shows the general strike directions

FIGURE 21: Image of a thrust fault observed along the ridge structure east of Domes field

resistivity, gravity and seismic studies carried out in Olkaria (Onacha, 1989; Simiyu *et al.,* 1995; Simiyu and Keller, 1997). However, the lack of a complete loci of domes around the entire volcanic system has not been explained. The western and northern segments of the volcanic complex do not show arcuate domes or remnants of caldera ring faults.

Lipman (1997) classified different types of calderas based on their geometry and morphology. The

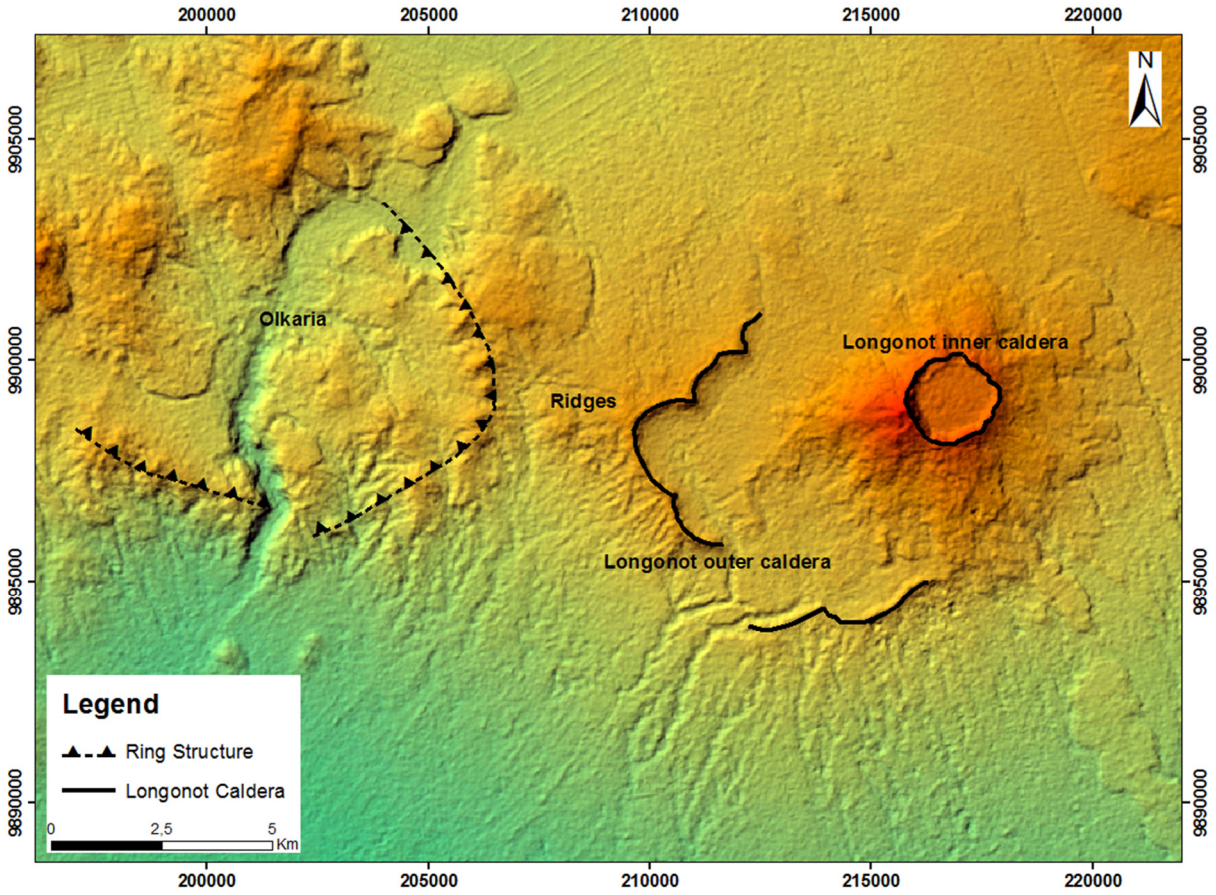

FIGURE 22: Map showing Olkaria ring structure and both outer and inner Longonot caldera rims. The ring structure is defined by arcuate domes

classifications include piecemeal, trapdoor, downsag and funnel calderas. The trap door caldera is bounded by a hinged structure and a partial ring structure caused by incomplete piston collapse. The formation of trap door calderas may be attributed to smaller eruptions, an asymmetrical magma chamber, or regional tectonic influences. Lipman (1997) also observed that many pre-Holocene calderas are filled by tuffs and other younger lava flows from other vents or from neighbouring volcanic centres. Caldera formation is usually in response to explosive eruptions that lead to deposition of tuffaceous material. These flows obscure the primary volcanic structures which cause difficulties in surface structural mapping.

Olkaria volcanic system may be classified as a trap door system formed due to asymmetrical geomorphology of the magma chamber or smaller magma chambers forming numerous sources of eruptions. During the initial periods of volcanic eruptions, the emptying of the magma chamber may have been irregular, resulting in an uneven collapse of the eastern and southern segments which shows the arcuate ring structure. The northwestern part acted as the hinge and had less deformation. Due to intense deformation on the east and south, subsequent magma chamber depressurisation led to formation of ring dykes along the ring faults but due to the high viscosity of the magma, most of it was arrested to form the numerous domes along the ring structure. The shallow magma chamber and higher deformation on the east, and south fields led to formation of more hydrofractures that eventually led to thermal conduction and hydrothermal alteration at shallower depth.

Part of Longonot outer caldera rim was mapped during the field work. The outer caldera of Mt. Longonot is however structurally well visible and one of its arcuate tips lies in the Olkaria geothermal license (Figure 22). The northeastern part of the caldera is however poorly exposed and may have been covered by younger trachytic lava flows. The Longonot inner caldera is conspicuous in satellite images and shows a central vent system with a symmetrical ellipse of about 2km in diameter.

4.3.4 Dykes

Dykes are important magma movement channels that are formed when magma chamber overpressure results in uprising of magma towards Earth's surface. Magma moves through fractured crustal surfaces due to their weak resistance. Dykes that reach Earth's surface are known as feeder dykes while those that are arrested along the way are known as non-feeder dykes. During extrusion in active volcanism, magma moves to the surface as dykes that propagate in fractured zones. They normally propagate parallel to principle stress trajectories. Therefore, those dykes ejected from circular magma chambers move in a steeply vertical direction or as inclined cone sheets until encountering an arresting point. Dyke arrest is caused by changes in rock shear strength due to differences in composition. The arrested dyke would either end there or change its direction to horizontal and move along bedding planes of strata to form a sill (Gudmundsson, 2011). Studying propagation of dykes is important in geothermal research since dykes encourage rejuvenation of older buried faults, which enhance permeability. They also act as potential heat sources in geothermal systems that form upflow zones of hydrothermal fluids. Since dykes intrude younger strata, their rate of cooling has been proven to be low (Tsang and Neretnieks, 1998). During well siting, they are key targets to tap their heat and enhanced permeability.

Factors influencing the propagation of dykes and sheets

The plumbing system of Olkaria volcanic complex is different from most volcanic centres along the rift system. The volcanic system does not display a caldera depicting that the magma chamber may have been emptied via feeder dykes mainly occurring along the ring structure. The Olkaria ring structure may have been more porous towards the east and south hence the existence of numerous volcanic domes. Dykes play a critical role in the plumbing system and are therefore important in this study. Gudmundsson (2011) refers to dykes as hydrofractures and they propagate depending on fracture regimes of host rocks. There are three main factors that influence dyke behaviour as detailed below.

(i) *Stress barriers*

Tensile stress variations between the dyke and host rocks may lead to successful dyke propagation. The dyke tensile strength should largely exceed the rock strength of between 0.5-6 MPa (Gudmundsson, 2011). The direction of propagation will always be parallel to the trajectories of the principle stress, σ_1 and perpendicular (or normal) to σ_3. However, if the dykes reach a stress barrier, the dykes may be forced to change orientation or halt at the intersection with the stress barrier. The stress barrier is defined as a layer or unit where the local stress field is unfavourable for the propagation of a particular type of fracture (Gudmundsson, 2011) (Figure 23).

(ii) *Elastic mismatch*

It is a result of variations in rock mechanical properties of different strata hosting dykes and those directly in front of the dyke tip. Dykes mainly follow these extension fractures until such fractures meet and form mixed mode structures (Hutchinson and He, 1989; Xu *et al.*, 2003).

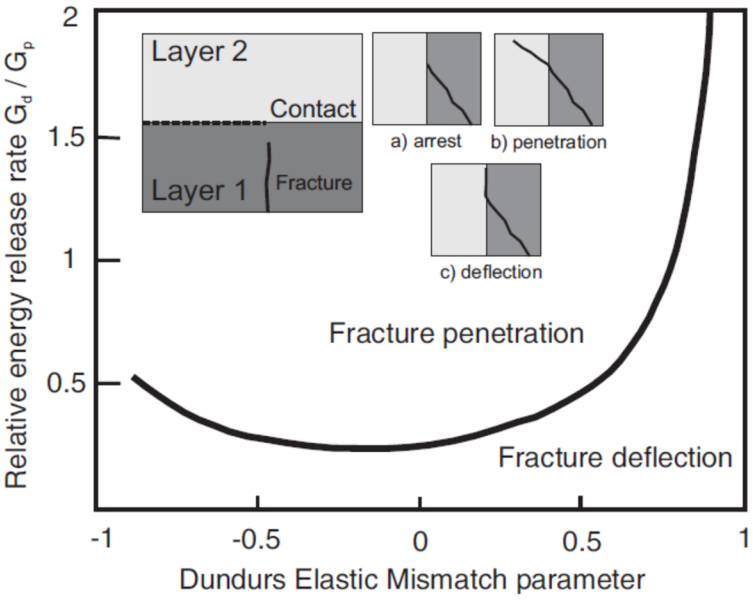

FIGURE 23: Conditions for dyke propagation: upon meeting a contact between two layers with contrasting material properties, a fracture will either a) arrest, b) penetrate the contact or c) deflect at the contact. The ratio of strain energy release rate for fracture deflection (Gd) against fracture penetration (Gp) is plotted as a function of the Dundurs elastic mismatch parameter, see text for details (He *et al.,* 1994)

(iii) *Cook-Gordon mechanism*

According to Xu *et al.*, (2003); Wang and Zu, (2006); Browning and Gudmundsson (2015), there have been several experiments on crack propagation which have shown that Cook-Gordon de-bonding is partly responsible for delamination of composite materials. The results proved that tensile strength on the tip of a propagating dyke causes discontinuities ahead of the host formation. The fractures caused by the dyke may further change orientation due to the changes in mechanical properties of rocks. The propagating dyke will in most cases follow the propagated fracture until the magma pressure is in equilibrium with the tensile strength of the host rock.

In the present study, several dykes were encountered in the Domes field and were well observed on the exposed surfaces of the Ol Njorowa Gorge (Figure 24). The rhyolitic dykes are mostly feeder dykes occurring in close relations with volcanic plugs. A section to the south of Ol Njorowa Gorge showed the presence of an arrested dyke that formed a sill. The dyke was arrested due to an encounter with a stress barrier. The sill moves horizontally along bedding planes of different strata. Most of the dykes observed cross cutting the gorge are believed to have extruded along prominent fractured surface of the Olkaria caldera system where magma found weak points. Ring dykes may have been responsible for the formation of arcuate ring domes that lie along the ring structure formed as a result of dyke arrests beneath the Earth's surface due to encounter of stress barriers.

OW-918A is a directional well (azimuth 90°) located about 350 m from the ring structure. The well penetrated the Olkaria ring structure and encountered rhyolitic intrusions beneath basaltic and trachytic lava flows at depth of between 1180 to 1700 m below ground level. The encountered rhyolite was described as light grey, moderately porphyritic, compact rock rich in quartz and sanidine phenocrysts. It is relatively fresh and appears to be slightly altered to oxides and clays (KenGen, 2014 and Musonye, 2012). The penetrated rhyolitic rock may be part of the arrested dyke system which formed volcanic domes along the ring structure.

FIGURE 24: Dykes extrusion along the Ol Njorowa Gorge that have been exposed by erosion. The dykes have near vertical dips with thickness of 2 to 7m

More dykes were identified along erosion gullies close to the Central Tower where they cut across the pyroclastic rocks (Figure 29). Where erosion has been extensive, the dykes form high cliffs along these gullies ranging from 15 to 40 m high due to resistance to erosion. They have near vertical dips and thicknesses ranges from 2 to 7 m (Figure 24). The dykes are believed to have fed the volcanic plugs with lava to reach the surface. Surface Earth processes such as deposition, erosion and weathering have led to burial or exfoliation of exposed dykes leading to visual constrains.

Dyke propagation has been proven to reduce chances of fault formation due to magma deflation during periods of crustal uplift (Wang and Xu, 2006). The dykes reduce the energy build up in the magma chamber as they propagate to evacuate magma to Earth's surface. These dykes also reduce risks of volcanic eruption by acting as punctured section of an over inflated ball (Gudmundsson, 2011).

4.3.5 Folds

Folds are formed when compressive forces act parallel to the bedding planes of ductile or plastic crustal material like pyroclastic deposits. The deposits are resistant to fracturing and form synclines and anticlines among other fold patterns.

In the field, folding is mostly observed on pyroclastic rocks lying on top of areas which may have experienced volcanic uplift (Figure 32). The cause of folding may thus be inferred to have been volcanicity. Most folds were encountered along gullies on the ridges between Olkaria and Longonot, while others occur along the ring structure where rhyolitic domes caused plastic deformation. Some folds slope gently with dips of up to 15°, while others cause inclines of above 40°. Other folds were encountered along the Olkaria ring structure where the accompanying pressure emanated from volcanic uplift of the rhyolitic domes (Figure 25). Alternatively, the pyroclastic rocks may have been deposited as thin sheets draping a pre-existing undulating ground. The occurrence of folds paralleling the domes suggests draping.

FIGURE 25: Plate showing folding along the ring structure. This may have been caused by volcanic intrusion of rhyolitic domes after dyking events

4.3.6 Altered ground

Hydrothermal alteration is a result of hydrothermal fluid contact with surface rocks. The hot rock-fluid interaction leads to chemical reactions that alter primary minerals. Since geothermal fluids have elevated temperatures, they easily dissolve primary minerals and transport them towards areas of lower pressure. The fluids move through preferred zones of permeability and tend to follow geological structures. Minerals saturated in hydrothermal fluids are later precipitation as secondary minerals when temperature and pressure conditions are lowered. The implication is that the fluids form very distinct alteration mineral assemblages with depth. Various alteration mineral assemblages appear in equilibrium and depict different temperature and pressure conditions. Precipitates that are deposited on the Earth´s surface mark zones of alteration, which may experience elevated temperatures compared to the surrounding environment. Geothermal fluids also alter the surface rocks to form alteration minerals which are further evidences of subsurface interaction.

Altered grounds are found widely distributed in the study area. They form an E-W pattern running along the southern part of the ring structure (Figure 26). They are also located in the Ol Njorowa Gorge where

they have high temperature. They host numerous sulphur deposits and have altered pyroclastics to brown and red clays (Figure 27). The occurrence of altered grounds is also related to geological structures as interpreted from the map (Figure 26). Most of the altered grounds along the gorge occur along fault planes. The red coloration is a result of iron rich source rocks, which is also exposed to atmospheric oxygen to form iron oxides. Smectite and kaolinite clays were the most common alteration products (argillic alteration).

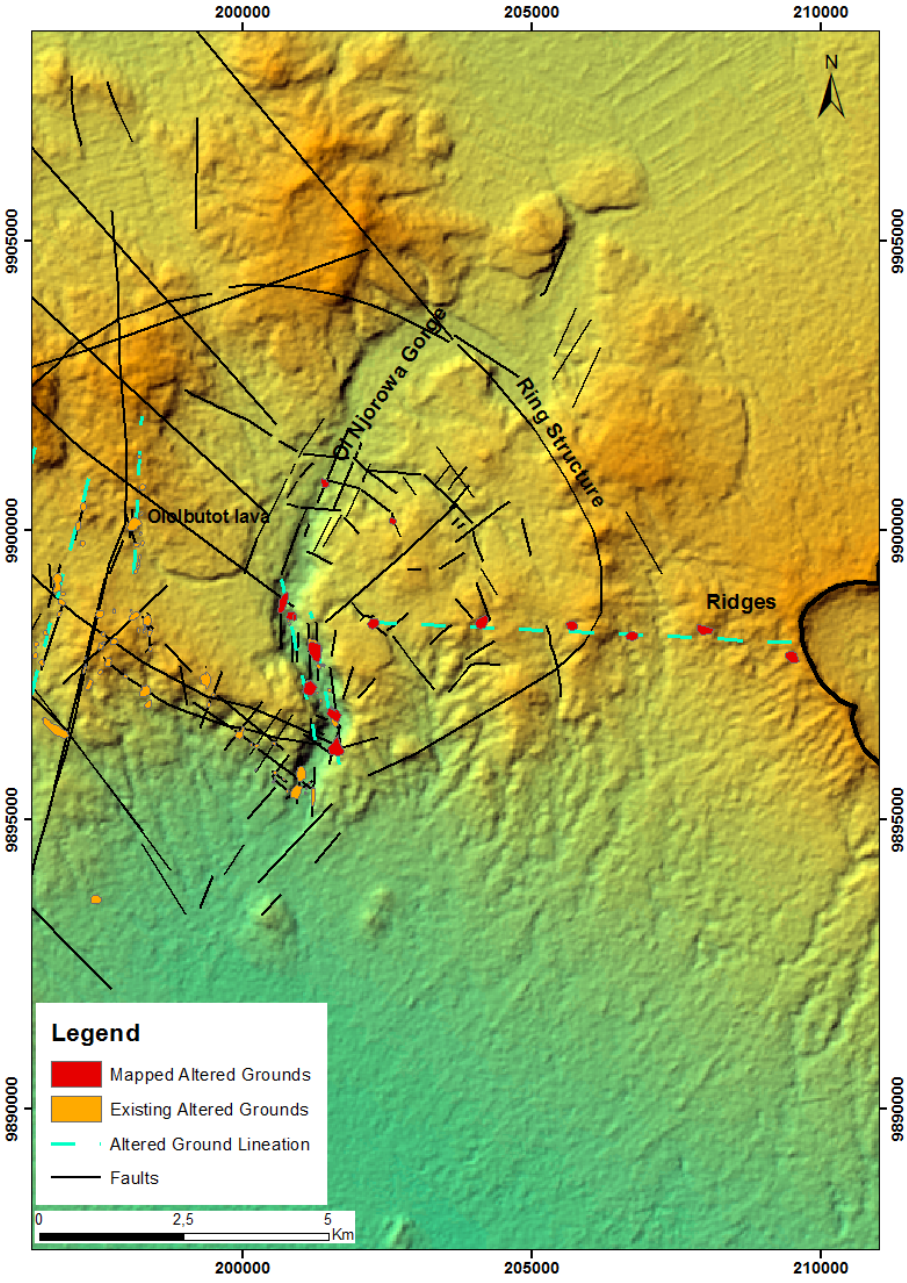

FIGURE 26: Map of the study area showing spatial distribution of altered grounds mapped during this study (red polygons) in the study area. The orange polygons indicate the previously mapped altered grounds to the southwest of Olkaria. Note the E-W trend from the ridges to the Ol Njorowa Gorge shown by the light blue dashed line

Extinct fumaroles also left altered grounds to the south of the study area along the ring structure (Figure 26). They may have been formed due to self-sealing of hydrothermal deposits that led to reduced permeability. Consequently, sudden burial by Longonot pyroclastics may have led to their extinction due to the thick overburden. They exhibit lower alteration rates and reduced temperatures of about 62 to 67°C. Geothermal grass is also found in close proximity.

Vegetation cover around altered ground is lacking or emaciated. Apart from geothermal grass that thrives in this hot and clayey environment, most of the shrubs and local grass have died due to chemical pollution. This characteristic feature has been applied in identifying altered grounds in infrared satellite images elsewhere. Limitations occur due to presence of other factors that have led to vegetation loss. Human encroachment in the study area for example, has led to deforestation making it difficult to distinguish this from chemical pollution caused by hydrothermal pollution. Other altered grounds were encountered in deep gullies covered with vegetation making them hard to detect using satellite images.

FIGURE 27: Altered grounds showing different levels of alteration. Plate A was taken on altered pyroclastic rock outcrop to the south of Olkaria ring structure where the ground temperatures were 67°C, while in plates B and C, there were no elevated temperatures. The dominant clays were smectite and kaolin altered from pyroclastics and rhyolites

4.3.7 Hot springs

Hot springs are formed when groundwater is heated by Earth's natural heat. They spring to the surface where permeability allows and pressure conditions are higher than the atmospheric pressure. Due to interaction with hot rocks beneath, their temperatures are higher than the surroundings and sometimes reach boiling (Otieno *et al.,* 2014). The elevated temperatures are also responsible for increased pressure. Hot springs may also emanate from contact with convective magmatic fluids that conduct heat to shallow groundwater. The groundwater becomes highly mineralised and reaches the surface where the water table intersects the surface due to topographic lows. A good example of this is along the Ol Njorowa Gorge where erosion has formed deep gullies.

Hot springs were observed along the Ol Njorowa Gorge where they discharge hot fluids (Figure 28). The fluid temperatures range from 56 to 96°C along the upper part of the gorge. The springs are structurally controlled and occur linearly along the NE-SW oriented normal faults. Their characteristics

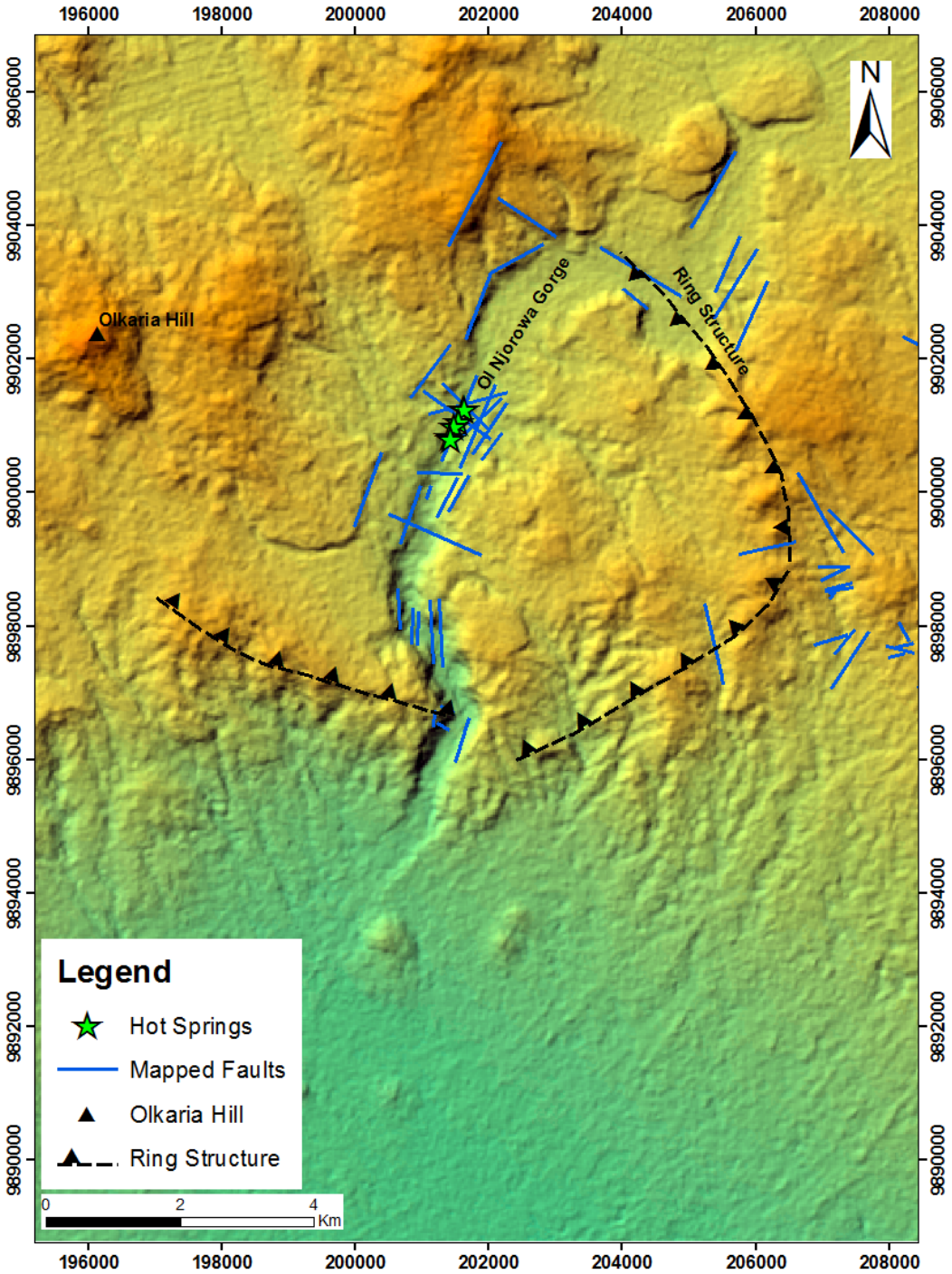

FIGURE 28: Map showing location of hot springs along Ol Njorowa Gorge with elevated temperatures. The hot springs are aligned along NE-SW faults

vary as to the amount of fluid they discharge and their temperatures. Some also occur on the valley floor where cooler water is flowing, making it difficult to measure their precise temperatures. Others occur along valley walls where the fluid is contaminated with meteoric water.

4.3.8 Volcanic plugs and eruption centres

During eruption periods, magma is transported from the magma chamber to the surface through the crust. Once the magma chamber pressure is in equilibrium with lithostatic pressure, the extrusion process ceases and solidification commences. Some of the magma solidifies along the magma movement channels to form volcanic plugs. These plugs seal the magma transport channel and subsequent eruptions

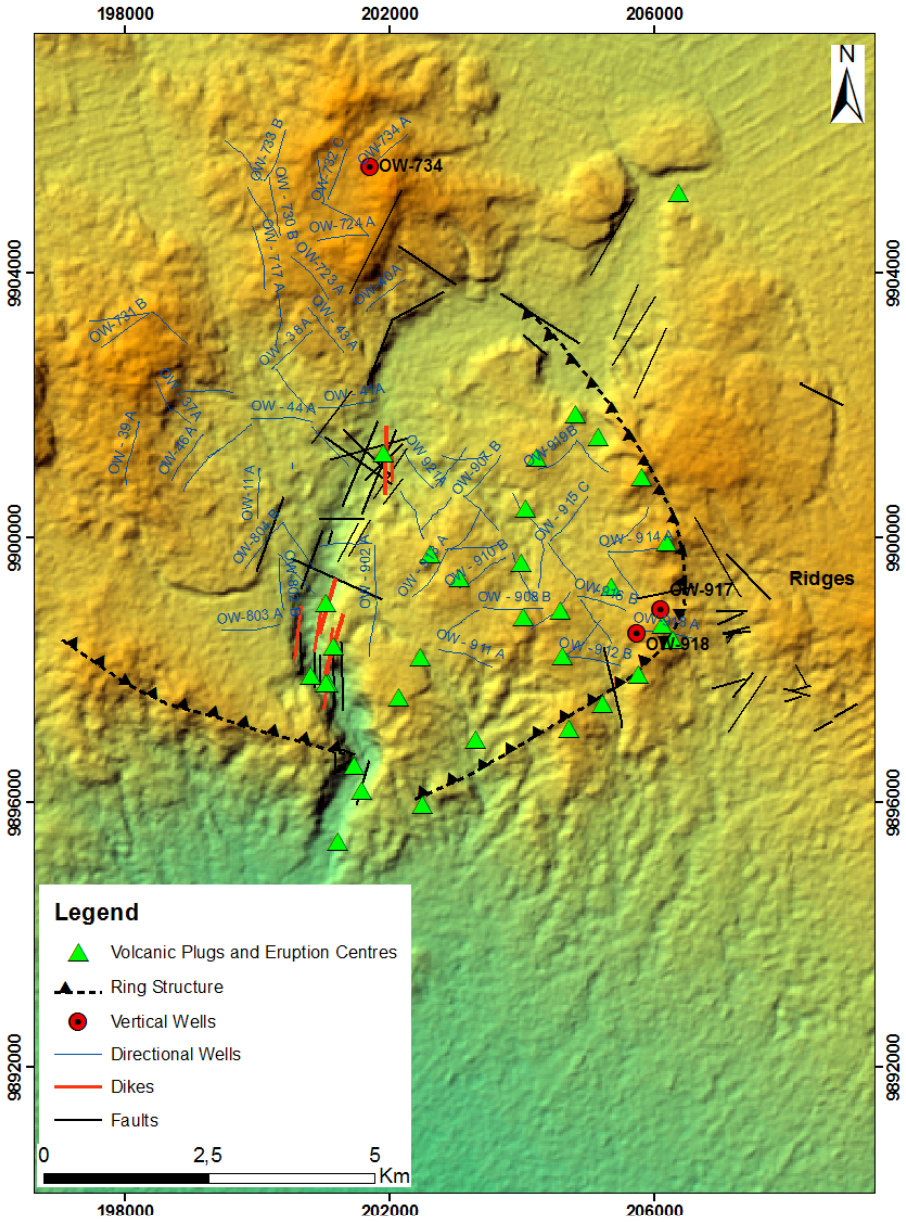

FIGURE 29: Map of the study area showing volcanic plugs and eruption centres marked with red triangles. Some directional wells are displayed to show position and azimuth of well OW-921A. The well may have intersected the dyke or volcanic plug at the Central Tower. Wells OW-917, 918 and 734 are also shown as vertical wells in the map

may result in formation of different channels or destroying the previous ones. When magma is violently erupted to the surface, there are remnants of the volcanic plugs characterised by eruption centres.

Volcanic plugs were widely distributed along Ol Njorowa Gorge where numerous rhyolitic dykes accompany them (Figure 29). These plugs are believed to be channels of magma movement to form the numerous rhyolitic lava flows on the surface. Plugs are important heat sources in geothermal resources. In cases where the magma chamber is still active, there is a possibility of heat conduction along these volcanic plugs and dykes accompanying them. In the current study, the volcanic plugs seem to be young as they cross cut all the other formations to extrude the surface. This means they may still possess significant heat resources at depth. The rocks around volcanic plugs and resultant dykes are often permeable due to reactivation of older structures which run deep below the surface. This allows deep hydrothermal fluid convection and efficient heat transfer. An example is well OW-921A which intersected the dyke observed close to the Central Tower at a depth of 2126 m b.g.l. (Figure 29). The well is one of the highest steam producers in Africa with a power rating of 25 MWe and 5 MWt.

4.4 Geochemical soil gas survey results

4.4.1 CO_2 gas survey

The CO_2 soil gas analyses were carried out during this study in Olkaria Domes field. They were compared to the background values of 0.03% and results showed spatial variations in soil gas

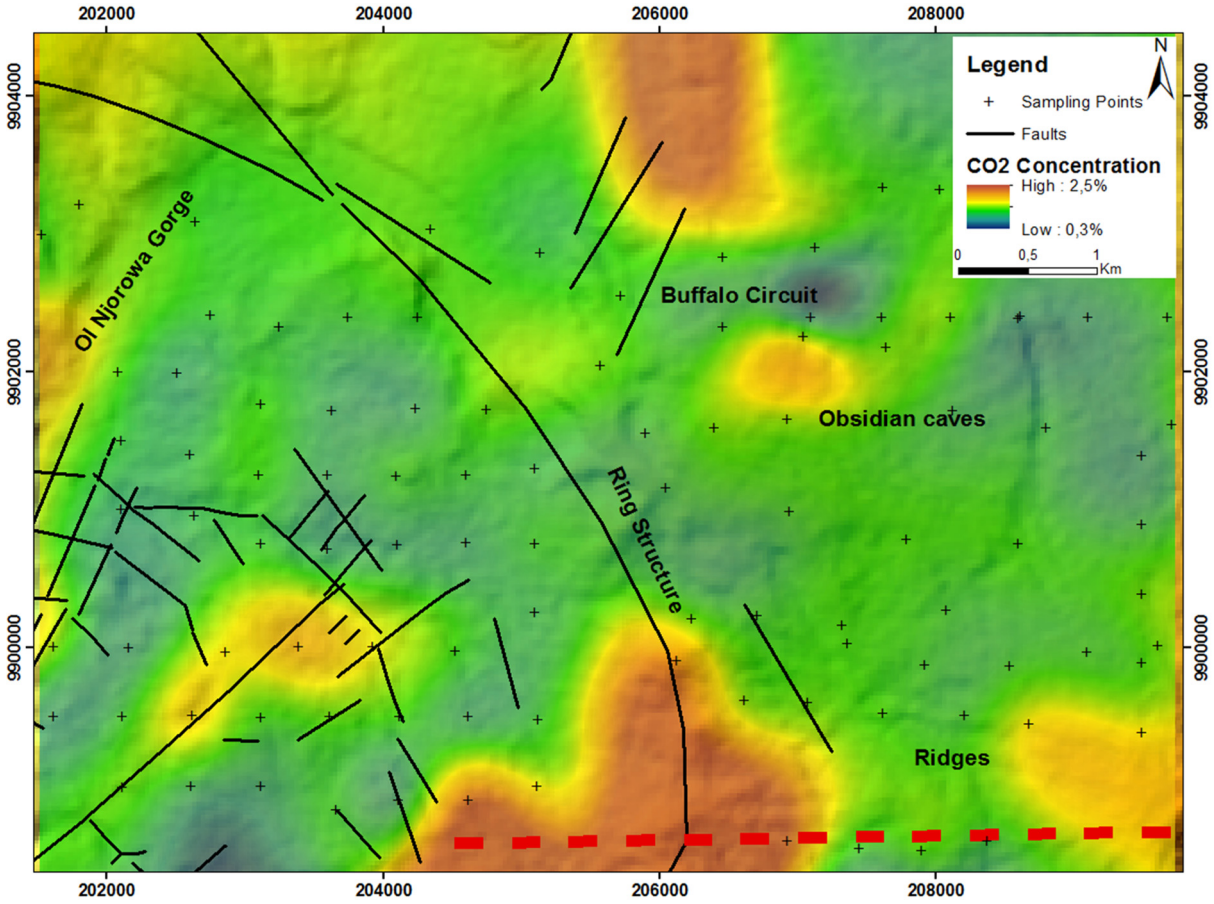

FIGURE 30: Soil gas map of CO2 gas survey carried out in Domes field. Station numbers are demarcated by the plus signs in the map and the red line to the south shows the preferred E-W alignment of CO2 anomalies

concentrations. High CO_2 concentrations were interpreted as sections of greater permeability causing accelerated gas diffusion from crustal magmatic sources. There is an E-W trend of high gas concentrations marked by the red dashed line, consistent with the occurrence of altered grounds (Figure 30). The trend runs from the ridge to the gorge at the southern part of the study area. Gas values range from 0.55 to 1.25% volume of the total gas phase. Some parts of the caldera floor show significantly lower CO_2 flux of 0.05% probably due to thick pyroclastics burial of their sources. CO_2 degassing of the soil along the E-W trending zone may have either been sourced from deep volcanic origin or from shallow organic sources. However, an anomaly occurs at the southern part of caldera floor with values of about 1% volume, which may be indicative of deep seated faults, eruption centres or shallow magmatic bodies (marked with a red dashed line in Figure 30). This appears cognate to the altered ground mapped close to the same area (Figure 26). The anomaly may be attributed to presence of fault intersections which may have been reactivated to allow partial permeability. Alternatively, the anomaly may be in close proximity to an upflow zone.

The area south of the ring structure has the highest CO_2 concentrations with values of 1.35% in volume (Figure 30). This zone hosts the major upflow zone in Domes field. This shows high level of permeability to the surface with a localised radial extent. A similar high anomaly is present to the southeast outside the ring structure but no wells have been drilled there to prove the extent of the geothermal resource.

Buffalo Circuit lies to the North east of the study area. It shows relatively low values compared to the rest of the field. The circuit is relatively flat with a thick pyroclastic cover. It is assumed to harbour limited geological structures due to its poor permeability. There is only one rhyolitic lava flow exposed at the Obsidian Caves tourist site (Figure 30). The rhyolite eruption centre may be the source of the CO_2 anomaly observed at these caves (Figure 30). Correlation of thermal and diffuse degassing anomalies

should be approached cautiously due to influences from gases emanating from magmatic bodies in the crust.

4.4.2 Radon gas survey

Radon gas surveys were also carried out simultaneously with CO_2 soil gas survey in this study. The Radon soil gas amounts were subtracted from background values specific to each station (see Appendix III). Radon is a decay product of Uranium-238 (U^{238}), which originates from deep magmatic sources. It is a naturally occurring radioactive noble gas produced from the radioactive decay of radium isotopes, which are the decay products of Uranium (U^{238}), Thorium (Th^{232}) and Uranium (U^{235}). The amount of concentration of Uranium and thorium in the bedrock is directly proportional to the volumes of radon in the soil. After radioactive decay of uranium and thorium, radon migrates through the soil by diffusion and convection. It moves along areas of weaknesses such as pore spaces, shear zones, faults and fractures. Due to its effective solubility in water, it is mainly used to infer areas of high permeability as well as upflow zones. Since radon gas has a short lived half-life of 3.8 days, it is a better indicator of permeability since it´s emanations may depend on other factors such as the degree of rock fracture.

Radon gas survey results show relatively low values with only two anomalies in the south of the ring structure of about 700 counts per minute (Figure 31). The two anomalies also show a preferred E-W orientation (marked with a red dashed line) similar to the altered grounds with high CO_2 soil concentrations which might be indicative of a similar magmatic source. This coincidence is an indication of faster travel rate of radon gas to the surface. It is not clear if the gas moves through fracture systems or is transported in solution by upwelling geothermal fluids. However, it is certain that the anomalies indicate permeability. Alternatively, the anomalies may be indicative of a short travel distance, probably from shallow magmatic sources.

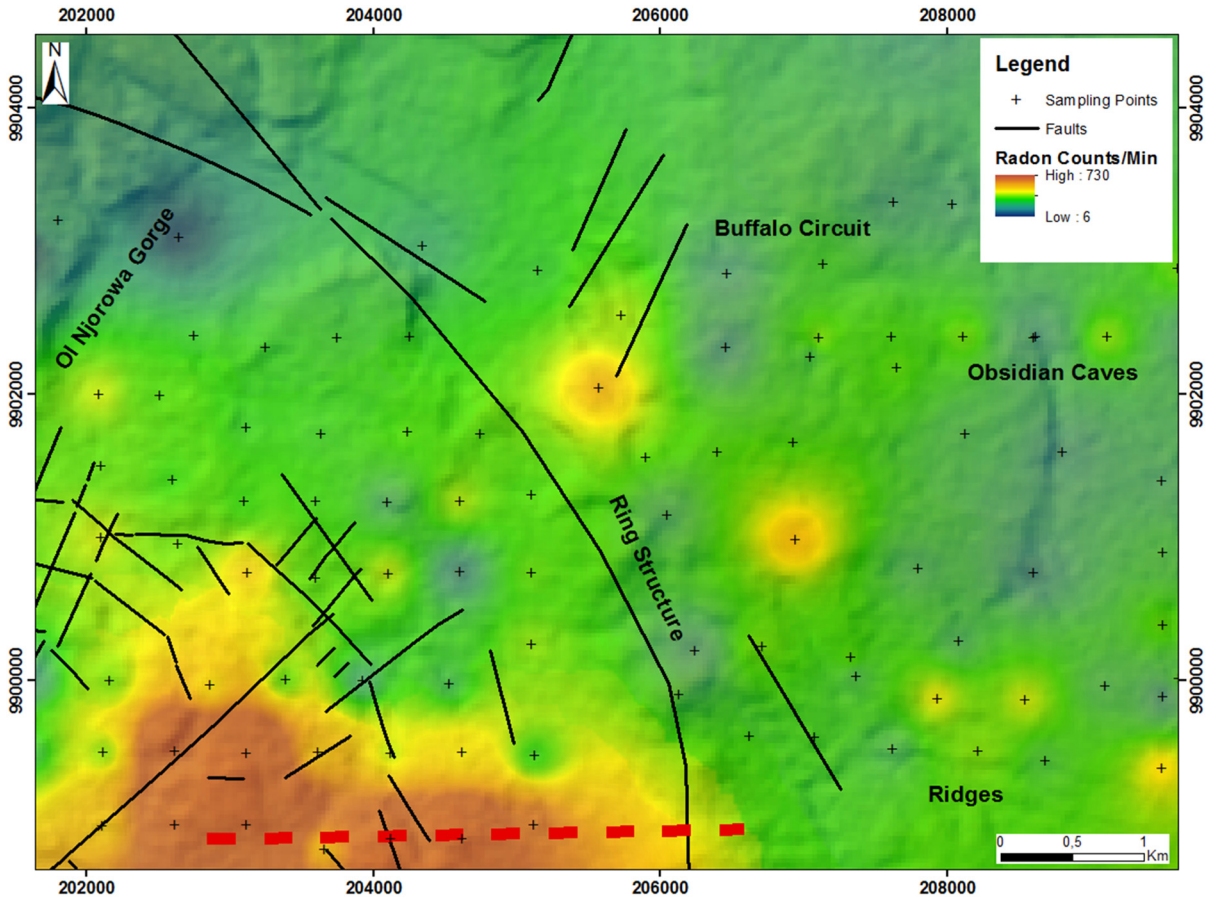

FIGURE 31: Map of radon gas values measured in Domes field showing the distinct red anomaly on the south of the study area. The red dashed line shows an E-W preferred orientation

5. DISCUSSION

The Greater Olkaria volcanic complex is a high temperature geothermal system with proven potential of more than 600 MWe (KenGen, 2015). The geothermal license lies within the Greater Olkaria volcanic complex. The current study was focused on Olkaria Domes geothermal field, which is the most recently developed field supplying bulk steam for electricity production. Olkaria IV geothermal power plant was commissioned in 2014 with a total installed capacity of 149.8 MWe (KenGen, 2015). An additional 140 MWe Olkaria V power plant is proposed to be constructed in the Domes field. The geology of the Olkaria Volcanic Complex is dominated by Pleistocene and Holocene lava flows and more recent pyroclastic deposits, mainly composed of ash falls from Longonot caldera (Woodhall, 1987 and Marshall *et al.,* 2009). The topography is dotted by at least 80 volcanic centres of Quaternary age forming steep sided domes formed as thick lava piles with limited lateral flow (Marshall *et al.,* 2009). Ololbutot comenditic lava is the youngest, erupted at 180 ± 50 yr BP (Clarke *et al.,* 1990).

5.1 Updated structural map of Olkaria Domes geothermal field

Faults in the Greater Olkaria Volcanic Complex are categorised under five types based on their strikes. They are; N-S, NE-SW, NW-SE, NNW-SSE and E-W. Fault average displacements range from 5 to 50 m. Ol Njorowa Gorge has a high density of NE-SW and NNE-SSW faults. Faults mapped during this study are mainly oriented NW-SE, NNW-SSE and NNE-SSW (Figure 32). Normal faults are the most dominant in Domes field dipping to the west, while compressional faults are rare depicting limited periods of crustal compression. Normal faults were formed by tensional forces during periods of rift spreading. There is a unique set of E-W faults along the ridges east of the Olkaria ring structure (Figure 32). The faults may have been formed by lateral movement of the lithosphere. They cut across pyroclastic layers and were observed along gullies east of Domes field.

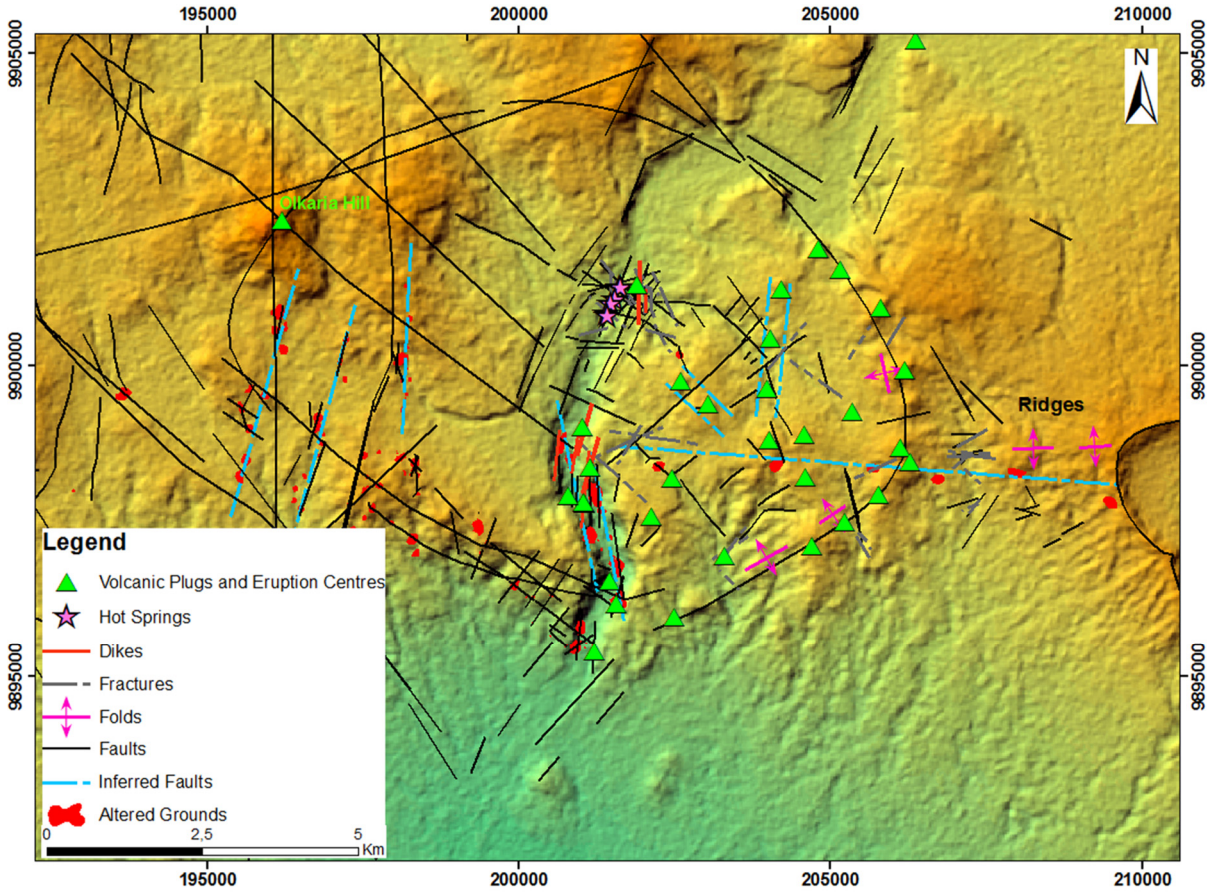

FIGURE 32: Updated structural map of Olkaria Domes field showing all features mapped during this study

Bosworth and Strecker (1997) dated the E–W and ENE–WSW oriented faults along the Kenyan rift and reported that they were formed between 12 and 0.6 Ma, while the NE–SW faults date back to 0.6 Ma. The constant change in direction is caused by changes in kinematic regimes being attributed to volcanic activities on both local and regional scales. Delvaux *et al.*, (1992) found evidences of compressional forces on the East African rift during the Cenozoic period. The Aswa lineament is one of the major transform zones with several NW-SE striking faults. These faults host some of the major volcanic centres on the EARS and produce major earthquakes in Africa (Chorowicz, 2005).

Left-lateral strike slip of rift shoulder faults was observed from DEMs affecting most parts of the Central Kenyan rift. The lateral movement is connected to the Aswa lineament which connects the Eastern and Western rifts to form the Victoria micro-plate (Chorowicz, 2005). Faults occur in close association with tectonic fractures. They show evidence of recent tensional forces whose sources are tectonic and volcanic in origin along the Kenyan rift system. They are formed due to negative principal compressive stress, σ_3, making them prominent only within the uppermost 1 km of the Earth's crust (Gudmundsson, 2011). Many fractures in Olkaria geothermal field therefore arise from tensile stress related to the Olkaria domal uplift. Both faults and fractures form good permeability when they are interconnected. Meteoric fluids move through these openings to recharge the geothermal reservoir.

Eruption centres and volcanic plugs were widely distributed in Domes field (Figure 32). They are sources of lava formed when magma conduits have successfully penetrated Earth's surface. Some eruption centres formed craters erupted under water along the ring structure due to flooding of Lake Naivasha (Omenda, 1998). Other eruption centres within domes field occur linearly and are believed to have been extruded along fault planes (Clarke *et al.,* 1990) (Figure 32). Volcanic plugs were observed along the Ol Njorowa Gorge. They form volcanic vertical elliptical pipes.

Altered grounds mainly occur along the Ol Njorowa Gorge and along the ring structure. Slightly altered grounds were also observed along the ridges where geothermal grass was noted. They are a result of surface alteration by hydrothermal fluid. Occurrence of surface alteration is closely associated with near surface permeability that encourages fluid movements. They are also indicative of an upflow region where hot hydrothermal fluids reach to near surface and cause argillic alteration, responsible for higher CO_2 and radon soil gas concentrations. The hot fluids may also come into contact with shallow groundwater to form hot springs found along the Ol Njorowa gorge (Figure 32). Their lateral distribution may be interpreted to show buried structures.

5.2 Olkaria conceptual model

Attempts have been made to improve understanding of the Olkaria geothermal system and create an accurate Olkaria Conceptual Model based on geology, geophysics and geochemistry data (SWECO and Virkir, 1976; Ofwona, 2002; West-JEC, 2009; MANNVIT/ÍSOR/Vatnaskil/Verkís Consortium, 2011). Reservoir characteristics over long time periods have also helped build the model by showing upflow and downflow zones (Ambusso and Ouma, 1991; Ofwona, 2002). This information has been key in developing and sustaining production from the geothermal reservoir.

Exploration of the geothermal potential began in 1956 when geological mapping and geophysical studies were carried out (Odongo, 1984). Deep drilling commenced in 1973 when two exploration wells were drilled. A basic conceptual model showing a boiling geothermal reservoir overlain by a steam zone capped by tuffaceous caprock was presented by SWECO and Virkir (1976). Feasibility studies carried out in 1976 proved that geothermal development in Olkaria was feasible. This decision led to the construction of the first geothermal power plant with a capacity of 15 MWe in 1981 (Ouma, 2009). Continued drilling increased the levels of understanding and the conceptual model extended towards the east covering Olkaria East Production field and extended eastwards to the Gorge Farm fault (Ofwona, 2002). Optimisation studies were carried out by West-JEC (2009), where the conceptual model was also revised to incorporate even more recent surface and subsurface data. The report recommended geothermal expansion towards the Olkaria Domes field. More recent studies have been carried out by

MANNVIT/ÍSOR/Vatnaskil/Verkís Consortium, (2011), where a more updated conceptual model has been constructed.

Despite many studies carried out in the last 40 years, there is still a challenge in understanding the Greater Olkaria volcanic complex. None of the proposed models confirm the presence of a caldera system in Olkaria geothermal field. The only evidence showing the presence of a caldera is the ring structure. The Greater Olkaria Volcanic Complex is bound by a ring structure formed by arcuate rhyolitic domes to the east, south and south west (Omenda, 1998) (Figure 32). This ring structure is presumed to represent remnants of a buried caldera that was later intruded by younger rhyolitic rocks (Naylor, 1972). Lack of sufficient subsurface data outside the ring structure has been a major setback in unearthing the evidence of a caldera system. However, an attempt to correlate the stratigraphic information outside the ring structure has been made using lithological logs from well OW-922 which was drilled about 2km east of the Domes field (Musonye, 2015). Rhyolites are lacking in the upper stratigraphic column outside the ring structure. This may imply that most of the comenditic lavas were post-caldera extrusions (Marshall *et al.,* 2009), which could not flow outside Olkaria volcanic complex, probably due to presence of a depression formed by the uneven collapsed slab.

According to Lipman (1997), uneven slab collapse may be caused by an asymmetrical morphology of a magma chamber that results to variations in lithostatic pressure. Evidence of uneven slab collapse in Olkaria would be ascertained by lack of a system of rhyolitic ring domes or a ring structure towards the northeast and east segments of the proposed caldera system. Deformation may be interpreted to be significantly higher to the east (towards Longonot) than to the west (towards Olkaria Hill) of Olkaria volcanic complex. This assumption is based on presence of shallow heat sources towards Olkaria East and Northeast production fields of the volcanic complex that are at minimum to the west of Olkaria hill (MANNVIT/ÍSOR/Vatnaskil/Verkís Consortium, 2011). Increased NE-SW faulting, dyking and fracturing episodes along Ol Njorowa Gorge and in Domes field may also be interpreted to mean more deformation, which may have been caused by greater subsidence to the east. This kind of uneven subsidence is categorised as trapdoor collapse where the west part forms a hinge of a door and the east is the panel that opens or subsides like a trapdoor (Lipman, 1997).

The Greater Olkaria Volcanic Complex has vast networks of faults that were formed during different tectonic episodes. The oldest faults are NW-SE and WNW-ESE which are related to formation of the Kenyan rift system (Mungania, 1999). The NE-SW are much younger and are related to the caldera collapse (Omenda, 1998). Their frequency is significantly high along the Ol Njorowa Gorge and in Domes field (Figure 32). They are also dominant along the south western arm of the ring structure (Otieno *et al.*, 2014). They are poorly distributed to the west. Most of the caldera faulting is also towards the east consistent with the deformation patterns forming the trapdoor collapse slab.

Dykes have a N-S trend and are exposed along the Ol Njorowa Gorge. They are associated with most recent N-S and NNE-SSW faulting and attest to the recent fault rejuvenation forming numerous fumeroles and craters along Ololbutot fault and at the gorge (Lagat, 2004; Musonye, 2015). Since dyke propagation is dependent on rock tensile strength, they were extruded when magma pressure superseded lithostatic pressure (Gudmundsson, 2011). The faults along the Ol Njorowa Gorge created weak points along fault planes. The young dykes form important heat sources as well as good permeability. When the dykes are intersected at deeper depths during geothermal drilling, they improve steam production. During drilling of well OW-921A, a dyke was intersected at a depth of 2126 m b.g.l. (KenGen, 2014). This may have improved the productivity of the well making it one of the biggest producers in Africa.

Figure 33 shows a chematic geological conceptual model of Olkaria showing relative locations of mapped faults east of Domes field

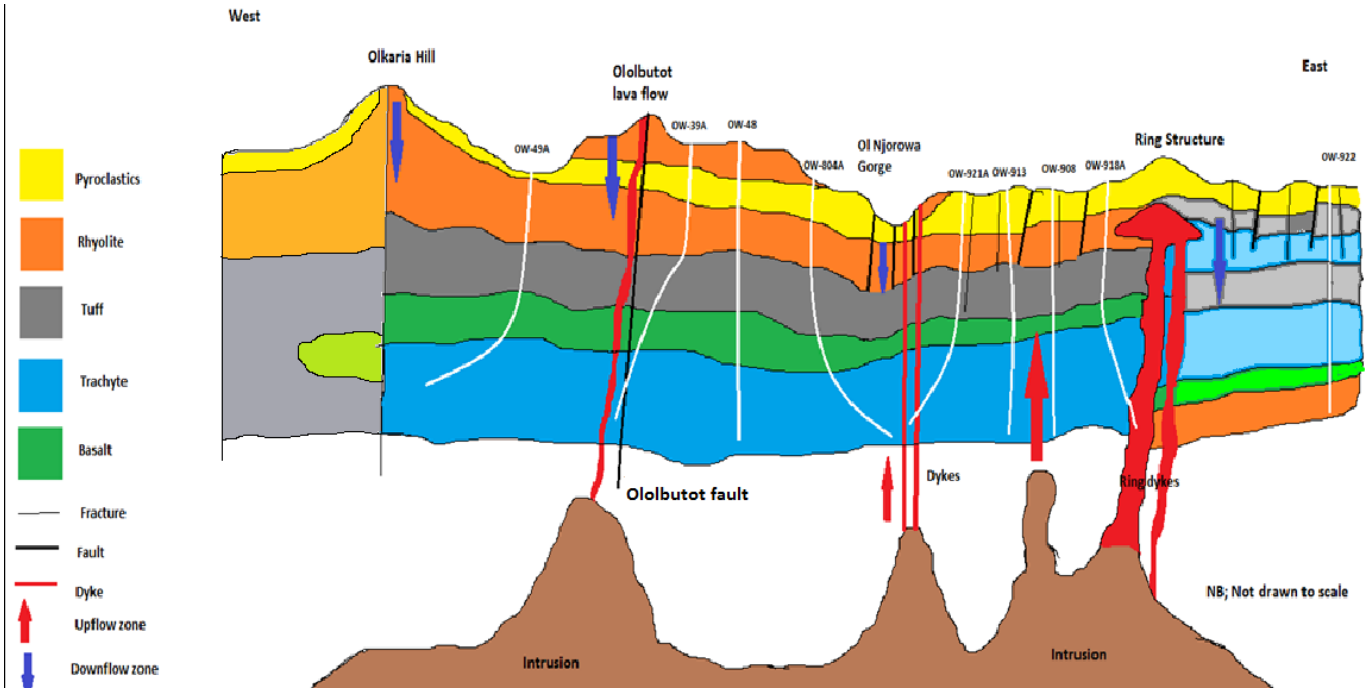

FIGURE 33: Schematic geological conceptual model of Olkaria showing relative locations of mapped faults east of Domes field. The figure is not drawn to scale

5.3 The knee joint structure

Preliminary structural geology study of the Central Kenyan rift was carried out by analysing Digital Elevation Models from ASTER GDEM. Regional normal fault trends depict periods of extensional deformation leading to lithostatic brittle failure (Corti, 2012). Deformation was initiated by the Kenyan plume whose origin is the upper mantle. Tensional forces favoured formation of normal faulting with near vertical inclinations. Regional transform faulting affected the Kenyan rift leading to changes in rift orientation from NW-SE to NE-SW. The lateral shift introduced the E-W oriented faults mapped east of Olkaria Domes field and Eburru massif (Mwania *et al.,* 2014). Study of DEMs led to the discovery of the knee joint structure which is a circular depression of 50 by 30 km similar to a collapsed caldera. It may have been formed during the period of lateral transform faulting leading to a brittle piston collapse. The subsidence resulted in dyke intrusions within Kijabe area, along the eastern scarp of the rift. Kijabe hill may have also been formed during this process. The shallow high density basaltic intrusions may be responsible for gravity reversals noted in several parts of Kenton area during field work, where localised negative gravity anomalies were experienced. Hot rock-water interactions are believed to form hot springs along the rift escarpment in Kijabe area.

Magnetic survey data from the Africa Magnetic Mapping Project (AMMP) analysed by Kuria *et al.*, (2010) was used to estimate the Curie Point Depth (CPD) of magnetic rocks in this region. Results show a shallow CPD on the Central Kenyan rift, immediately south of Lake Naivasha (Figure 14). These findings correspond to our observations in DEMs which envisages presence of a collapsed slab forming the knee joint structure. The shallow CPD may explain the heat source fuelling geothermal manifestations along the eastern escarpment. This magma reservoir may be the source of the peralkaline rocks dominating Olkaria and Longonot volcanoes (Figure 33). However, the differences in rock evolution may be due to presence of localised magma chambers for both Olkaria and Longonot which may have encouraged different degrees of magma fractionation and anatexis. More sub-surface data is required to ascertain this theory.

Kiyoo (1958) studied volcanic eruptions in Japan and concluded that primary volcanic landforms are created by the ascent and eruption of magma. The ascending magma displaces and interacts with surrounding rock and fluids as it creates new pathways. It causes propagation of cracks or conduits,

vesiculates, and accumulates in underground reservoir cavities. The formation of new pathways and pressure changes within existing conduits and reservoirs is responsible for causing stress build up and deforming the surrounding rock.

Dzurisin (2007) also studied many volcanic edifices in other parts of the World and carried out volcanic eruption simulations in controlled laboratory environments. Results show that surface deformation depends on the shape and size of the pressure source, pressure increment, and the elastic properties of the medium. For any particular source depth and geometry, the surface deformation scales with the ratio of the cavity pressure change to the half-space elastic modulus, and to a lesser extent with Poisson's ratio. Mathematical models are then created representing the Earth's crust as an ideal semi-infinite elastic body, known as an elastic half-space that is materially homogeneous and mechanically isotropic and it obeys Hooke's law. The models created are used to estimate surface deformation caused by changes in magma chamber pressure during periods of volcanic unrest. The magma chambers are conceptualised as fluid pressurised ellipsoidal cavities that cause ellipsoidal surface deformation in an elastic half space.

The current study concludes that the knee joint structure (Figure 34) is an ellipsoidal deformed structure that may have been formed by pressure changes in the magma cavity beneath. Presence of a magma chamber have been confirmed by the shallow CPD observed by Kuria *et al.,* (2010).

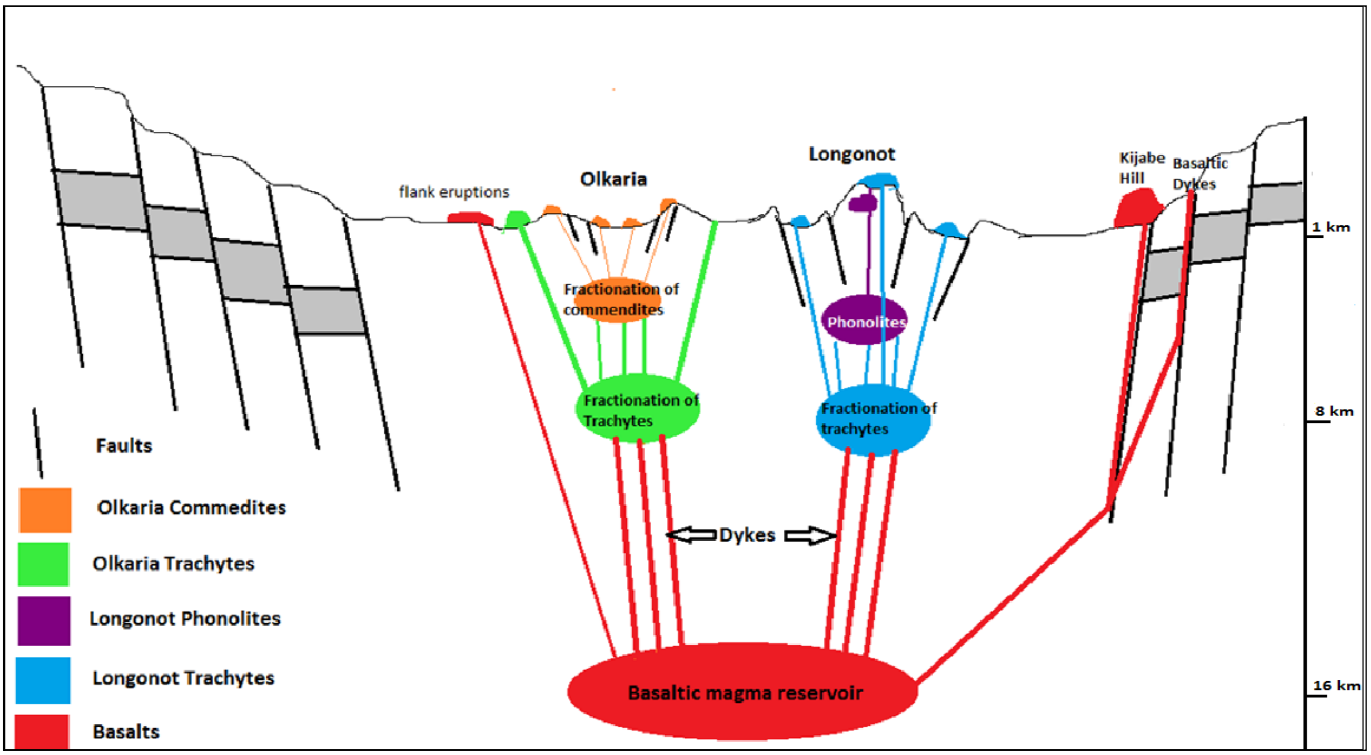

FIGURE 34: The schematic model of the knee joint structure located on the Central Kenyan rift showing an expression of its geometry; the figure is not drawn to scale

6. CONCLUSION

Olkaria geothermal field is a high temperature geothermal system with a proven potential of more than 650 MWe. The geothermal potential is enhanced by interconnected fracture and fault networks creating a percolation threshold that sustains hydrothermal fluid flux. The faults are classified under five types based on their strikes. They include; N-S, NE-SW, NW-SE, NNW-SSE and E-W. Fault average displacements range from 5 to 50 m based on field measurements. The N-S faults are located along the Ol Njorowa Gorge and Ololbutot fault. They were formed by young magma resurgence evidenced by dykes, volcanic plugs and eruption centres erupted less than 3280±120 Bp.

The ring structure may have a system of rhyolitic dykes and cone sheets which may have fed the shallow rhyolitic domes at shallow depths. The ring dykes may act as barriers preventing cold fluids from infiltrating Olkaria Domes field from the east. Olkaria geothermal complex may be classified as a trap door volcanic system formed due to asymmetrical geomorphology of its magma chamber. During the pre-caldera volcanic eruptions, the emptying of the magma chamber may have been uneven, resulting in a larger collapse of the southeast and southwest parts and formed the arcuate ring structure. The north and west parts may have acted as the hinges where less deformation and lack of ring faults was observed.

The geothermal potential of the ridges east of Domes field has not yet been proven. Subsurface data along the ridge is lacking since no deep drilling has been carried out. An exploratory well, OW-922, was drilled a few kilometres north of the ridge but it did not sustain discharge upon testing. Based on geophysical resistivity profiles, the ridge may contain a localised intrusion which may form a localised heat source. The envisaged intrusions may have originated from either Olkaria or Longonot peripheral eruptions. The company should manage their expectations while investing capital resources to explore this region.

The Central Kenyan Rift may have been subjected to transform faulting during the rifting process. Left lateral strike slip movement was observed in DEMs along rift shoulder faults. The knee joint structure may have been formed by piece meal type subsidence of a piston due to under-pressurised shallow magma cavity at a depth of about 15.9 km b.g.l. Extrusion of basaltic dykes along Kijabe area may have resulted to emanation of hot springs and CO_2 rich grounds which form prominent surface geothermal manifestations in Kenton and Kereita areas.

7. RECOMMENDATIONS

The area east of the Domes field has not been explored fully. Geophysical data is scarce and only one well has been drilled. There is need to carry out additional interdisciplinary scientific work in the area to understand the geothermal potential.

Volcanology and geodetic research of the Greater Olkaria Geothermal Complex is required to monitor reservoir pressure changes. GPS deformation measurements as well as InSAR studies will assist in observing surface deformation caused by magma chamber pressure changes and contribute in creating more precise deformation models based on Mogi point source modelling method. The surveys could also be used to determine pressure reduction in the geothermal reservoir due to mass abstraction of steam in Olkaria geothermal field. The geodetic surveys can be complemented by gravity measurements which can also show density reduction due to mass geothermal fluid abstraction. Trace element and isotope studies of all volcanic rocks penetrated during drilling in Olkaria would considerably improve understanding of magma sources and process involved in magma movement.

The knee joint structure was discovered during this study but there is insufficient data to classify it to a caldera. Intensive geophysical measurements should be done to confirm the existence of the shallow magma source as well as local intrusions in the Kijabe area that may host geothermal potential. Bulk rock petrochemistry and trace element analysis of subsurface rocks, which may be obtained during deep drilling in Longonot, Suswa and Mt. Margaret, needs to be carried out in the long term. This will determine or confirm any relation of magma evolution processes.

REFERENCES

Abrams, M., Tsu, H., Hulley, G., Iwao, K., Pieri, D., Cudahy, T., and Kargel, J., 2015: The Advanced Spaceborne Thermal Emission and Reflection radiometer (ASTER) after fifteen years. Review of global products. *Intern. J. Applied Earth Observation and Geoinformation, 38,* 292-301.

Ambusso, W.J., and Ouma, P.A., 1991: Thermodynamic and permeability structure of Olkaria Northeast field: Olkaria fault. *Geothermal Resource Council, Transactions, 15*, 237-242.

Awange, J.L., Forootan, E., Kusche, J., Kiema, J.B.K., Omondi, P.A., Heck, B., Fleming, K., Ohanya, S.O., and Gonçalves, R.M., 2013: Understanding the decline of water storage across the Ramsar - Lake Naivasha using satellite-based methods. *Advances in Water Resources, 60*, 7-23.

Baker, B.H., 1970: The structural pattern of the Afro-Arabian rift system in relation to plate tectonics. *Philosophical Transactions, Royal Society of London, Series A267,* 383-391.

Baker B.H., Mohr, P.A., and Williams, L.A.J., 1972: Geology of the Eastern Rift System of Africa. *Geological Society of America, Special Paper 136*, 1-67.

Baker, B.H., Williams, L.A.J., Miller, J.A., Fitch, F.J., 1971: Sequence and geochronology of the Kenya rift volcanics. *Tectonophysics, 11*, 191-215.

Baker B.H., and Wohlenberg, J., 1971: Structure and evolution of the Kenya rift valley. *Nature, 229,* 538-542.

Biggs J., Anthony, E.Y., and Ebinger, C.J., 2009: Multiple inflation and deflation events at Kenyan volcanoes, East African Rift. *Geological Society of America, 37-11*, 979–982

Bonini, M., Corti, G., Innocenti, F., Manetti, P., Mazzarini, F., Abebe, T., and Pecskay, Z., 2005: Evolution of the Main Ethiopian Rift in the frame of Afar and Kenya rifts propagation. *Tectonics, 24-1.*

Bosworth, W., and Strecker, M.R., 1997: Stress field changes in the AfroArabian rift system during the Miocene to recent period. *Tectonophysics, 278*, 47–62.

Browne P.R.L., 1984: Subsurface stratigraphy and hydrothermal alteration of the eastern section of the Olkaria geothermal field, Kenya. *Proceedings of the 6th New Zealand Geothermal Workshop, Geothermal Institute, Auckland, NZ,* 33-41.

Browning, J., and Gudmundsson, A., 2015: Caldera faults capture and deflect inclined sheets: An alternative mechanism of ring-dyke formation. *Bulletin of Volcanology,* 77, 889, 33 pp.

Chorowicz, J., 2005: The East African rift system. *J. African Earth Sciences, 43-1/3,* 379–410.

Chorowicz J. Le Fournier J., and Vidal, G., 1987: A model for rift development in Eastern Africa. In: Bowden, P., and Kinnaird, J. (eds.), *African Geology Reviews, Geological Journal, 22 (thematic issue)*, 495–513.

Clarke, M.C.G., Woodhall, D.G., Allen, D., and Darling, G., 1990: *Geological, volcanological and hydrogeological controls of the occurrence of geothermal activity in the area surrounding Lake Naivasha, Kenya.* Ministry of Energy, Kenya, report.

Corti, G., 2012: Evolution and characteristics of continental rifting: Analog modelling-inspired view and comparison with examples from the East Africa Rift System. *Tectonophysics, 522-523-1,* 1-33.

Corti G., van Wijk, J., Cloetingh S., and Morley, C.K., 2007: Tectonic inheritance and continental rift architecture: Numerical and analogue models of the East African Rift system. *Tectonics, 26,* 13 pp.

Darling, W.G., Griesshaber, E., Andrews, J.N., Ármannsson, H., and O'Nions, R.K., 1995: The origin of hydrothermal and other gases in the Kenya Rift Valley. *Geochim. Cosmochim. Acta, 59-12,* 2501-2512.

Delvaux, D., Levi, K., Kajara, R., and Sarota, J., 1992: Cenozoic paleostress and kinematic evolution of the Rukwa-North Malawi rift valley (East African rift system). *Bulletin des Centres de Recherche, Exploration Production Elf-Aquiaine, 16-2, 383–406.*

Dimitrios, G., 1989: *Magnetotelluric studies in geothermal areas in Greece and Kenya.* University of Edinburgh, PhD thesis, Edinburgh.

Dzurisin D., 2007: *Volcano deformation geodetic monitoring techniques*. Springer and Praxis publishing, Chichester, UK, 435 pp.

EEE, Ltd., 2016: *Orsat apparatus*. Eternal Engineering Equipment - EEE, webpage: *www.eeepune.com/images/thr15big.gif.*

ESA, 2010: *Using ASAR*. European Space Agency – ESA, webpage: *www.esa.int/Our_Activities/Observing_the_Earth/Living_Planet_Symposium/Volcanic_uplift.*

Furgerson R.B., 1972: *Electrical resistivity survey of the Olkaria project, Kenya*. East African Power & Lighting Co., Ltd., Geothermal Exploration Project, report.

Galland, O., Burchardt, S., Hallot, E., Mourgues, R., and Bulois, C., 2014: Dynamics of dykes versus cone sheets in volcanic systems. *J. Geophysical Research, 119-8,* 6178-6192.

Giordano, G., Pinton, A., Cianfarra, P., Baez, W., Chiodi, A., Viramonte, J., Norini, G.,Groppelli, G., 2013: Structural control on geothermal circulation in the Cerro Tuzgle - Tocomar geothermal volcanic area (Puna plateau, Argentina). *J. Volcanol.& Geotherm. Res., 249*, 77–94.

Gregory, J.W., 1896: *The Great Rift Valley*. John Murray, London, 422 pp.

Gudmundsson, A., 2011: *Rock fractures in geological processes.* Cambridge University Press, Cambridge, 594 pp.

Gudmundsson, A., and Nielsen, K., 2006: Ring-faults in composite volcanoes: structures, models and stress fields associated with their formation. *Geological Society of London, Special Publications, 269,* 83-108.

Guth, A., and Wood, J., 2013: *Geological map of the Southern Kenyan Rift.* The Geological Society of America, Colorado.

Harkin, P.A., 1960: The Rungwe volcanics at the northern end of lake Nyasa. *Memoir Geological Survey of Tanganyika, 2,* 172.

Harris, R.P., 1969: Basalt type and African Rift valley tectonism. *Tectonophysics 8-4/6,* 567–577.

He M.Y., Evans, A.G., and Hutchinson, J.W., 1994: Crack deflection at an interface between dissimilar elastic materials: role of residual stresses. *Int. J. Solids Struct., 31,* 3443–3455.

Heath, R.C., 1983: *Basic groundwater hydrology*. US Geological Survey, Reston, VI, 86 pp.

Hutchison, J.W., and He M.Y., 1989: Crack deflection at an interface between dissimilar elastic materials. *Int. J. Solids Struct., 25-9,* 1053–1067.

Hutchison, J.W., Mather, T.A., Pyle, D.M., Biggs, J., and Yirgu, G., 2015: Structural controls on fluid pathways in an active rift system: A case study of the Aluto volcanic complex. *Geosphere, 11-3, 542-562.*

Karingithi, C.W., 1999: *Olkaria Domes geochemical model*. KenGen - Kenya Electricity Generating Company, Ltd, Kenya, internal report, 30 pp.

KenGen, 2014: *Stratigraphy logs for well OW-918A and OW-921A*. KenGen, Kenya, internal report.

KenGen, 2015: *Audited annual results for the year ending June 2015*. KenGen - Kenya Electricity Generating Company, Ltd, Kenya, report.

KenGen, 2016: *Geothermal projects status April 2016*. KenGen – Kenya Electricity Generating Comp., Ltd., Kenya, internal report.

Kenya Power, 2015: *Annual report and financial statements for financial year ended 30 June 2015.* Kenya Power and Lighting Company, Ltd. - KPLC, Kenya, report.

Kiyoo, M., 1958: Relations between the eruption of various volcanoes and the deformations of the ground surfaces around them. *Earthquake Research Institute, 36*, 99-134.

KRISP Working Group, 1991: The Kenya Rift: pure shear extension above a mantle plume. *Nature, 345,* 223–227.

Kuria Z.N., Woldai, T., van der Meer, F.D., and Barongo, J.O., 2010: Active fault segments as potential earthquake sources: Inferences from integrated geophysical mapping of the Magadi fault system, southern Kenya Rift. *J. African Earth Sci., 57-4,* 345–359.

Lagat, J.L., 2004: *Geology, hydrothermal alteration and fluid inclusion studies of Olkaria Domes geothermal field, Kenya.* University of Iceland, MSc thesis, UNU-GTP, Iceland, report 2, 71 pp.

Lichoro, C.M., 2009: Joint 1-D inversion of TEM and MT data from Olkaria Domes geothermal area, Kenya. Report 16 in: *Geothermal training in Iceland 2009*. UNU-GTP, Iceland, 289-318.

Lillesand, T.M. & Kiefer, R.W., 2004: Remote sensing and image interpretation (4th ed.). John Wiley & Sons, NY, 736 pp.

Lipman, P.W., 1997: Subsidence of ashflow calderas: relation to caldera size and magma geometry. *Bull. Volcanol., 59,* 198–218.

Liu, J.G., and Mason, P.J., 2009: *Image processing and GIS for remote sensing*. Wiley Blackwell publication, John Wiley and Sons Ltd., NY, 472 pp.

MacDonald R., Belkin, H.E., Fitton, J.G., Rogers, N.W., Nejbert, K., Tindle, A.G., and Marshall, A.S., 2008: The roles of fractional crystallization, magma mixing, crystal mush remobilization and volatile-melt interactions in the genesis of a young basalt-peralkaline rhyolite suite, the Greater Olkaria Volcanic Complex, Kenya Rift Valley. *J. Petrology, 49,* 1515-1547.

MANNVIT/ÍSOR/Vatnaskil/Verkís Consortium, 2011: Consultancy services for geothermal optimization study of the Greater Olkaria geothermal fields, Report 3: Revision of the conceptual model of the Greater Olkaria Geothermal System – Phase I. Mannvit/ÍSOR/Vatnaskil/Verkís, Reykjavík, November 2011, 100 pp.

Marshall A.S.l., Macdonald, R., Rogers, N.W., Fitton, J.G., Tindle, A.G.N., Nejbert, K., and Khinton, R.W., 2009: Fractionation of peralkaline silicic magmas: The Greater Olkaria volcanic complex, Kenya Rift Valley. *J. Petrol., 50,* 323-359.

McCall, G.J.H., 1957: The Menengai caldera, Kenya Colony. *The 20th International Geological Congress, Section I-1,* 55–69.

McConnel, R.B., 1959: Outline of the geology of the Ruwenzori Mountains. *Colonial Geological Mining Research, 7,* 245–268.

McKenzie, D.P., Davies, D., and Molnar, P., 1972: Plate tectonics of the Red Sea and East Africa. *Nature, 224*, 125–133.

MOE, 2015: *Draft national energy and petroleum policy*. Ministry of Energy and Petroleum, Kenya Government, Press.

Mohr, P.A., 1962: The Ethiopian rift system. *Bull. Geophysical Observatory Addis Ababa, 5,* 33-62.

Mohr, P.A., 1970. The Afar triple junction and sea-floor spreading. *J. Geophysical Research, 75*, 7340–7352.

Muchemi, G.G., 1992: *Structural map of Olkaria geothermal field showing inferred ring structures.* Kenya Power Company, internal report.

Muchemi G.G., 1998: Geothermal exploration in the Kenyan rift. *Proceedings of the "20th Anniversary Workshop of the United Nations University Geothermal Training Programme", organized by UNU-GTP, Reykjavik, 121*-130.

Muchemi, G.G., 2000: *Conceptual model of Olkaria geothermal field*. KenGen, Kenya, internal report.

Mungania, J., 1999: *Geological report of well OW-714*. Kenya Power Company, internal report.

Musonye, X.S., 2012: Borehole geology and alteration mineralogy of well OW-914A, Domes Area, Olkaria geothermal field, Central Kenya Rift. Report 23 in: *Geothermal training in Iceland 2012*. UNU-GTP, Iceland, 501-540.

Musonye X.S., 2015: *Sub-surface petrochemistry, stratigraphy and hydrothermal alteration of the domes area, Olkaria geothermal field, Kenya.* University of Iceland, MSc thesis, UNU-GTP, Iceland, report 3, 100 pp.

Mwangi, M.N., 1986: *Interpretation of additional sounding data at Olkaria, Kenya*. Kenya Power Company, internal report.

Mwania, M., Kandie, R., Kubai, R., and Oketch, E., 2014*: Structural mapping of Eburru geothermal field, 5th May - 20th July, 2014.* KenGen, Kenya, internal report, 46 pp.

Naylor, W.I., 1972: *Geology of the Eburru and Olkaria prospects.* UN Geothermal Exploration Project, report.

Odongo, M.E.O., 1984: *Geology of Olkaria geothermal field.* Kenya Power Company, Ltd., Geothermal project, Kenya. report GL/OW/020.

Ofwona, C.O., 2002: *A reservoir study of Olkaria East geothermal system, Kenya*. University of Iceland, MSc thesis, UNU-GTP, Iceland, report 1, 74 pp.

Omenda, P.A., 1994; The geological structure of the Olkaria west geothermal field, Kenya. *Proceedings of the 19th Stanford Geothermal Reservoir Engineering Workshop, Stanford, Ca*, 125-130.

Omenda P.A., 1998: The geology and structural controls of the Olkaria geothermal system, Kenya. *Geothermics, 27-1,* 55-74.

Omenda P.A., 2000: Anatectic origin for Comendite in Olkaria geothermal field, Kenya Rift; geochemical evidence for syenitic protholith. *African J. Science and Technology, Science and Engineering series, 1,* 39-47.

Omenda P., 2014: Geothermal country update report for Kenya: 2014. *Presented at Short Course IX on Exploration for Geothermal Resources, organized by UNU-GTP, GDC and KenGen, at Lake Bogoria and Lake Naivasha, Kenya,* 10 pp.

Omenda P., and Simiyu, S., 2015: Country update report for Kenya 2010-2014. *Proceedings of the World Geothermal Congress 2015, Melbourne, Australia,* 11 pp.

Omenda P., Simiyu, S., and Muchemi, G., 2014: Geothermal country update report for Kenya: 2014. *Proceedings of the ARGeo-C5, Conference, Arusha, Tanzania*, 29-31.

Onacha, S.A., 1989: *An electrical resistivity study of the area between Mt. Suswa and the Olkaria geothermal field, Kenya*. University of Nairobi, MSc Thesis.

Onacha, S.A. 1999: *Geophysical model of Olkaria-Domes geothermal field*. Kenya Electricity Generating Company (KENGEN), internal report.

Ormat, 2015: *Ormat global project map*. Ormat, webpage: *www.ormat.com/global-project*.

Otieno, V., Munyiri, S., Wanjohi, D., Okoo, J., and Wanjohi, A., 2014: *Structural mapping of Olkaria Southwest, Olkaria geothermal field, 5th May - 20th July, 2014.* KenGen, Kenya, internal report, 46 pp.

Ouma, P., 2009: Geothermal exploration and development of the Olkaria geothermal field. Presented at *Short Course IV on Exploration for Geothermal Resources, Lake Naivasha, Kenya*, organized by UNU-GTP, KenGen and GDC, 16 pp.

Peacock, D.C.P., Knipe, R.J., and Sanderson, D.J., 1999: *Glossary of normal faults. J. Structural Geology, 22,* 291-305.

Saemundsson, K., 2007: Structural geology – tectonics, volcanology and geothermal activity. *Presented at Short Course II on Surface Exploration for Geothermal Resources, Naivasha, Kenya, organized by UNU-GTP and KenGen*, 11 pp.

Simiyu, S.M., 2010: Status of geothermal exploration in Kenya and future plans for its development. *Proceedings of the World Geothermal Congress 2010, Bali, Indonesia*, 11 pp.

Simiyu, S.M., and Keller, G., 1997: An integrated analysis of the lithospheric structure across the east African plateau based on gravity analysis and recent seismic studies. *Tectonophysics, 278,* 291-313.

Simiyu, S.M., Omenda, P.A., Keller, G.R and Antony, E.Y., 1995: Geophysical and geological evidence of the occurrence of shallow intrusion in the Naivasha sub-basin of the Kenya rift. *AGU Fall 1995 Meeting, Abst. F657,* V21A-12.

Smith, M., and Mosley, P., 1993: Crustal heterogeneity and basement influence on the development of the Kenya Rift, East Africa. *Tectonics 12-2,* 591–606.

Smith, W.C., 1931: A classification of some rhyolites, trachytes and phonolites from part of Kenya Colony, with a note on some associated basaltic rocks. *P.J. Geological Society London, 87,* 212–258.

Suess, E., 1891: Die Brüche des östlichen Africa (in German). *Beitrage zur Geologischen Kenntnis des östlichen Africa, Denkschriften Kaiserlichen Akademie der Wissenschaftl. Klasse, Wien, 50,* 555–556.

SWECO-Virkir, 1976: *Feasibility report for the Olkaria geothermal project.* United Nations, Government of Kenya, report.

Thompson A.O., 1964: *Geology of Kijabe area*. Ministry of Natural Resources, Mines & Geology department, Kenya Government Press.

Todd, D.K., and Larry, W.M., 2005: *Groundwater hydrology* (3rd ed.) John Wiley and Sons, Inc., NY, 656 pp.

Tole, M.P., 1996: Geothermal energy research in Kenya: a review. *J. African Earth Sciences, 23-4,* 565-575.

Tsang, C.F., and Neretnieks, I., 1998: Flow channelling in heterogeneous fractured rocks. *Reviews of Geophysics, 36-2,* 275–298.

Van der Meer, F., Hecker, C., van Ruitenbeek, F., van der Werff, H., de Wijkerslooth, C., and Wechsler, C., 2014: Geologic remote sensing for geothermal exploration: A review. *Internat. J. Applied Earth Observation and Geoinformation, 33,* 255-269.

VIRKIR Consulting Group, 1980: *Geothermal development at Olkaria.* Report prepared for Kenya Power Company, 40 pp.

Wamalwa R.N., 2014: Structural controls on the chemistry and output of the wells in the Olkaria geothermal field, Kenya. *Proceedings of the ARGeo-C5 Conference, Arusha, Tanzania*, 14 pp.

Wambugu, J.M., 1995: *Geochemical update of Olkaria West geothermal field.* Kenya Power Company, Ltd., internal report, 40 pp.

Wambugu, J.M., 1996: *Assessment of Olkaria Northeast geothermal reservoir, based on well discharge chemistry.* Kenya Power Company, Kenya, internal report.

Wang P. and. Xu L.R., 2006: Dynamic interfacial debonding initiation induced by an incident crack. *Int. J. Solids Struct., 43,* 6535–6550.

Wanjohi, A.W., 2014: *Geophysics report of the Great Olkaria geothermal area*. KenGen, Kenya, internal report.

West-JEC, 2009: *The Olkaria optimization study (phase II) – Final reservoir analysis report.* West Japan Engineering Consultants, Inc., report, 301 pp.

Wheildon, J., Morgan, P., Williamson, K.H., and Swanberg, C.A., 1994: Heat flow in the Kenya rift zone. *Tectonophysics, 236,* 131-149.

Wohlenberg, J., 1969: Remarks on the seismicity of East Africa between 4 N – 12 S and 23 E – 40 E. *Tectonophysics 8-4/6,* 567–577.

Wood, J., and Guth, A., 2015: *East Africa's Great Rift Valley: A complex rift system*. Michigan Technological University, webpage: *geology.com/articles/east-africa-rift.shtml.*

Woodhall, D.J., 1987: *Geology of Longonot volcano, The Greater Olkaria Volcanic Complex and adjacent areas.* British Geological Survey, report BGSGENKEN/5, 15-16.

Xu W., Zheng, R.Z., Ma, W., Song F.M., and Yu, G.H., 2003: Pattern of latest tectonic motion and its dynamics for active blocks in Sichuan-Yunnan region, China. *Science in China, Series D: Earth Sciences, 46-2,* 210-226.

Yong Technology Inc., 2016: *On-line rose diagram*. Yong Technology Inc., webpage: *www.yongtechnology.com/yong-lab/online-rose-diagram.*

APPENDIX I: Clay analysis data for selected samples

STATION 16 OLKARIA

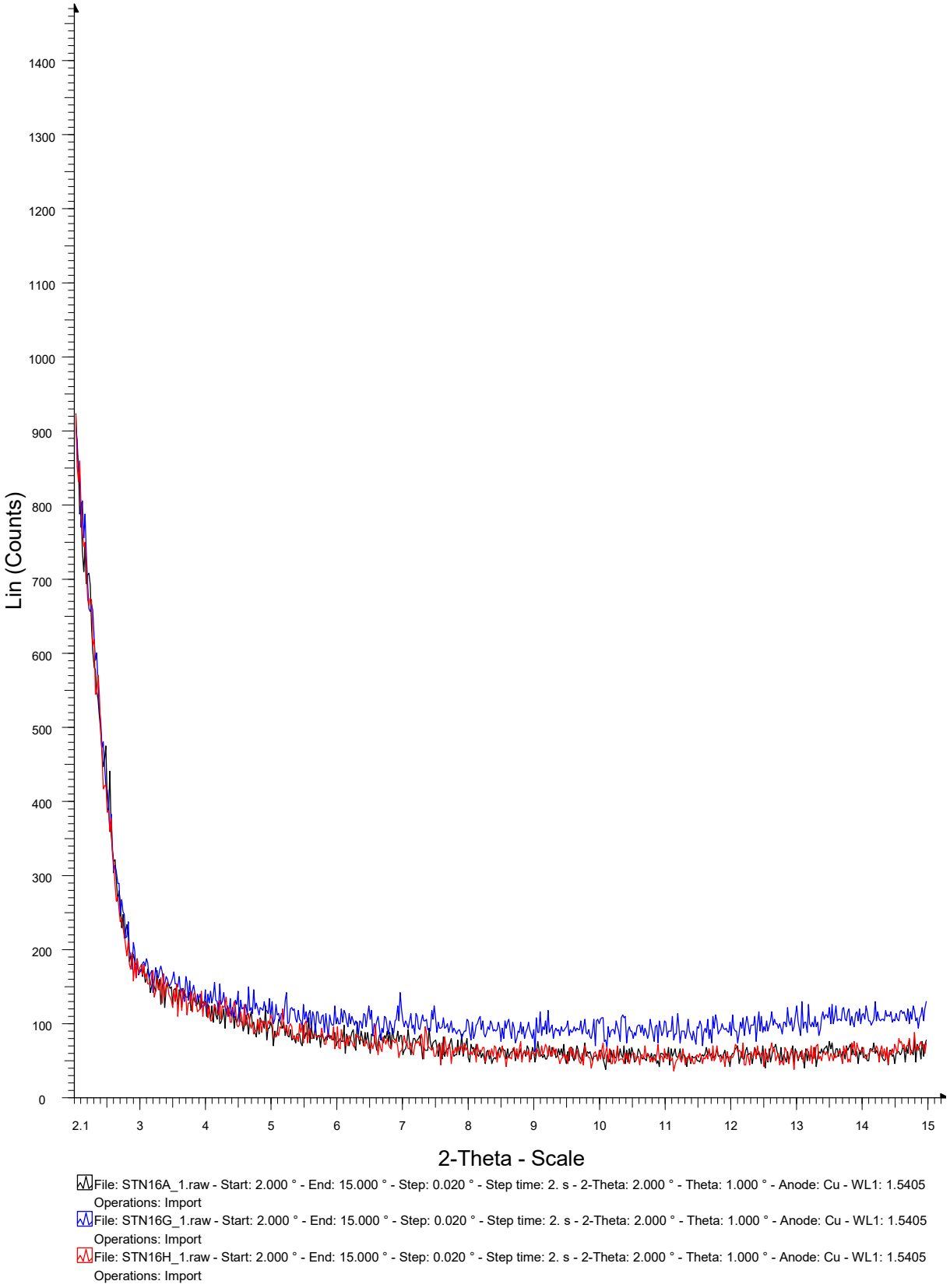

STATION 32 OLKARIA

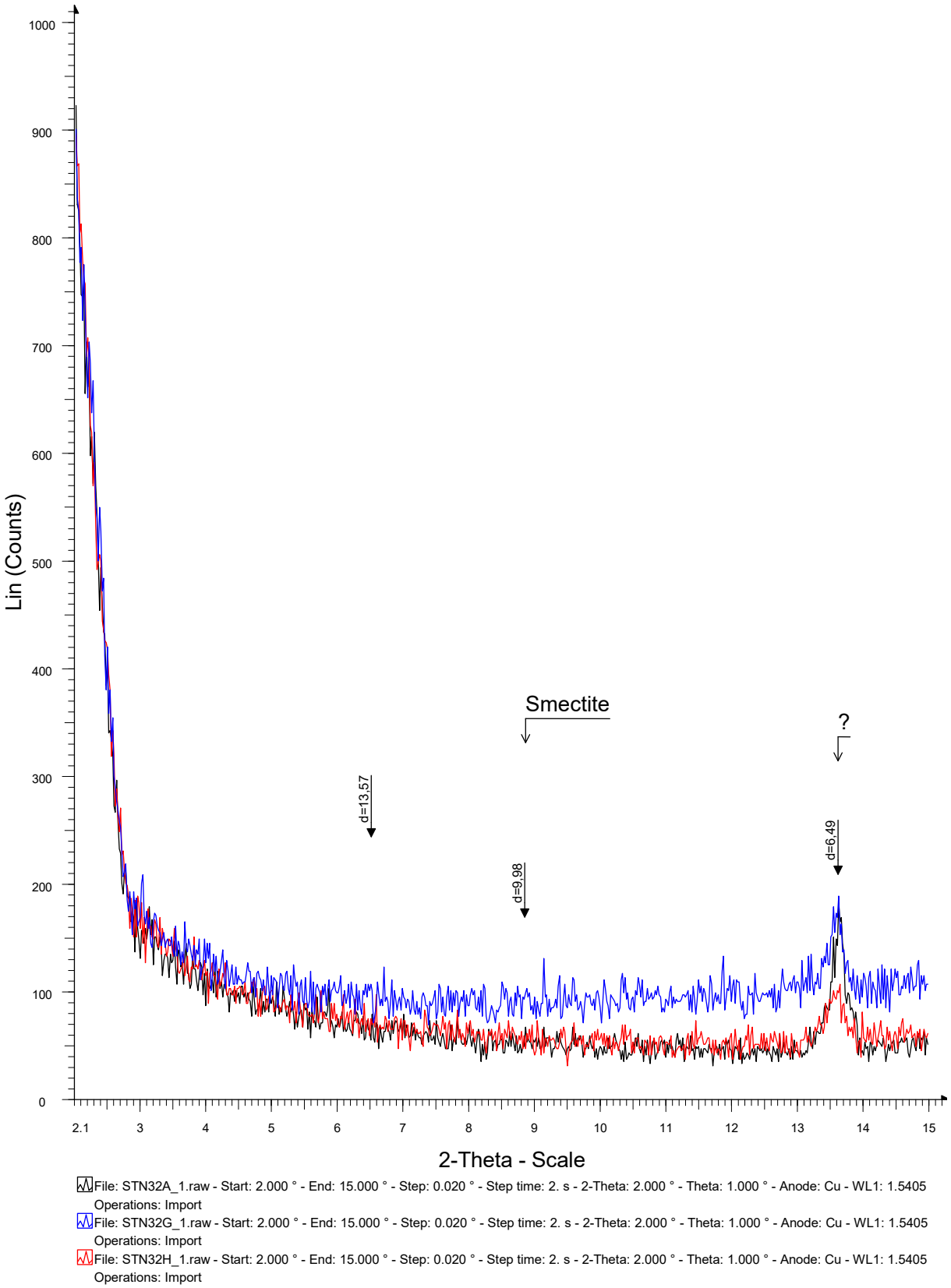

STATION 53 OLKARIA

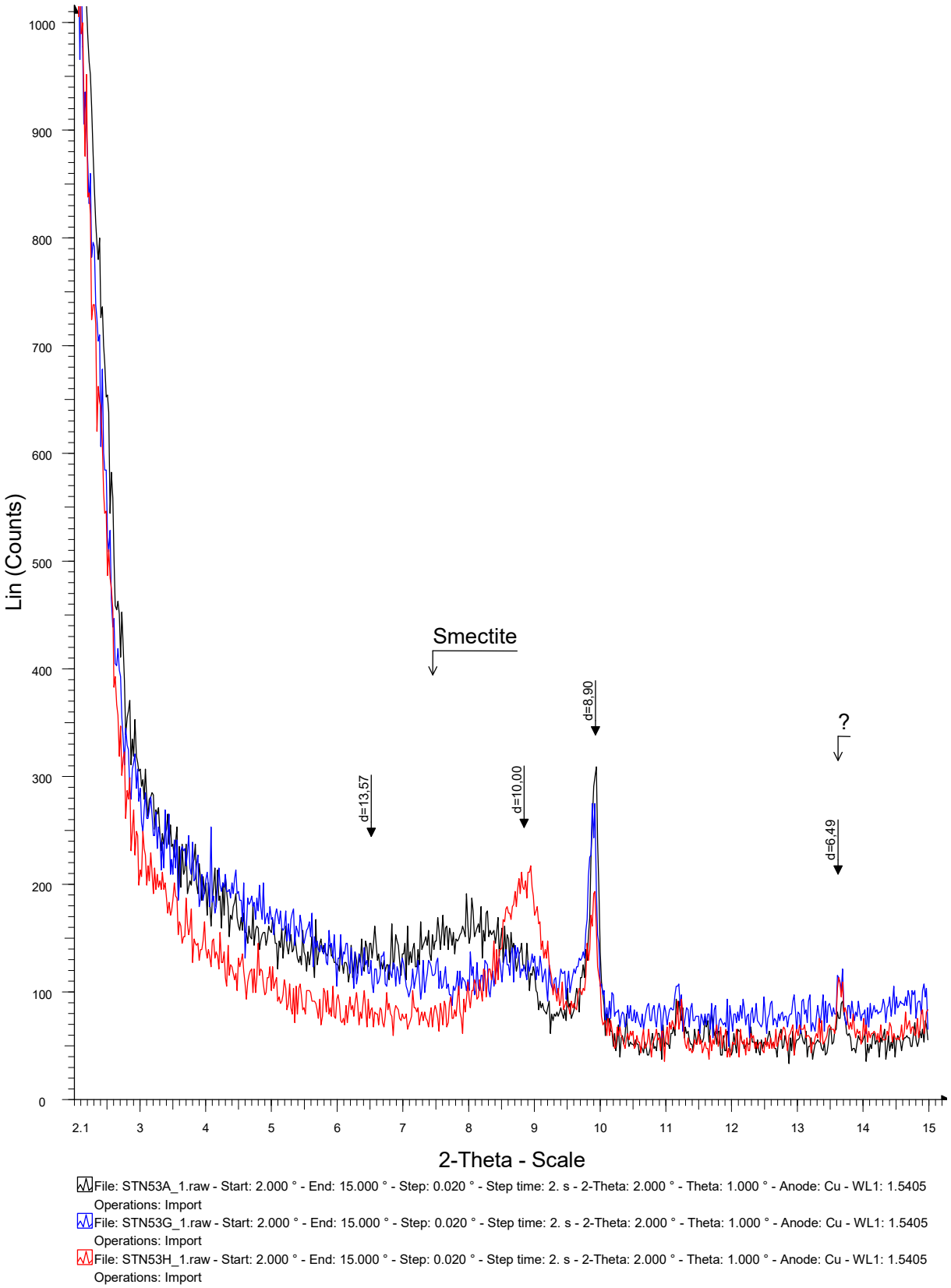

STATION 69 OLKARIA

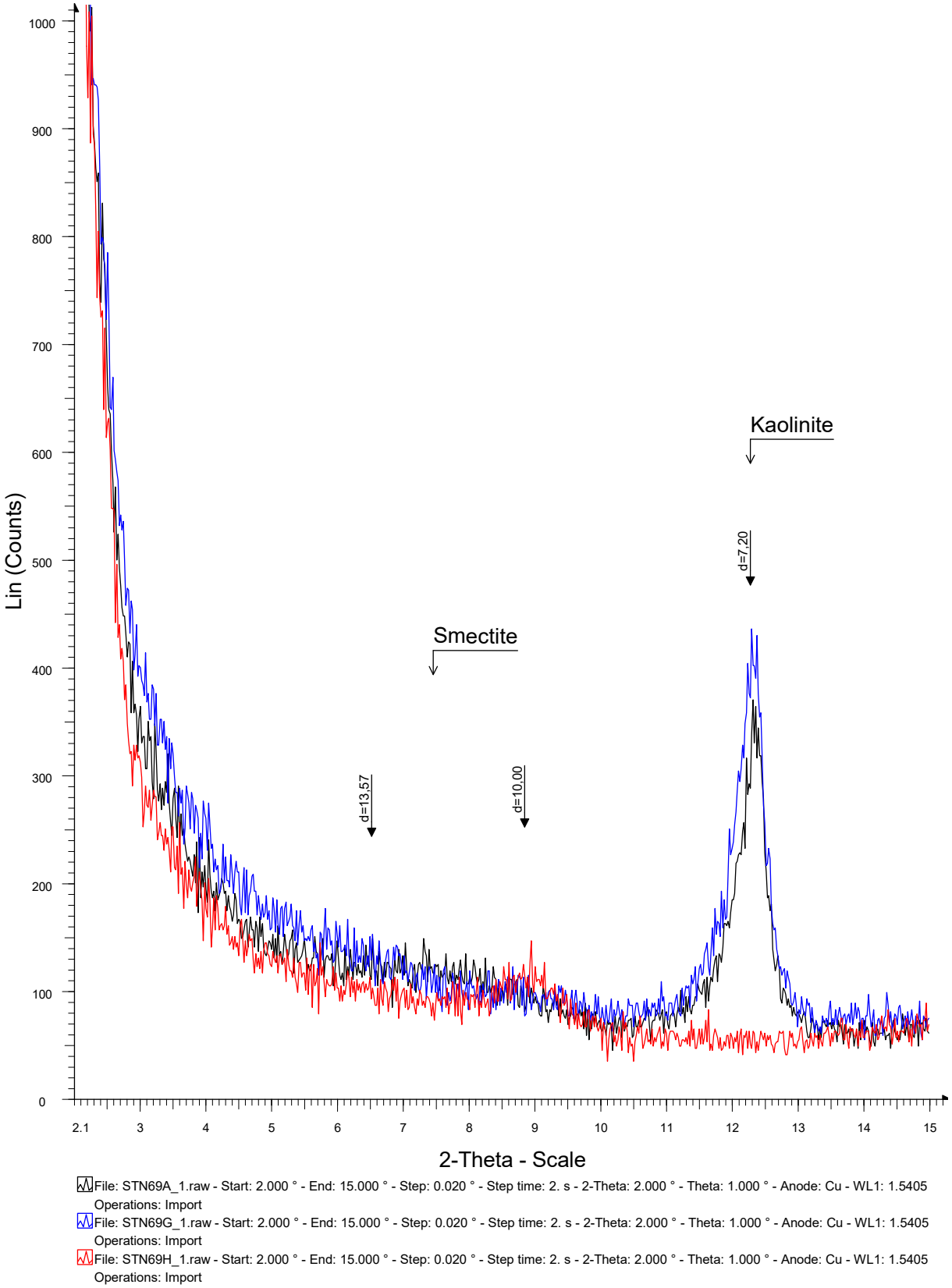

STATION 70 OLKARIA

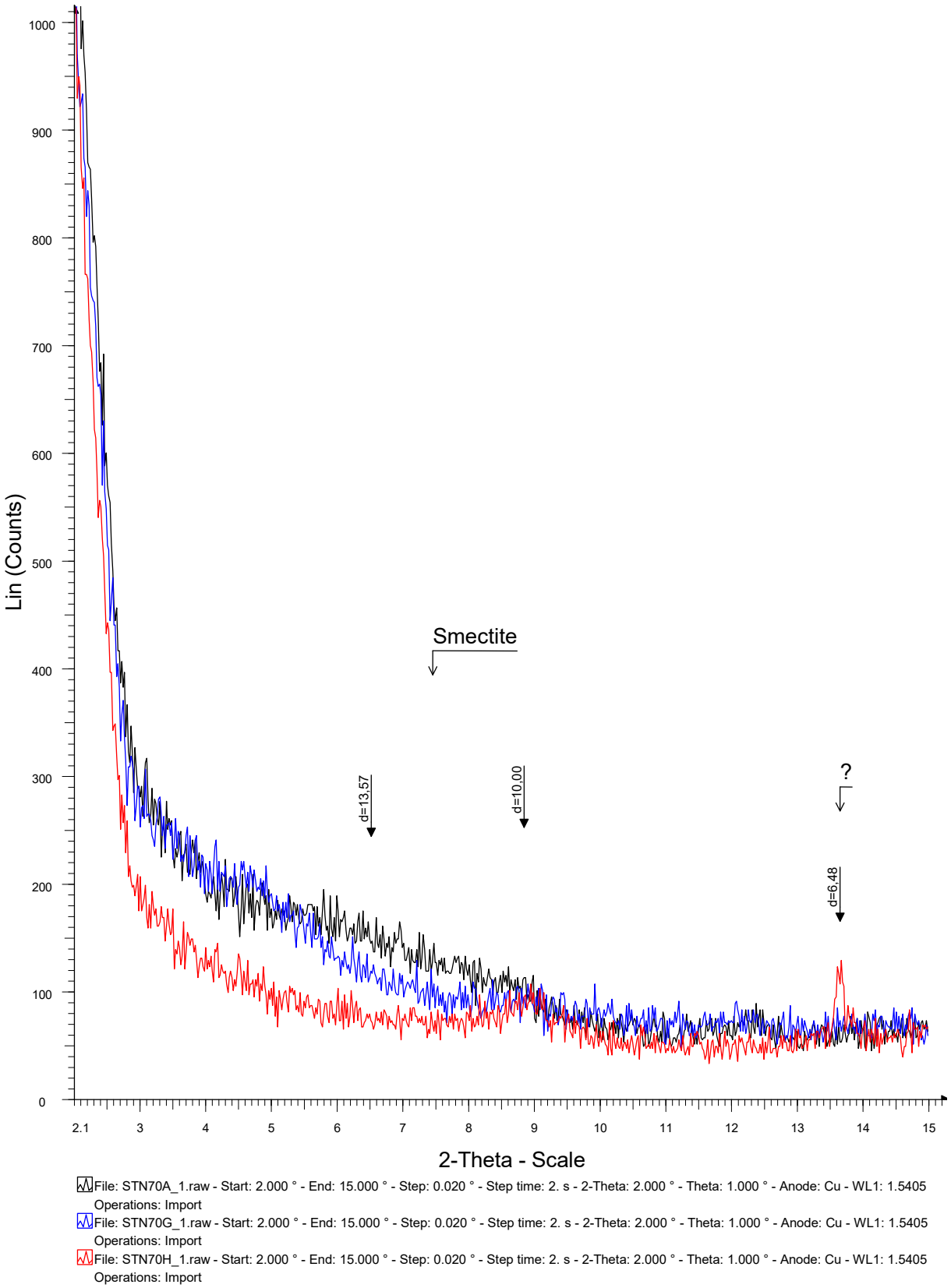

STATION 78 OLKARIA

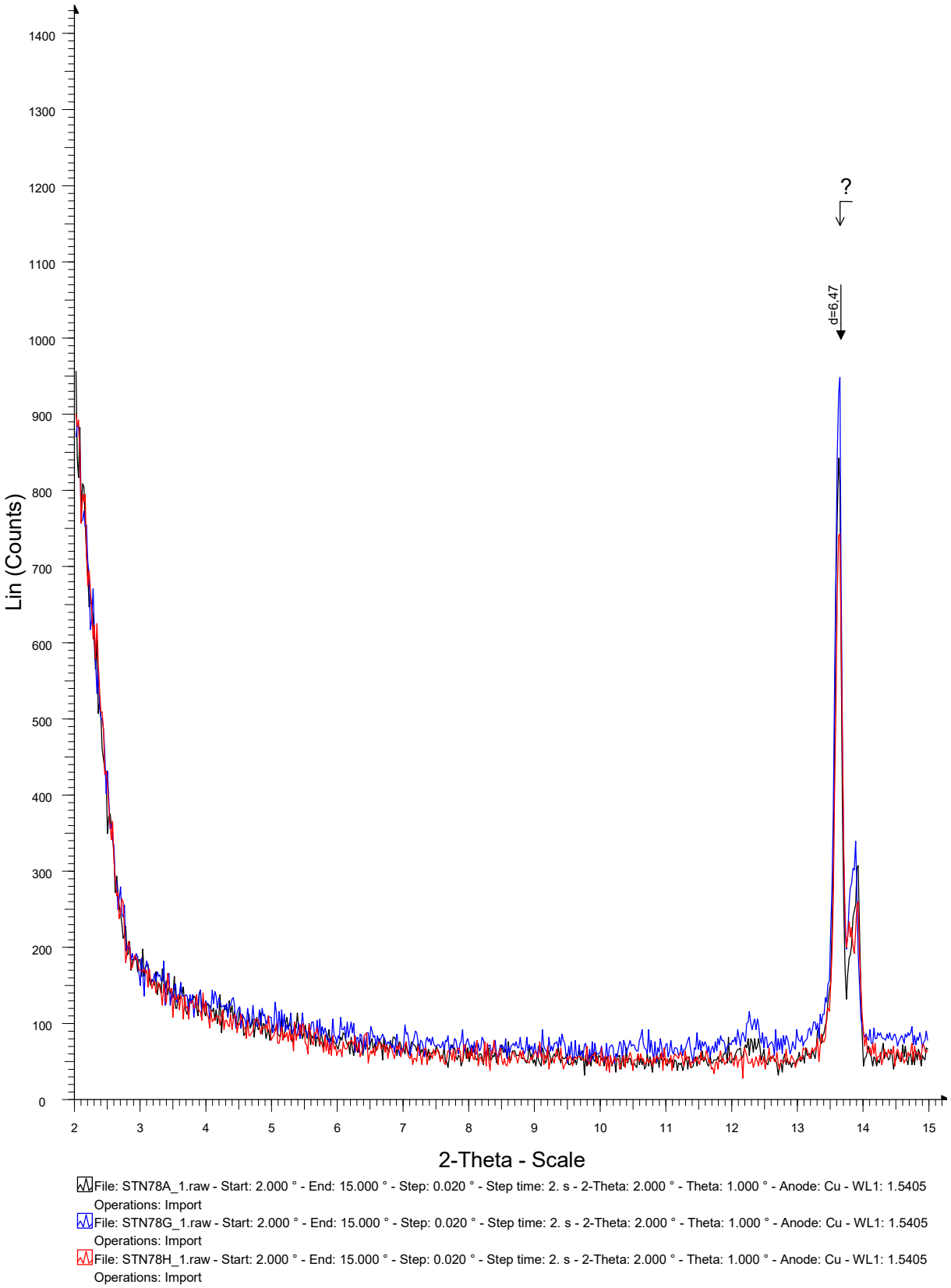

STATION 83 OLKARIA

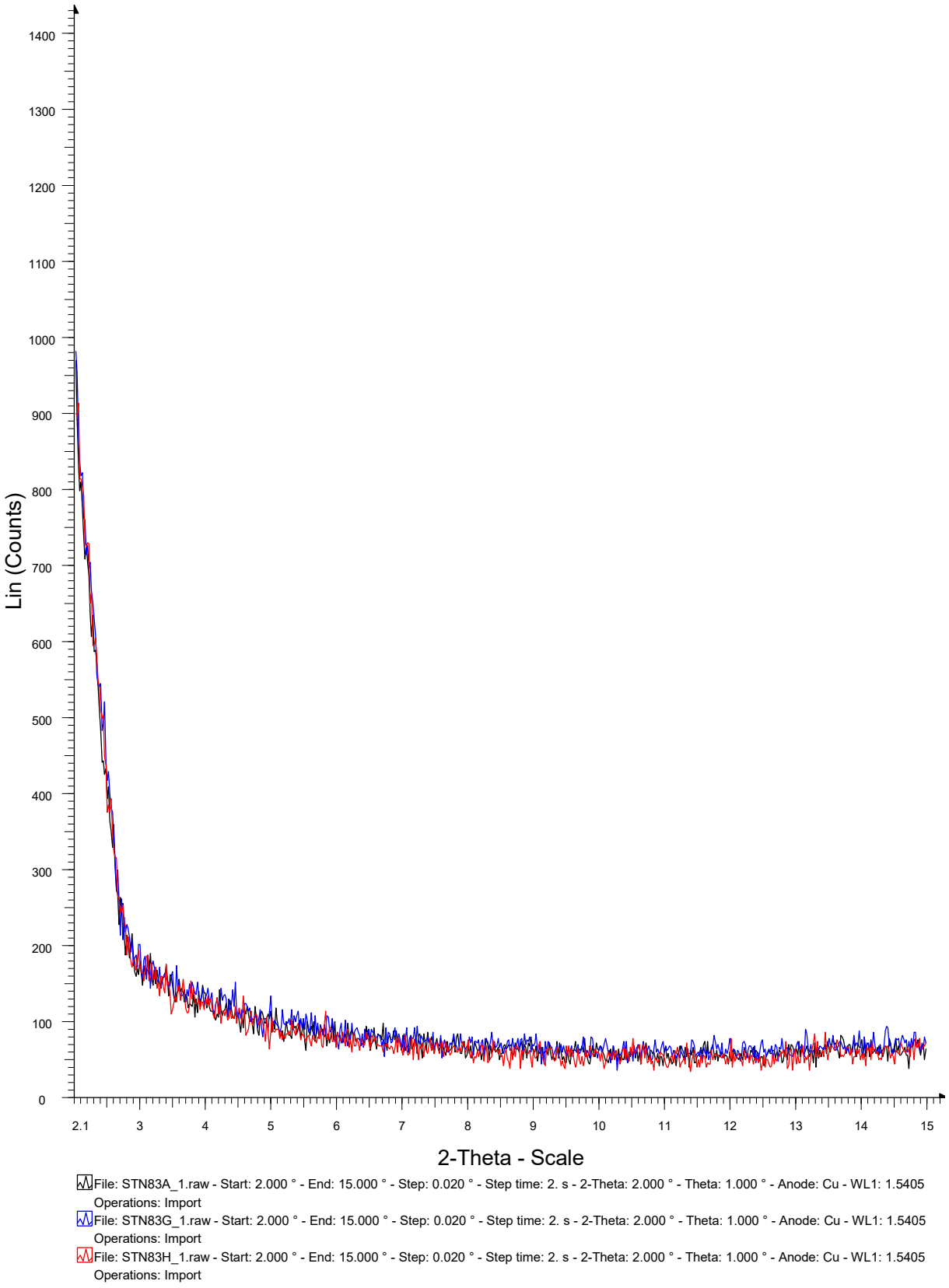

STATION 120 OLKARIA

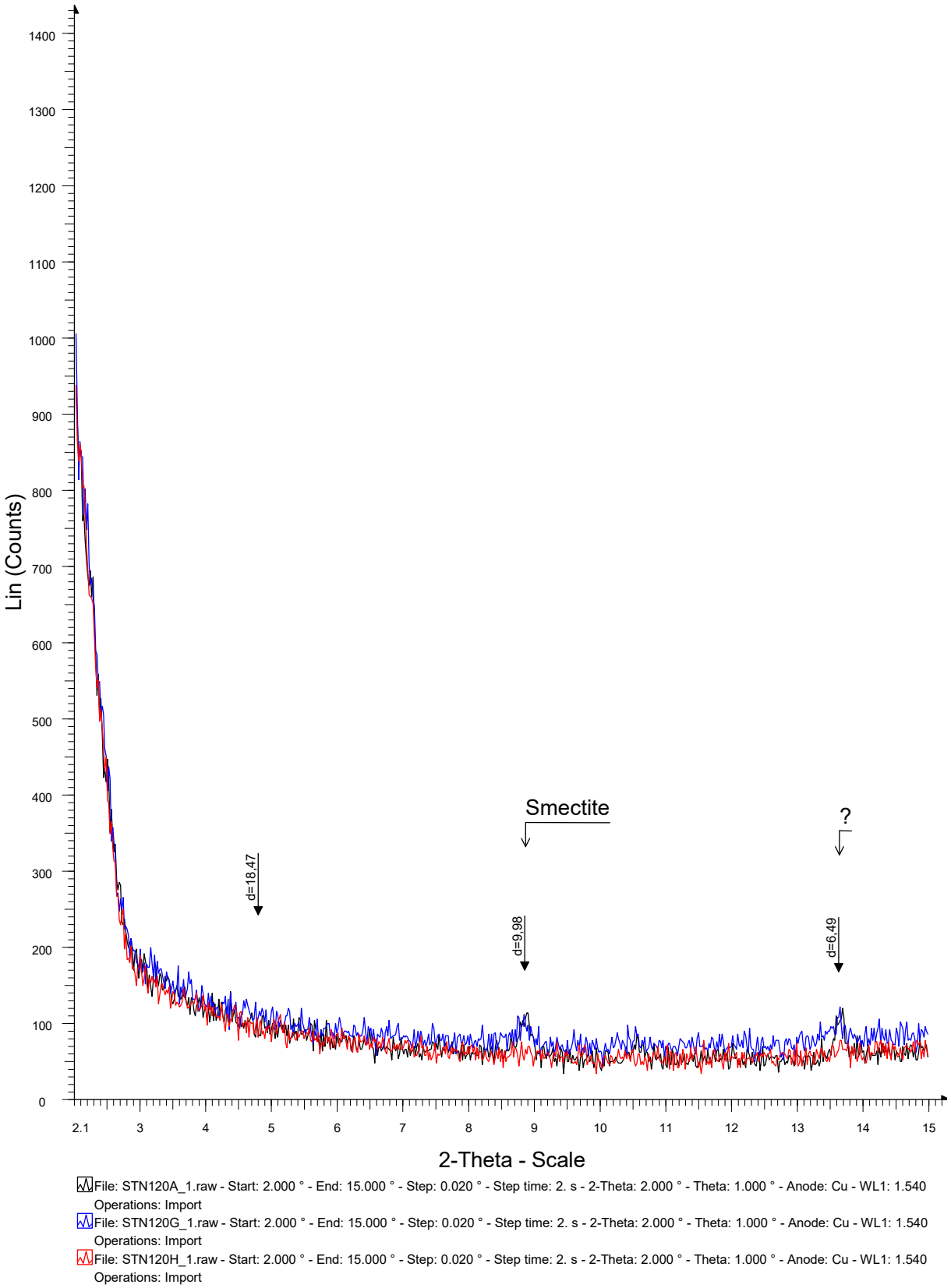

An identification key for the simplest clays

A = 13-15 Å, G = 14-17 Å, H = ~10 Å	Smectite
A = 7.2 Å, G = 7.2 Å, H = destroyed	Kaolinite
A = 10 Å, G = 10 Å, H = 10 Å	Illite
A = 13-14 / 7 AÅ, G = 13-14 / 7 Å, H = 13-14 / 7 Å	Chlorite
A = 13-14 / 7AÅ, G = 13-14 / 7 Å, H = 13-14 Å / 7Å peak destroyed	"Unstable" chlorite

The peak seen very often in Olkaria wells' samples, appearing at about 6.5 Å in A/G/H is not fully understood and identified. Also worth noting is that in KenGen report on the borehole geology of OW-905A by John Lagat, chlorites are routinely identified with a peak at approx. 12 Å (A/G) and disappearing in the heated sample. Similar samples are often associated with a mineral interpreted as illite, occurring with the chlorite and appearing at approx. 10 Å in A/G. Chlorite is also interpreted in samples only having a ~7 Å peak in A/G/H, and sometimes even when the H peak is destroyed.

APPENDIX II: Sampling stations

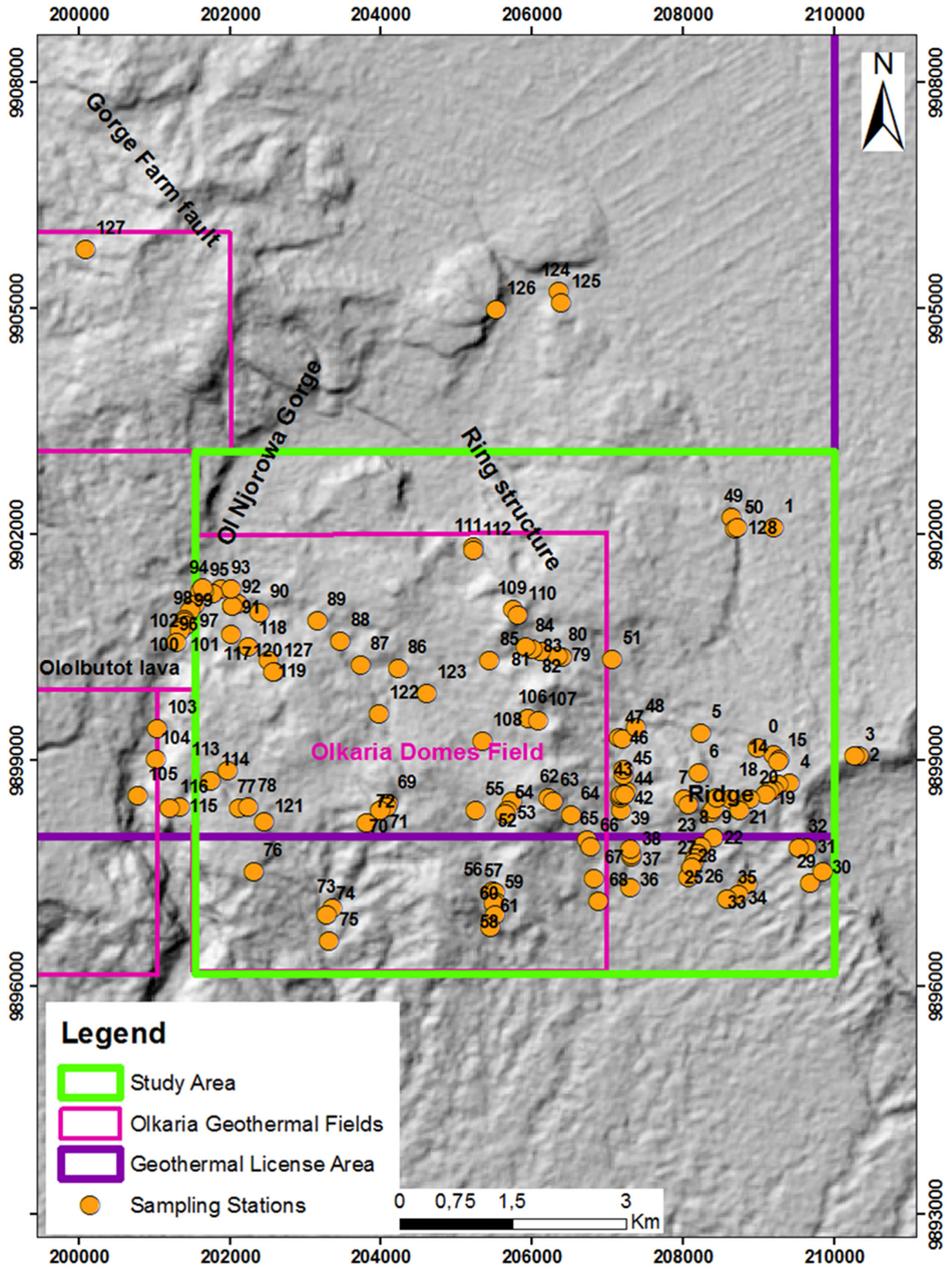

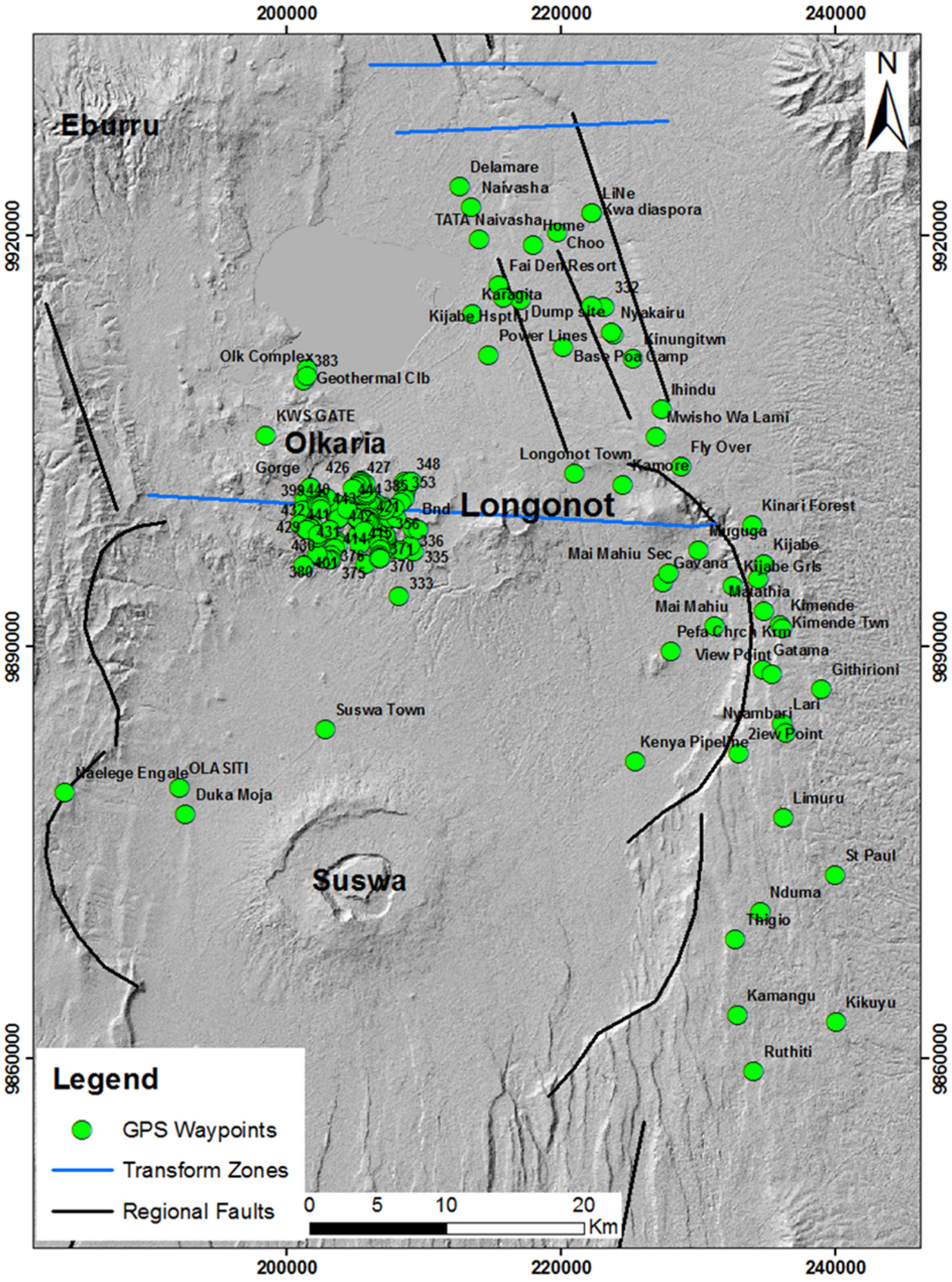
200000
220000
240000
9920000
9890000
9860000
N
Eburru
Delamare
Naivasha
LiNe
Kwa diaspora
TATA Naivasha
Home
Choo
Fai Den Resort
Karagita
332
Kijabe Hspt
Dump Site
Nyakairu
Power Lines
Kinungitwn
Base
Poa Camp
Olk Complex
383
Geothermal Clb
Ihindu
KWS GATE
Olkaria
Mwisho Wa Lami
Fly Over
Longonot Town
Kamore
Gorge
426
427
348
353
385
Bnd
Longonot
Kinari Forest
Muguga
Kijabe
Mai Mahiu Sec
Gavana
Kijabe Grls
Maiathia
Mai Mahiu
Kimende
Kimende Twn
Pefa Chrch
Krm
View Point
Gatama
Githirioni
Lari
Suswa Town
Nyambari
2iew Point
Kenya Pipeline
Naelege Engale
OLA SITI
Duka Moja
Limuru
St Paul
Suswa
Nduma
Thigio
Kamangu
Kikuyu
Ruthiti
Legend
GPS Waypoints
Transform Zones
Regional Faults
0
5
10
20
Km

APPENDIX III: Geochemical data for radon survey

					Radon					
					Background values			Soil gas measurements counts/minute		
Northings	Eastings	Elevation (m)	Temp (°C)	CO_2(%)	B1	B2	B3	R1	R2	R3
9904578	207860	2005,32	28,5	0	3	2	0	51	67	65
9902878	209612	2072,37	29,1	0,4	4	4	5	117	173	149
9902396	209685	209685	31,8	0,3	13	10	8	76	87	75
9901398	209499	2119,44	27,2	0	4	8	4	67	83	82
9900896	209501	2144,79	26,8	0,2	29	31	20	104	103	107
9900393	209502	2153,83	25	0,5	17	20	15	95	114	147
9899889	209501	2179,77	25,1	0,4	6	18	13	47	51	65
9899388	209500	2214,43	22	0,8	35	17	25	193	219	206
9902398	209113	2080,44	26,5	0	4	5	5	183	138	161
9902403	208616	2060,03	29,5	0	12	25	12	31	26	35
9902402	208114	2096,35	28,2	0,5	16	14	7	110	159	151
9902402	207615	2130,55	27,3	0,3	39	17	56	143	158	136
9902395	207102	2115,35	30	0	7	6	7	137	160	155
9902393	208600	2144,91	27,7	0	9	8	15	50	67	102
9900756	208604	2121,77	32,7	0,4	0	0	0	36	38	52
9900276	208081	2114,23	27,1	0,3	6	4	4	78	103	99
9903323	208036	2019	29,5	0,4	1	1	0	40	84	77
9900164	207329	2168	29,3	0,4	30	29	11	102	146	143
9900987	206942	2218	27,7	0,3	15	13	17	129	222	235
9901160	206047	2182	26,8	0,2	0	1	0	65	83	95
9899877	207929	2106	27	0,3	117	99	89	140	173	196
9899868	208544	2116	29,1	0,3	10	9	8	135	145	184
9899969	209100	2137	22,4	0,3	23	28	18	94	107	100
9900019	209617	2154	24,6	0,5	6	2	3	84	113	115
9900033	207363	2109	25,3	0,4	6	6	14	67	104	110
9900238	206711	2138	25,4	0,3	2	5	15	118	130	151
9900208	206238	2142	26,7	0,5	7	11	17	49	74	70
9901616	209719	2091	25	0,3	3	1	2	66	125	95
9901599	208806	2052	23,9	0,2	2	2	0	49	63	56
9901724	208129	2091	26,2	0,2	7	10	13	59	84	102
9900783	207797	2155	26,8	0,4	4	3	4	49	61	95
9898600	208377	2137	23,3	0,3	4	1	4	118	141	138
9898526	207906	2152	28,8	0,4						
9898542	207454	2074	25,5	0,3						
9898285	207180	1992	26	0,4						
9898600	206933	2074	27,5	1,5						
9899445	208684	2129	24,4	0,8	1	0	0	76	99	118
9899512	208218	2111	27,2	0,3	6	6	6	125	142	159
9899523	207620	2095	24,6	0,4	15	7	2	78	96	103
9899605	207077	2103	28,4	0,5	13		13			
9899619	206618	2125	31,7	0,6						
9899908	206128	2224	31,7	1,2						
9903338	207624	2065	28	0,4	0	1	0	43	65	78
9902905	207136	2068	23,9	0,3	27	12	10	94	117	124
9902837	206466	2050	27,3	0,4	34	24	26	34	63	61
9902553	205725	2001	28,8	0,4	33	35	33	119	157	176
9902866	205143	1931	27,8	0,3	33	15	33	70	92	124
9902183	207648	2032	25	0,5	48	36	19	105	173	144
9902261	207044	2041	27,6	0,6	20	14	24	104	142	116
9902328	206460	2115	28,6	0,3	24	17	20	54	67	60
9902045	205573	2056	27	0,5	19	8	17	189	212	256
9903035	204345	1906	31,8	0,5	26	26	20	64	98	88
9903093	202642	1896	26,5	0,4	0	0	0	20	12	12
9902998	201525	2034	27,6	0,4	0	0	0	14	10	6

					Radon					
					Background values			Soil gas measurements counts/minute		
Northings	Eastings	Elevation (m)	Temp (°C)	CO_2(%)	B1	B2	B3	R1	R2	R3
9903214	201799	2017	27	0,6	11	2	9	74	78	78
9901660	206930	2195	29,1	0,6						
9901597	206400	2181	31,5	0,5						
9901560	205901	2110	30,2	0,2						
9902412	202749	1928	29,1	0,3						
9902327	203249	1976	25,1	0,3			202614			
9902396	203749	1999	25,1	0,3			202114			
9902400	204250	1986	25,4	0,4						
9901727	204747	2017	28,7	0,5						
9901736	204236	2011	24,6	0,1	0	0	0	71	117	141
9901724	203633	1980	25,9	0,1	18	15	11	87	115	125
9901771	203114	1950	29,7	0,4	0	0	0	110	129	128
9901993	202508	1937	25,5	0,1	0	0	3	113	131	149
9902000	202083	1883	26,7	0,5	20	30	22	116	161	191
9901299	205102	1986	24,3	0,2	37	38	40	97	138	142
9901251	204600	2025	24,1	0,3	24	30	21	108	174	176
9901250	204100	2075	27,5	0,3	19	22	21	57	83	89
9901251	203600	1990	25,2	0,1	16	23	21	93	122	132
9901251	203100	1963	26	0,4	23	20	21	90	131	137
9901400	202602	1926	28,3	0,2	15	20	21	116	119	139
9901500	202100	1898	24,5	0,3	6	5	5	74	142	156
9901002	202100	1903	28	0,1	19	16	11	94	159	193
9900958	202634	1905	32,5	0,2	70	46	38	119	146	161
9900754	203118	1963	28	0,3	41	38	31	156	201	236
9900715	203596	1964	31,4	0,1	34	37	44	53	88	151
9900751	204101	1997	26	0,1	32	25	25	124	192	182
9900760	204601	1996	26,5	0,1	3	6	2	39	56	48
9900754	205101	2017	26,7	0,3	6	8	9	107	113	149
9900254	205103	2002	27,1	0,2	13	13	22	93	152	165
9899981	204525	1989	28,1	0,4	1	0	1	65	105	108
9900005	203927	1955	30,2	0,8	27	19	14	55	68	84
9900009	203386	2018	27,2	1,1	16	17	13	94	143	153
9899973	202860	2045	26,8	0,8	0	3	2	121	206	220
9900002	202160	2000	28,4	0	12	30	17	52	149	161
9900009	201616	1950	25,2	0,6	17	21	15	45	63	66
9899500	201615	1966	26	0	16	17	16	102	136	113
9899500	202115	1999	29,3	0,3	16	16	19	119	165	170
9899508	202615	2016	23,6	0,9	1	5	6	307	511	533
9899498	203115	2060	24	0,4	34	30	27	261	407	524
9899500	203615	2018	30,2	0,5	65	83	80	159	204	245
9899499	204116	1984	26,1	0,4	79	68	65	151	160	187
9899500	204615	2014	31,6	0,1	55	61	46	159	216	211
9899480	205125	2005	21,1	0,3	8	3	6	69	99	130
9898995	205114	2039	20,4	0,81	11	13	1	176	297	321
9898898	204615	2086	22	1,4	22	27	38	354	524	603
9898898	204115	2075	21,4	0,1	65	60	59	217	350	428
9898823	203657	2031	22,1	0,3	64	62	52	157	228	256
9899000	203113	2055	24,6	0,1	8	9	7	273	515	733
9899000	202613	2031	25,2	0,2	259	201	144	294	351	383
9898990	202110	1962	28,5	0,5	158	120	148	208	228	242